SOI: 1.1/TAS
DOI: 10.15863/TAS
Scopus ASJC: 1000

ISSN 2308-4944 (print)
ISSN 2409-0085 (online)
№ 10 (114) 2022

Teoretičeskaâ i prikladnaâ nauka

Theoretical & Applied Science

Philadelphia, USA

Teoretičeskaâ i prikladnaâ nauka

Theoretical & Applied Science

10 (114)

2022

International Scientific Journal
Theoretical & Applied Science

Founder: **International Academy of Theoretical & Applied Sciences**

Published since 2013 year. Issued Monthly.

International scientific journal «Theoretical & Applied Science», registered in France, and indexed more than 45 international scientific bases.

Editorial office: **http://T-Science.org** Phone: **+777727-606-81**

E-mail: **T-Science@mail.ru**

ISSN 2308-4944

9 772308 494225 10

International Scientific Journal

Theoretical & Applied Science

International Scientific Journal

Theoretical & Applied Science

ISJ Theoretical & Applied Science, 10 (114), 884.
Philadelphia, USA

Impact Factor ICV = 6.630

Impact Factor ISI = 0.829
based on International Citation Report (ICR)

The percentage of rejected articles:

ISSN 2308-4944

9 772308 494225 10

SOI: 1.1/TAS DOI: 10.15863/TAS
International Scientific Journal
Theoretical & Applied Science

p-ISSN: 2308-4944 (print) **e-ISSN:** 2409-0085 (online)

Year: 2022 **Issue:** 10 **Volume:** 114

Published: 24.10.2022 http://T-Science.org

Issue Article

Bekzod Matnazarovich Matyakubov
Mirzo Ulugbek National University of Uzbekistan
University of Public Security of the Republic of Uzbekistan
Doctor of Philosophy (PhD) in Physical and Mathematical Sciences

Mirzhalol Eslamasov
Mirzo Ulugbek National University of Uzbekistan
undergraduate

SOME CHARACTERISTICS OF NANOFIBER NANOPOROUS MATERIALS

Abstract: *The article presents the results of a study on the production of nanofibre anisotropic nanoporous materials based on silk fibroin (FS) and Acrylonitrile Copolymer (Co-An) of nanofibers in the form of a thin material. The dependence of the anisotropy, which characterizes the structural states of the obtained thin-layer polymeric materials, on the deformation effects, their sorption and filtration properties has been studied. Wide possibilities of using nanofiber nonwoven materials as nanofilters and the efficiency of the filtration process of nonwoven materials with an increase in the size of their nanopores.*

Key words: *nanofiber, nanomaterial, formation, polymer, structure, temperature.*
Language: *Russian*
Citation: Matyakubov, B. M., & Eslamasov, M. (2022). Some characteristics of nanofiber nanoporous materials. *ISJ Theoretical & Applied Science, 10 (114),* 301-306.
Soi: http://s-o-i.org/1.1/TAS-10-114-43 ***Doi***: crossref https://dx.doi.org/10.15863/TAS.2022.10.114.43
Scopus ASCC: *3100.*

НЕКОТОРЫЕ ХАРАКТЕРИСТИКИ НАНОВОЛОКОННЫХ НАНОПОРИСТЫХ МАТЕРИАЛОВ

Аннотация: *В статье представлены результаты исследований по производству нановолоконных анизотропных нанопористых материалов на основе фиброина шелка (ФШ) и сополимера акрилонитрила (Со-Ан) нановолокон в виде тонкого материала. Исследована зависимость анизотропии, характеризующей структурные состояния полученных тонкослойных полимерных материалов, от деформационных воздействий, их сорбционных и фильтрационных свойств. Широкие возможности использования нановолоконных нетканых материалов в качестве нанофильтров и эффективность процесса фильтрации нетканых материалов с увеличением размера их нанопор.*

Ключевые слова: *нановолокно, наноматериал, формирование, полимер, структура, температура.*

Введение

Динамичное развитие современной нанонауки и нанотехнологии тесно связано со созданием новых наноматериалов, в частности, нановолокон полимеров с уникальными свойствами [1]. Нановолокна формуют из прядильных растворов и расплавов полимеров путем вытягивания жидкой струи посредством сильного электрического поля, т.е. методом электроформования (электроспиннинга) [2]. Метод основан на осуществление превращения «струя-нановолокно» в воздухе между анода (фильера) до катода (барабан или экран). Высокое напряжение, подаваемое на анод не только вытягивает молекул полимеров из струи в направление катода, но и осуществляет ориентационно-скрученное структурообразование макромолекул в форме нановолокон [3]. Технически принятие нановолокон на стационарный экран является простым, что позволяет непосредственной укладки формируемого нановолокна на поверхность экрана в виде нетканого материала. Причем, полученный нетканый материал характеризуется нанопористостою [4].

Характеристики нановолоконных нетканых материалов и их нано пористость во многом зависит от условий электроспиннинга и укладки нановолокон на поверхности экрана – приемника [5]. В этом большой интерес представляет получение нановолоконных нанопористых нетканых материалов на основе местных биосовместимых полимеров, в частности, фиброина и целлюлозы, выделенных, соответственно, из отходов переработки кокона шелка и хлопкового сырья, например, лигнина. Нановолокна фиброина характеризуются с выраженной био- активностью, которой наиболее ярко проявляется на поверхностном слои нанопористого нетканого материала. Внутри таких материалов нановолокна находится в произвольно-уплотненной форме, т.е. в неупорядоченном состоянии [6].

В таком случае пространства между нановолокнами образованные поры, нанопоры в том числе, имеют различные размеры и размерности. Поскольку, нановолокна проявляют выраженной поверхностной активности, то это явление в таких разноразмерных порах и нанопорах проявляется различной степени, и главное в зависимости от формы и размеры данных пор проходит через поры различные количества вещества в газообразном и жидкофазном состоянии. Проявление таких разнообразных свойств активности в нановолоконных нетканых материалах усложняют проявление свойств характерных для наноматериала. Например, при практическом применении нановолоконных материалов в качестве биоактивных покрытий открытых ран очень важно наличие в них нанопоры с определенными размерами, способными пропуксать через себя определенного объема вещества, воздуха и т.п. Поэтому, целесообразно получение нетканых материалов, в которых поверхностный слой состоял из биоактивных биосовместимых нановолокон и внутри были нанопоры с определенными размерами. Такие нанопористые наноматериалы, безусловно, находят широкое практическое применение в области медицины, фармацевтики, косметологии, текстиля, экологии и т.п [7].

Для получения таких нанопористых материалов необходимо усовершенствование способа (установки и метода) электроспиннинга со специальным устройством приёмника (экрана), способного осуществлять равномерной укладки нановолокон с образованием однотипных нанопор в получаемом нетканом материале.

В целом, усовершенствование способа электроспиннинга нановолокон на уровне нанотехнологии современных материалов, прежде всего, нанопористых нетканых материалов на основе местных много тоннажных биополимеров является весьма актуальным научным направлением прикладных исследований [8].

Выявлено, что в зависимости от условий формования получают нановолокна с толщиной 5 - 500 nm, а толщина нетканого материала может быть регулирована от 10 mkm до десятки mm. В случае полиэлектролитов высокое напряжение способствует локализацию мобильных ионогенных групп макромолекул на поверхности нановолокон и в результате полученный нановолоконный нетканый материал обладает выраженной поверхностной активностью [9]. Особое внимание привлекает следующие моменты: - формование нановолокон на основе биополимеров (например, фиброина, коллагена, хитозана), содержащих положительно заряженных аминных групп позволяет получить нетканые бактерицидные материалы, поскольку, аминные группы блокируют отрицательно заряженных бактерий. Такие материалы могут быть применены в качестве биоразлагаемые перевязочные средства или покрытия для открытых ран [10]; - в случае формования нановолокон на основе ионогенных биосовместимых полимеров, в частности, сополимера акрилонитрила (АК:МА:ИК) получаются нетканые материалы с высокой гибкостью и выраженной поверхностной активностью, проявляющие взаимодействия с различными веществами. Такие нетканые материалы могут быть использованы в качестве высокоэффективные нанофильтры для газообразных и жидкофазных веществ. Исходя из этого исследовали поверхностно-активных свойств нановолокон на основе фиброина шелка и сополимера акрилонитрила [11].

В качестве объектов исследования выбрали волокон фиброин шелка (ФШ), очищенного от серицина и жировосков, а также волокон сополимера акрилонитрила (Со-АН), произведенного в ОАО «Навоиазот». Волокна ФШ растворяли в 50 % $CaCl_2$ в целях исключения возможных деструкций цепей. Далее, проводили диализ против ионов $CaCl_2$, и полученный порошок аморфизированного фиброина растворяли в муравьиной кислоте (HCOOH). Опыты показали, что растворы ФШ с концентрацией С = 5 – 20 % в HCOOH пригодны для получения нановолокон с толщиной 100-300 nm методом электроспиннинга при напряжении 3 - 6 kV/cm.

Прядильные растворы со-АН приготовили в ДМФА с С = 5 – 10 % в ДМФА. Выявлено, что при таком же диапазоне напряжения 3 - 6 kV/cm формируются нановолокон со-АН, однако толщина нановолокон при этом колеблется в интервале 50 - 500 nm.

При этом было очевидно концентрирование ионогенных групп макромолекул на поверхности нановолокон, следовательно, проявление выраженных поверхностно-активных свойств их при контакте составляющими (атомами, молекулами, ионами, частицами) окружающей среды. Такие особенности нановолокон исследовали методами физической химии, в частности, сорбции паров, нанофильтрации жидкостей, электроосмоса ζ-потенциала, а также испытали в качестве биопокрытия [12].

Сорбции паров. Опыты проводили на высоковакуумной установке с ртутными затворами и кварцевыми весами Мак-Бэна при 298 К и остаточном давлении воздуха 10^{-3}-10^{-4} Па. В качестве сорбата выбрали этанола и воды. Получили типичные S-образные изотермы сорбции, которые приведены на рис.1 в виде зависимости показателя сорбции (*x/m*) от относительной влажности (P/P_o) для нановолокон фиброина и Со-АН.

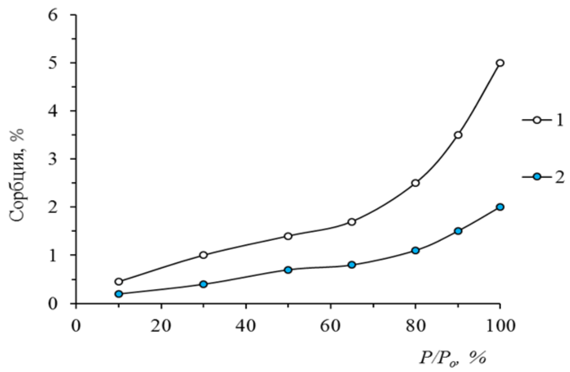

Рис. 1. Изотермы сорбции паров этанола (1, 2) и воды (1', 2') для нановолокон ФШ (1, 1') и со-АН (2, 2').

Видно, что нановолоконные образцы сравнительно больше сорбируют паров воды, чем этанола. Причем, такое явление заметно ярче проявляется в случае образца ФШ. Данное различие по-видимому, обусловлено с плотной упаковкой гибкоцепных молекул со-АН по сравнению жесткоцепных молекул ФШ в нановолокнах. А также наличием сравнительно больших количествах гидрофильных групп в цепях ФШ. Подобные различия обнаружили при расчете капиллярно-пористых и структурных показателей нановолокон, а именно, сорбционного объема (X_m), удельной поверхности ($S_{уд}$), суммарного объема пор (W_o), среднего радиуса пор (r_k) нановолокон приведены в табл. 1. Видно, что значение показателей сравнительно низкое в случае паров этанола, чем воды как для со-АН, так и для ФШ. Заметно завешенное значение в случае ФШ, т.е. большие объемы пор обусловлены наличием в молекулах фиброина крупных аминокислотных остатков типа аспаргиновых и глутаминовых, которые не укладываются как в α-спиральных, так и в β-структурных формах данного белка в волокнах. Тем не мнение радиусы пор достаточно большие для проникновения атомов и не больших молекул в объем нановолокон [13].

Таблица 1. Капилярно-пористые и структурные показатели нановолокон

Образец	ФШ	Со-АН	ФШ	Со-АН
	Этанол		Вода	
X_m, g/g	0,0045	0,0041	0,0054	0,0052
$S_{уд}$, m^2/g	14,72	12,91	23,04	18,33
W_o, cm^3/g	0,028	0,020	0,042	0,037
r_k, Å	38,27	31,41	45,26	36,55

Таким образом, из полученных результатов следуют, что нановолокна ФШ и со-АН являются наноматериалов, способных сорбировать паров атомов и молекул с размерами не более 30-40 Å сохраняя свои формы без существенных деформационных изменений [14].

Нанофильтрация. Безусловно, нетканые нанопористые материалы на основе поверхностно-активных нановолокон проявляют специфические взаимодействия с газообразными и жидкофазными веществами, и могут селективно фиксировать или удержать их составляющих в зависимости от химической природы, строения и размерности. Такая селективность наиболее ярко проявляется, когда через поверхностно-активный нанопористый материал пропускается коллоидная и молекулярно-дисперсная система.

Это обусловливало проведения настоящего опыта в целях выявления эффективности нановолоконного нанопористого материала со-АН в качестве нанофильтра, пропуская через него отработанного машинного масла, содержащего микро- и наноразмерных частиц. Причем, машинное масло является химически нейтральным относительно нановолокон со-АН. Это дало дополнительная возможность для проведения сравнительных опытов образцов нетканого материала со-АН, различающихся по размерам пор: 50, 100, 300 nm. При этом толщина нетканого материала составляла d_n = 0,5 mm.

Исследование проводили следующим образом, т.е. через нанофильтр массой (m_n), находящийся в длительном воронке, пропускали m_o=100 ml отработанного машинного масла, имеющего коричневого цвета. На выходе, т.е. после протекания масло через нанофильтр имело светло-желтый цвет и масса его уменьшалась (m_i), т.е. определенная часть массы (m_p) из состава удержалась на нанофильтре. Это свидетельствовало о протекании фильтрации масла, которая протекала интенсивно в течение 60 -80 min. При этом эффективность фильтрации судили по отношению m_i/m_o по времени (t) наблюдения, построив графики, представленные на рис.2. Видно, что процесс фильтрации носит кинетический характер, т.е. с увеличением времени и размеров нанопор масса продукта фильтрации (m_i) повышается монотонно до 60-80 min, далее стабилизуется. Причем, уменьшение размеров поры нанофильтра способствует росту эффективности удержания примесей. Выявлено, что степень очистки отработанного машинного масла при пропускании через нанофильтры без всяких внешних давлений или деформационных воздействий составляет примерно 25 % в случае использования нанопоры 80 nm, почти 65 % в случае нанопоры 50 nm.

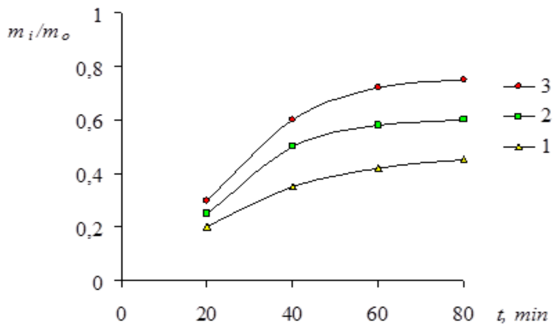

Рис.2. Зависимость относительной изменения массы (m) от времени (*t*) при пропускании машинного масла через нанофильтры Со-АН с различными размерами пор: 1 – 50 nm, 2 – 100 nm, 3 – 300 nm.

Это в принципе хорошей результат для рекомендации нановолоконного нетканого нанопористого материала на основе Со-АН на практическое применение в качестве нанофильтров.

Электроосмос. Взаимодействие поверхностно-активных нановолоконных нетканых материалов с ионами металлов исследовали с помощью метода электроосмоса [15]. При этом в качестве нанопористой мембраны использовали нановолоконного нетканого материала на основе ФШ и подвижной дисперсной фазы водного раствора $CuSO_4$ (2%). Определяли значения ζ-потенциала, характеризующего устойчивости взаимодействия ионов с функциональными группами нановолокон при перемещении дисперсной среды через мембраны под действием постоянного тока (рис.3.). Выявлено, что значение ζ-потенциала повышается от 40 до 80 mV при росте концентрации $CuSO_4$ от 0,5 до 2 %. Данные результаты свидетельствует об устойчивости взаимодействий ионов с элементами нановолокон из-за поверхностной активности нетканого материала.

Таким образом, результаты показывают, что на основе фиброина возможно получение нановолоконных нетканых материалов с поверхностно-активными свойствами, достаточно устойчиво взаимодействующие и удерживающие ионов металлов в дисперсных средах.

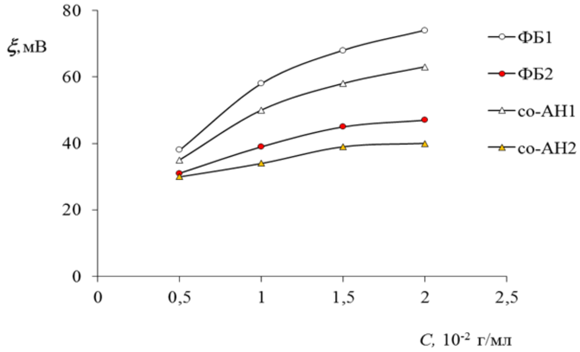

Рис.3. Зависимость значения ζ-потенциала от концентрации (*C*) раствора $CuSO_4$ для нановолоконного нетканого материала на основе ФШ.

Нановолоконные биопокрытия. Поверхностно-активные нетканых материалы на основе Со-АН является биосовместимым, а на основе ФШ не только биосовместимым, но и биоактивным. Это представляло интерес проведения медико-биологических испытаний, например, в качестве покрытия открытых ран. Для этого из нановолоконных материалов Со-АН и ФШ нарезали квадратики с размерами 2х2 $см^2$ и согласно [16] проводили стерилизации посредством этилового спирта. Далее, в медико-биологическом лабораторном условии на поверхность открытых ран у крыс наложили квадратиков и фиксировали их с краев посредством пластыров. Сравнительные наблюдения за заживлением ран проводили в прочих равных условиях с использованием для каждого образца наноматериалов по 10 крыс в течение 30 дней.

Результаты наблюдения обнаружили, что заживление открытых ран в случае использования биоактивных наноматериалов протекало значительно интенсивнее, чем биосовместимого образца. Биоактивные нанопокрытия способствовали практически полному заживлению ран в течение 14 суток, тогда как заживление ран при биосовместимом образце продолжалось до 21 суток. В конце заживления ран наноматериальные покрытия отпадали без всяких дополнительных усилий [17]. Отделившие от ран наноматериалы были анализированы на предмет сохранности структуры. Поляризационно-оптические и электронно-микроскопические наблюдения показали, что в целом нановолоконные структуры образцов сохранились. Контрольные наблюдения за физическим и медико-биологическим состоянием заживленных участков крыс, проведенные в течение трех месяц не характеризовались с каким-либо серьезным структурным изменением [18].

Таким образом, испытания нановолоконных материалов Со-АН и ФШ показали принципиальной возможности их применения в качестве покрытий открытых ран. На основе проведенных исследований показано, что на основе фиброина шелка и сополимера акрилонитрила, имеющихся функционально-активных групп возможно получение нановолоконные нетканые материалы с выраженными поверхностно-активными свойствами. Иссследование данных материалов на предмет выявления сорбционных характеристик, фильтрующих способностей, электрокинетических устойчивостей, биоактивных покрытий дали положительные результаты, на основе которых на последующем этапе возможна разработки наноматериалов со специальными свойствами [19].

ЗАКЛЮЧЕНИЕ

Определены некоторые физико-химические и медико-биологические характеристики нановолоконных нанопористых нетканых материалов, необходимые для практического применения. В частности, выявлены сорбционные характеристики, фильтрующие способности, электрокинетические устойчивости, которые имею важные значения для разработки нановолоконных нетканых материалов. Повышенное значение электрокинетического потенциала выше ±30 мВ показало стабильность и устойчивость взаимодействия нетканых анизотропных материалов с ионами электролита. со специальными свойствами.

References:

1. Valery, F., Kurenkov, H.-G.H., & Lobanov, F.I. (2002). Application of Polyacrylamide Flocculants for Water Treatment. *Chem. & Comp. Simul., Butlerov Communications*, 11(3), 31-40, 2002. https://doi.org/10.4236/oalib.1106948
2. Kurenkov, V.F., Snigirev, S.V., Churikov, F.I., et al. (1869). Preparation of Anionic Flocculant by Alkaline Hydrolysis of Polyacrylamide (Praestol 2500) in Aqueous Solutions and Its Use for Water Treatment Purposes. *Russ. J. of Appl. Chem.* 74, 445-448, 2001. https://doi.org/10.1023/A:1012745611869
3. Pilgunov, V.N., & Efremova, K.D. (2015). The outflow of a viscous fluid through round holes at low Reynolds numbers. *Aer.Sc. Jour*. (01), 31-57. 2015. https://doi.org/10.7463/aersp.0115.0775178
4. Davlyud D.N., et al. (2018). Rheological properties and concentration transitions in water-salt solutions of polyacrylamide and anionic (co) polymers of acrylamide. *Pro. of the Nat. Acad. of Sc. of Belarus Chem. Ser*. 54(3): 329-337. https://doi.org/10.29235/1561-8331-2018-54-3-329-337
5. Kholmuminov, A.A., & Matyakubov, B.M. (2021). Anisotropic properties of nanofiber porous materials of fibroin silk and cotton cellulose. *Mod. Phy.Let. B.*, 35(16), 2150276. https://doi.org/10.1142/S0217984921502766
6. Kholmuminov, A.A., Ashurov, N.S., Yunusov, M.Y., et al. (2013). Acrylonitrile copolymer nanofibers and their structural characteristics. *Polym. Sci. Ser. A* 55, 39-42. https://doi.org/10.1134/S0965545X13010021
7. Kholmuminov, A.A., Matyakubov, B.M., & Rakhmonov, T.T. (2021). Anisotropic, sorption and filtering properties of thin-layer polymer materials. *Chem. Mat. Sc. Res. J.*, 3(2). https://doi.org/10.51594/CMSRJ.V3I2.216
8. Umarbek, A., Vaxitovich, A., Raximova, Y., Karabayeva, M., Saidkulov, D., & Matyakubov, B. (2022). An Investigation of the Electrophysical Properties of Composite Ceramic Materials Containing Nickel Nanoparticles. *Phy. Chem. Res*., 11(2), 231-239. https://doi.org/10.22036/pcr.2022.335151.2063
9. Shatat, R.S., Niazi, S.K., & Ariffin, A. (2017). Synthesis and Characterization of Different Molecular Weights Polyacrylamide. *IOSR Jour. of Appl. Chem.* 10(4). 67-73. https://doi.org/10.9790/5736-1004016773
10. Wever, D.A.Z., Raffa, P., Picchioni, F., & Broekhuis, A.A. (2012). Acrylamide Homopolymers and Acrylamide−N-Isopropylacrylamide Block Copolymers by Atomic Transfer Radical Polymerization in Water. *Macromolecules*. 45(10), 4040-4045. https://doi.org/10.1021/ma3006125
11. Ma, J., Zheng, H., Tan, M., Liu, L., Chen, W., Guan Q., & Zheng, X. (2013). Synthesis, characterization, and flocculation performance of anionic polyacrylamide P (AM-AA-AMPS). *Jour. of Appl. Poly. Sc*. 129(4). 1984-1991. https://doi.org/10.1002/app.38900
12. You, L., Lu, F., Li, D., Qiao, Z., & Yin, Y. (2009). Preparation and flocculation properties of cationic starch/chitosan crosslinking-copolymer., *J. Hazard Mater*. 172(1), 38-45. https://doi.org/10.1016/j.jhazmat.2009.06.120
13. Kholmuminov, A.A., & Matyakubov, B.M. (2019). Nano-Fiber Nonwoven Materials of Polymers with Surface-Active Properties. *Journal of Scientific and Engineering Research*, Vol 6(11): pp. 232-235 ISSN: 2394-2630 CODEN(USA): JSERBR www.jsaer.com
14. Perepelkin,K. E. (2005). "Principles and Methods of Modification of Fibers and Fiber Material," *Fibre, Chemistry*, Vol. 37, pp. 123-140. https://doi.org/10.1007/s10692-005-0069-6
15. Ryo, U., Yutaka, S., Hiraku, I., Munenori, S., & Takeki, M. (1991). "Shrink Resist Treatment for Wool Using Mul-tifunctional Epoxides," *Textile Research Journal*, Vol. 61, No. 2, pp. 89-93. https://doi.org/10.1177/004051759106100206
16. Jeanette, M. C., Yao, J., & Alberto, N. (2004). "DCCA Shrink Proofing of Wool Part 1: Importance of Antichlor Natio- n," *Textile Research Journal*, Vol. 74, 2004, pp. 555-560. https://doi.org/10.1177/004051750407400616
17. Jeanette, M. C., Yao, J., & John, G. P. (2005). "Combined Bleaching, Shrinkage Prevention and Biopolishing of Wool Fabrics," *Textile Research Journal*, Vol. 75, No. 2, pp. 169-1764. https://doi.org/10.1177/004051750507500215
18. Jeanette, M. C. (2007). "En-zyme—Mediated Cross Linking of Wool, Part 1: Transgluta-minase," *Textile Research Journal*, Vol. 77, No. 4, pp. 214-221. https://doi.org/10.1177/0040517507076327
19. Zhang, Y. O. (2002). "Applications of Natural Silk Protein Sericin in Biomaterials," *Biotechnology Advances*, Vol. 20, pp. 91-96. https://doi.org/10.1016/S0734-9750(02)00003-4.

SOI: 1.1/TAS DOI: 10.15863/TAS
International Scientific Journal
Theoretical & Applied Science
p-ISSN: 2308-4944 (print) **e-ISSN:** 2409-0085 (online)
Year: 2022 **Issue:** 10 **Volume:** 114
Published: 25.10.2022 http://T-Science.org

Issue Article

Denis Chemezov
Vladimir Industrial College
M.Sc.Eng., Corresponding Member of International Academy of Theoretical and Applied Sciences, Lecturer, Russian Federation
https://orcid.org/0000-0002-2747-552X
vic-science@yandex.ru

Aleksandr Popov
Vladimir Industrial College
Student, Russian Federation

Anton Ilin
Vladimir Industrial College
Student, Russian Federation

Grigoriy Lushin
Vladimir Industrial College
Student, Russian Federation

Sergey Lukashov
Vladimir State University named after Alexander & Nikolay Stoletovs
Institute of Mechanical Engineering & Automobile Transport
Student, Russian Federation

Mikhail Chebotaryov
Vladimir Industrial College
Student, Russian Federation

Ilya Yakovlev
Vladimir Industrial College
Student, Russian Federation

REFERENCE DATA OF PRESSURE DISTRIBUTION ON THE SURFACES OF AIRFOILS HAVING THE NAMES BEGINNING WITH THE LETTER M

***Abstract**: The results of the computer calculation of air flow around the airfoils having the names beginning with the letter M are presented in the article. The contours of pressure distribution on the surfaces of the airfoils at the angles of attack of 0, 15 and -15 degrees in conditions of the subsonic airplane flight speed were obtained.*

***Key words**: the airfoil, the angle of attack, pressure, the surface.*
***Language**: English*
***Citation**: Chemezov, D., et al. (2022). Reference data of pressure distribution on the surfaces of airfoils having the names beginning with the letter M. *ISJ Theoretical & Applied Science, 10 (114)*, 307-392.
Soi: http://s-o-i.org/1.1/TAS-10-114-44 ***Doi***: crossref https://dx.doi.org/10.15863/TAS.2022.10.114.44
***Scopus ASCC**: 1507.*

Introduction

Creating reference materials that determine the most accurate pressure distribution on the airfoil surfaces is an actual task of the airplane aerodynamics.

Materials and methods

The study of air flow around the airfoils was carried out in a two-dimensional formulation by means of the computer calculation in the *Comsol Multiphysics* program. The airfoils in the cross section were taken as objects of research [1-28]. In this work, the airfoils having the names beginning with the letter *M* were adopted. Air flow around the airfoils was carried out at the angles of attack (α) of 0, 15 and -15 degrees. Flight speed of the airplane in each case was subsonic. The airplane flight in the atmosphere was carried out under normal weather conditions. The geometric characteristics of the studied airfoils are presented in the Table 1. The geometric shapes of the airfoils in the cross section are presented in the Table 2.

Table 1. The geometric characteristics of the airfoils.

Airfoil name	Max. thickness	Max. camber	Leading edge radius	Trailing edge thickness
M06-13-1	12.84% at 33.2% of the chord	5.16% at 33.2% of the chord	0.982%	0.015%
M3 - HB396	9.59% at 31.0% of the chord	2.98% at 47.0% of the chord	0.4853%	0.0%
M6 (65%)	7.81% at 30.0% of the chord	1.44% at 30.0% of the chord	0.4573%	0.0%
M6 (85%)	10.21% at 30.0% of the chord	1.88% at 30.0% of the chord	0.9315%	0.0%
MA409 (original)	6.79% at 25.0% of the chord	4.31% at 40.0% of the chord	0.6961%	0.07%
MA409 (smoothed)	6.69% at 23.8% of the chord	3.33% at 49.3% of the chord	0.4323%	0.07%
Marquardt	11.53% at 20.0% of the chord	7.05% at 40.0% of the chord	1.923%	0.0%
Marsden	27.88% at 31.6% of the chord	9.61% at 34.5% of the chord	7.7426%	0.0%
MARSKE MONARCH	12.22% at 20.0% of the chord	3.38% at 15.0% of the chord	1.9108%	0.0%
MARSKE PIONEER IA	12.05% at 25.0% of the chord	2.69% at 15.0% of the chord	1.7183%	0.0%
MARSKE PIONEER IID ROOT	12.06% at 30.0% of the chord	2.76% at 15.0% of the chord	1.5706%	0.0%
MARSKE PIONEER IID TIP	10.19% at 20.0% of the chord	2.82% at 15.0% of the chord	1.4576%	0.0%
MARSKE XM-1D	13.99% at 24.9% of the chord	3.03% at 24.9% of the chord	2.357%	0.0%
Martin M 1	8.8% at 30.0% of the chord	0.0% at 0.0% of the chord	0.8135%	0.0%
MATWIES6	6.0% at 20.0% of the chord	8.3% at 40.0% of the chord	2.7985%	0.3%
MB253515	14.96% at 35.0% of the chord	2.43% at 37.5% of the chord	1.42%	0.0%
MB253515 15,0% smoothed	14.96% at 35.0% of the chord	2.43% at 37.5% of the chord	1.42%	0.0%
MB303515	14.96% at 35.0% of the chord	2.98% at 35.0% of the chord	1.65%	0.38%
mb7136	7.04% at 26.1% of the chord	1.22% at 38.4% of the chord	0.4918%	0.048%
mb714	7.0% at 26.1% of the chord	1.45% at 38.4% of the chord	0.5224%	0.0477%

mc813	8.0% at 25.8% of the chord	1.35% at 39.4% of the chord	0.4826%	0.0482%
md8135	8.01% at 28.8% of the chord	1.37% at 38.5% of the chord	0.4021%	0.047%
md814	8.0% at 26.3% of the chord	1.45% at 38.5% of the chord	0.4461%	0.0464%
MEG 59	10.95% at 30.0% of the chord	4.69% at 50.0% of the chord	1.1117%	0.0%
MEG 62-63137	13.68% at 30.0% of the chord	5.86% at 50.0% of the chord	1.5737%	0.0%
MEG 64	7.91% at 40.0% of the chord	2.55% at 20.0% of the chord	0.5884%	0.0%
MEG 66	9.71% at 40.0% of the chord	3.11% at 40.0% of the chord	0.5686%	0.0%
MEG 69-012	11.92% at 40.0% of the chord	0.05% at 70.0% of the chord	1.5272%	0.0%
MEG-197	10.0% at 30.0% of the chord	4.41% at 50.0% of the chord	0.9064%	0.0%
MG 08	8.67% at 30.2% of the chord	2.0% at 35.2% of the chord	0.5949%	0.0%
MG05	9.0% at 26.7% of the chord	0.0% at 0.0% of the chord	0.4237%	0.0%
MG06	7.37% at 22.4% of the chord	1.94% at 31.8% of the chord	0.4307%	0.0%
MH 102	17.0% at 27.7% of the chord	2.9% at 37.6% of the chord	2.006%	0.0%
MH 104	15.24% at 26.4% of the chord	1.92% at 31.0% of the chord	1.2786%	0.0%
MH 106	13.08% at 27.3% of the chord	0.92% at 27.3% of the chord	1.0054%	0.0%
MH 108	11.97% at 22.8% of the chord	1.05% at 18.7% of the chord	1.0607%	0.0%
MH 110	10.02% at 23.9% of the chord	1.07% at 15.8% of the chord	0.7333%	0.0%
MH 112	16.23% at 26.9% of the chord	7.16% at 48.8% of the chord	2.8472%	0.0%
MH 113	14.63% at 27.5% of the chord	6.86% at 49.4% of the chord	1.7997%	0.0%
MH 114	13.04% at 28.1% of the chord	6.51% at 50.0% of the chord	1.1733%	0.0%
MH 115	11.07% at 29.8% of the chord	5.51% at 46.0% of the chord	1.1499%	0.0%
MH 116	9.85% at 32.4% of the chord	4.03% at 48.5% of the chord	0.7086%	0.0%
MH 117	9.81% at 29.1% of the chord	2.69% at 44.6% of the chord	0.7948%	0.0%
MH 18	11.12% at 36.8% of the chord	2.77% at 36.8% of the chord	0.6678%	0.0%
MH 18 11,14%	11.12% at 36.8% of the chord	2.77% at 36.8% of the chord	0.6678%	0.0%
MH 18B	11.73% at 39.6% of the chord	1.95% at 39.6% of the chord	0.7392%	0.0%
MH 20	9.01% at 32.2% of the chord	2.0% at 32.3% of the chord	0.6162%	0.0%
MH 20 9,02%	9.01% at 32.2% of the chord	2.0% at 37.3% of the chord	0.6162%	0.0%
MH 22	7.2% at 27.0% of the chord	1.77% at 37.0% of the chord	0.5245%	0.0%

MH 22 7,21%	7.2% at 27.0% of the chord	1.77% at 37.0% of the chord	0.5245%	0.0%
MH 22-Mod,3	8.31% at 23.7% of the chord	1.6% at 27.9% of the chord	0.629%	0.0%
MH 23	8.0% at 37.5% of the chord	1.24% at 37.5% of the chord	0.5601%	0.0%
MH 24	9.0% at 37.2% of the chord	1.27% at 37.2% of the chord	0.5988%	0.0%
MH 25	9.97% at 42.2% of the chord	1.42% at 37.1% of the chord	0.6179%	0.0%
MH 26	10.98% at 42.3% of the chord	1.47% at 42.3% of the chord	0.6642%	0.0%
MH 27	11.98% at 42.4% of the chord	1.46% at 42.4% of the chord	0.7217%	0.0%
MH 30	7.82% at 31.0% of the chord	1.71% at 46.4% of the chord	0.3675%	0.0%
MH 31	7.98% at 26.9% of the chord	1.16% at 36.7% of the chord	0.4065%	0.0%
MH 32	8.71% at 30.2% of the chord	2.36% at 40.4% of the chord	0.5978%	0.0%
MH 33	7.25% at 26.9% of the chord	1.09% at 41.8% of the chord	0.2066%	0.0%
MH 34	8.5% at 31.7% of the chord	1.12% at 41.8% of the chord	0.2864%	0.0%
MH 42	9.02% at 30.9% of the chord	2.09% at 35.9% of the chord	0.4615%	0.0%
MH 42 8,94%	8.91% at 31.3% of the chord	1.84% at 36.3% of the chord	0.6285%	0.0%
MH 43	8.48% at 31.4% of the chord	1.72% at 36.4% of the chord	0.4127%	0.0%
MH 43 8,5%	8.48% at 31.4% of the chord	1.72% at 36.4% of the chord	0.6073%	0.0%
MH 44	9.66% at 27.1% of the chord	1.48% at 36.9% of the chord	0.7889%	0.0%
MH 45	9.84% at 26.9% of the chord	1.64% at 36.6% of the chord	0.6074%	0.0%
MH 46	11.34% at 27.2% of the chord	1.86% at 37.0% of the chord	1.0004%	0.0%
MH 49	10.49% at 28.8% of the chord	0.7% at 33.6% of the chord	0.7512%	0.0%
MH 60	10.07% at 26.9% of the chord	1.76% at 36.6% of the chord	0.5939%	0.0%
MH 60 10,08%	10.07% at 26.9% of the chord	1.76% at 36.6% of the chord	0.7573%	0.0%
MH 61	10.26% at 27.6% of the chord	1.47% at 37.3% of the chord	0.5093%	0.0%
MH 61 10,28%	10.26% at 27.6% of the chord	1.47% at 37.3% of the chord	0.6511%	0.0%
MH 62	9.29% at 26.9% of the chord	1.59% at 36.6% of the chord	0.5424%	0.0%
MH 62 9,3%	9.29% at 26.9% of the chord	1.59% at 36.6% of the chord	0.691%	0.0%
MH 64	8.6% at 26.9% of the chord	1.44% at 36.7% of the chord	0.4691%	0.0%
MH 78	14.43% at 22.1% of the chord	2.63% at 17.9% of the chord	2.2038%	0.0%
MH 91	15.0% at 27.2% of the chord	1.62% at 14.9% of the chord	1.5419%	0.0%

MH 92	15.5% at 27.4% of the chord	1.62% at 15.0% of the chord	1.6058%	0.0%
MH 93	15.99% at 27.5% of the chord	1.61% at 15.1% of the chord	2.2627%	0.0%
MH32 (8,71%)	8.71% at 30.2% of the chord	2.36% at 40.4% of the chord	0.4025%	0.0%
MH45	9.84% at 26.9% of the chord	1.64% at 36.6% of the chord	0.6074%	0.0%
mhmi2	9.31% at 23.7% of the chord	2.4% at 27.2% of the chord	0.8483%	0.0001%
mhmi3	9.59% at 25.1% of the chord	2.03% at 30.5% of the chord	0.9763%	0.0005%
MILEY M06-13-128	12.84% at 33.2% of the chord	5.16% at 33.2% of the chord	0.6521%	0.0%
MIRAGE	12.16% at 30.0% of the chord	2.97% at 30.0% of the chord	1.1514%	0.4%
Miser	9.0% at 30.0% of the chord	6.0% at 40.0% of the chord	0.8044%	0.0%
Misto 50-50 S1046-S8035	15.48% at 30.8% of the chord	0.0% at 0.0% of the chord	1.4846%	0.0%
mjp711f-3	7.0% at 28.1% of the chord	1.33% at 100.0% of the chord	0.3588%	0.0421%
mjp712	7.0% at 28.1% of the chord	1.19% at 31.7% of the chord	0.3571%	0.0427%
mjz 1211	12.0% at 28.6% of the chord	1.11% at 25.4% of the chord	1.215%	0.0729%
MM 007	7.0% at 28.3% of the chord	0.06% at 0.0% of the chord	0.3153%	0.0%
MM 008	8.0% at 28.3% of the chord	0.01% at 100.0% of the chord	0.3975%	0.0%
MM 009	9.01% at 27.4% of the chord	0.01% at 100.0% of the chord	0.5503%	0.0%
MM 010	10.0% at 27.5% of the chord	0.01% at 100.0% of the chord	0.6236%	0.0%
MM 012	12.0% at 29.5% of the chord	0.09% at 0.0% of the chord	0.743%	0.0%
MM 1,75-10	9.9% at 30.3% of the chord	1.75% at 30.3% of the chord	0.1442%	0.0%
MM 1,75-9	9.0% at 30.3% of the chord	1.75% at 30.3% of the chord	0.1276%	0.0%
MM 100	8.76% at 28.4% of the chord	2.12% at 39.8% of the chord	0.4966%	0.497%
MM 1010a	10.07% at 32.6% of the chord	0.99% at 40.8% of the chord	0.5668%	0.0%
MM 1010b	10.0% at 34.3% of the chord	1.0% at 37.5% of the chord	0.4879%	0.0%
MM 1100	11.0% at 34.5% of the chord	2.01% at 40.6% of the chord	0.3457%	0.0%
MM 11-29	11.0% at 28.3% of the chord	0.1% at 0.0% of the chord	0.5832%	0.0%
MM 1200	12.0% at 34.5% of the chord	2.01% at 40.6% of the chord	0.4572%	0.0%
MM 1300	13.0% at 35.1% of the chord	2.5% at 43.1% of the chord	0.8675%	0.0%
MM 1407	6.99% at 28.5% of the chord	1.45% at 38.0% of the chord	0.345%	0.0%
MM 1608	7.97% at 29.7% of the chord	1.61% at 37.6% of the chord	0.4272%	0.0%

MM 1609	9.8% at 29.4% of the chord	1.67% at 29.4% of the chord	1.0429%	0.0003%
MM 1710	10.74% at 28.1% of the chord	1.67% at 35.2% of the chord	0.9755%	0.0001%
MM 1711	11.12% at 30.5% of the chord	1.72% at 32.2% of the chord	0.9869%	0.0005%
MM 1809	9.2% at 27.7% of the chord	1.8% at 34.9% of the chord	0.9012%	0.0004%
MM 1810	10.35% at 30.1% of the chord	1.8% at 36.7% of the chord	0.6071%	0.5%
MM 1811b	11.0% at 30.3% of the chord	1.79% at 35.2% of the chord	0.671%	0.0232%
MM 1910	10.35% at 33.3% of the chord	1.94% at 36.5% of the chord	0.5014%	0.0%
MM 1995	9.6% at 30.3% of the chord	1.93% at 36.8% of the chord	0.4921%	0.0003%
MM 200	9.44% at 28.2% of the chord	2.14% at 40.2% of the chord	0.7986%	0.0%
MM 2-10 a	9.91% at 30.0% of the chord	2.0% at 30.0% of the chord	0.159%	0.0%
MM 2-12	11.89% at 30.0% of the chord	2.0% at 30.0% of the chord	0.2116%	0.0%
MM 2-9	9.01% at 30.0% of the chord	2.0% at 30.0% of the chord	0.1405%	0.0%
MM 300	9.8% at 30.2% of the chord	1.7% at 36.7% of the chord	0.4676%	0.0%
MM 400	10.2% at 28.6% of the chord	2.2% at 40.5% of the chord	0.4601%	0.0%
Mosca 317	10.2% at 30.0% of the chord	5.63% at 10.0% of the chord	1.7382%	0.0%
MRC-16	13.9% at 34.5% of the chord	3.12% at 38.5% of the chord	1.1618%	0.0745%
MRC-20	15.58% at 38.8% of the chord	2.93% at 46.7% of the chord	1.3632%	0.05%
ms1,9-8,7	8.78% at 30.0% of the chord	1.97% at 40.0% of the chord	0.4048%	0.0%
ms2-9,5	9.5% at 30.0% of the chord	2.02% at 40.0% of the chord	0.4745%	0.0%
MS3,3-11GP	11.0% at 30.7% of the chord	3.28% at 38.2% of the chord	0.6348%	0.0%
MS3,3-11GPT	11.0% at 30.7% of the chord	3.28% at 32.6% of the chord	0.5725%	0.0%
MS3,3-15GP	15.0% at 30.7% of the chord	3.28% at 38.2% of the chord	1.2257%	0.0%
msa812	8.0% at 26.4% of the chord	1.22% at 33.8% of the chord	0.5487%	0.0996%
MT172	10.0% at 33.1% of the chord	3.03% at 39.7% of the chord	0.3082%	0.277%
MT722	26.27% at 30.0% of the chord	7.97% at 40.0% of the chord	2.6492%	0.728%
MVA-101M	7.9% at 30.0% of the chord	3.95% at 30.0% of the chord	0.63%	0.0%
MVA-123	5.3% at 15.0% of the chord	6.55% at 40.0% of the chord	0.84%	0.3%
MVA-123M	5.3% at 15.0% of the chord	6.55% at 40.0% of the chord	0.84%	0.3%
MVA-173	7.7% at 20.0% of the chord	6.3% at 40.0% of the chord	0.7734%	0.2%

MVA-227	14.6% at 25.0% of the chord	11.65% at 50.0% of the chord	1.7205%	0.3%
MVA-301	9.8% at 25.0% of the chord	10.05% at 30.0% of the chord	1.3932%	0.3%
MVA30175	7.4% at 30.0% of the chord	6.95% at 40.0% of the chord	0.8434%	0.2%
MVA-301M	8.7% at 20.0% of the chord	7.15% at 30.0% of the chord	1.1769%	0.2%
MVA-342	5.5% at 25.0% of the chord	6.65% at 40.0% of the chord	0.8799%	0.3%
MVA-439	7.9% at 30.0% of the chord	5.7% at 40.0% of the chord	0.7004%	0.0%
mve8.516	8.5% at 26.8% of the chord	1.6% at 36.5% of the chord	0.5392%	0.0856%
mve8516 f 3	8.5% at 26.8% of the chord	1.6% at 36.5% of the chord	0.5392%	0.0861%
MZ 5411	11.25% at 35.0% of the chord	5.63% at 35.0% of the chord	0.8824%	0.2%
MZ 6409	9.1% at 25.0% of the chord	6.75% at 35.0% of the chord	0.8824%	0.2%

Note:
M3 - HB396 (Per HLG–F3J);
Marquardt (J. Marquardt (USA));
Martin M 1 (G.L. Martin (USA));
mb7136 (F5B fast airfoils edumolfino@ciudad.com.ar);
mb714 (F5B fast airfoils edumolfino@ciudad.com.ar);
mc813 (F5B fast airfoils edumolfino@ciudad.com.ar);
md8135 (F5B fast airfoils edumolfino@ciudad.com.ar);
md814 (F5B fast airfoils edumolfino@ciudad.com.ar);
MEG 59 (E. Gallazzi (Italy));
MEG 62-63137 (E. Gallazzi (Italy));
MEG 64 (E. Gallazzi (Italy));
MEG 66 (E. Gallazzi (Italy));
MEG 69-012 (E. Gallazzi (Italy));
MG 08 (Marcel Guwang volet a 30%);
MG05 (Marcel Guwang);
MG06 (Marcel Guwang volets a 30%);
MH 22-Mod,3 (Elaborato per Delta 400);
mhmi2 (By Matteo Gallizia – Italy);
mhmi3 (By Matteo Gallizia – Italy);
mjp711f-3 (Flying Wing airfoils flap 75% - 3 edumol);
mjp712 (edumolfino@ciudad.com.ar);
mjz 1211 (Flying Wing airfoils edumolfino@ciudad.co);
MM 007 (by Mario Marzocchi – Italy);
MM 009 (by Mario Marzocchi – Italy);
MM 010 (by Mario Marzocchi – Italy);
MM 012 (by Mario Marzocchi – Italy);
MM 1,75-10 (by Mario Marzocchi – Italy);
MM 1,75-9 (by Mario Marzocchi – Italy);
MM 100 (by Mario Marzocchi – Italy);
MM 1010b (by Mario Marzocchi – Italy);
MM 1100 (by Mario Marzocchi – Italy);
MM 11-29 (by Mario Marzocchi – Italy);
MM 1200 (by Mario Marzocchi – Italy);
MM 1300 (by Mario Marzocchi – Italy);
MM 1407 (by Mario Marzocchi – Italy);
MM 1608 (by Mario Marzocchi – Italy);

MM 1710 (by Mario Marzocchi – Italy);
MM 1809 (by Mario Marzocchi – Italy);
MM 1811b (by Mario Marzocchi – Italy);
MM 1910 (by Mario Marzocchi – Italy);
MM 1995 (by Mario Marzocchi – Italy);
MM 200 (by Mario Marzocchi – Italy);
MM 2-10 a (by Mario Marzocchi);
MM 2-12 (by Mario Marzocchi);
MM 2-9 (by Mario Marzocchi – Italy);
MM 300 (by Mario Marzocchi – Italy);
MM 400 (by Mario Marzocchi – Italy);
Mosca 317 (TsAGI (URSS));
ms1,9-8,7 (f3i, f3b matthieu.scherrer@supaero.fr);
ms2-9,5 (f3i, f3b root matthieu.scherrer@supaero.fr);
MS3,3-11GP (thermaling, scale, matthieu.scherrer@su);
MS3,3-11GPT (for tip; thermaling, scale matthieu.sc);
MS3,3-15GP (root of scale sailplane matthieu.scherr);
msa812 (F5B fast airfoils edumolfino@ciudad.com.ar);
mve8.516 (F3B airfoils edumolfino@ciudad.com.ar);
mve8516 f 3 (F3B airfoils flap 80% +3 edumolfino@ciudad.com.ar);
MZ 5411 (F. Zaic (USA));
MZ 6409 (F. Zaic (USA)).

Table 2. The geometric shapes of the airfoils in the cross section.

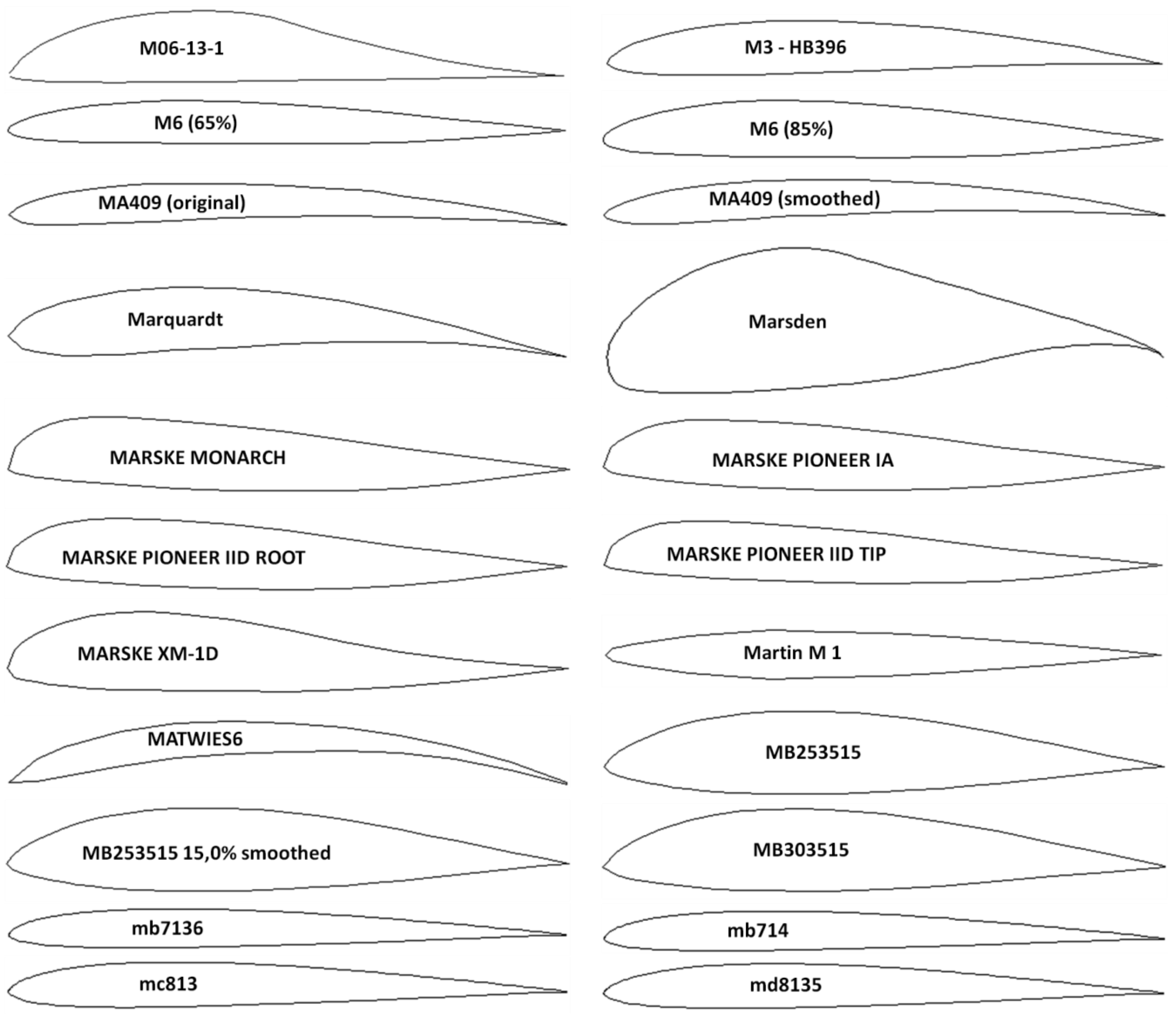

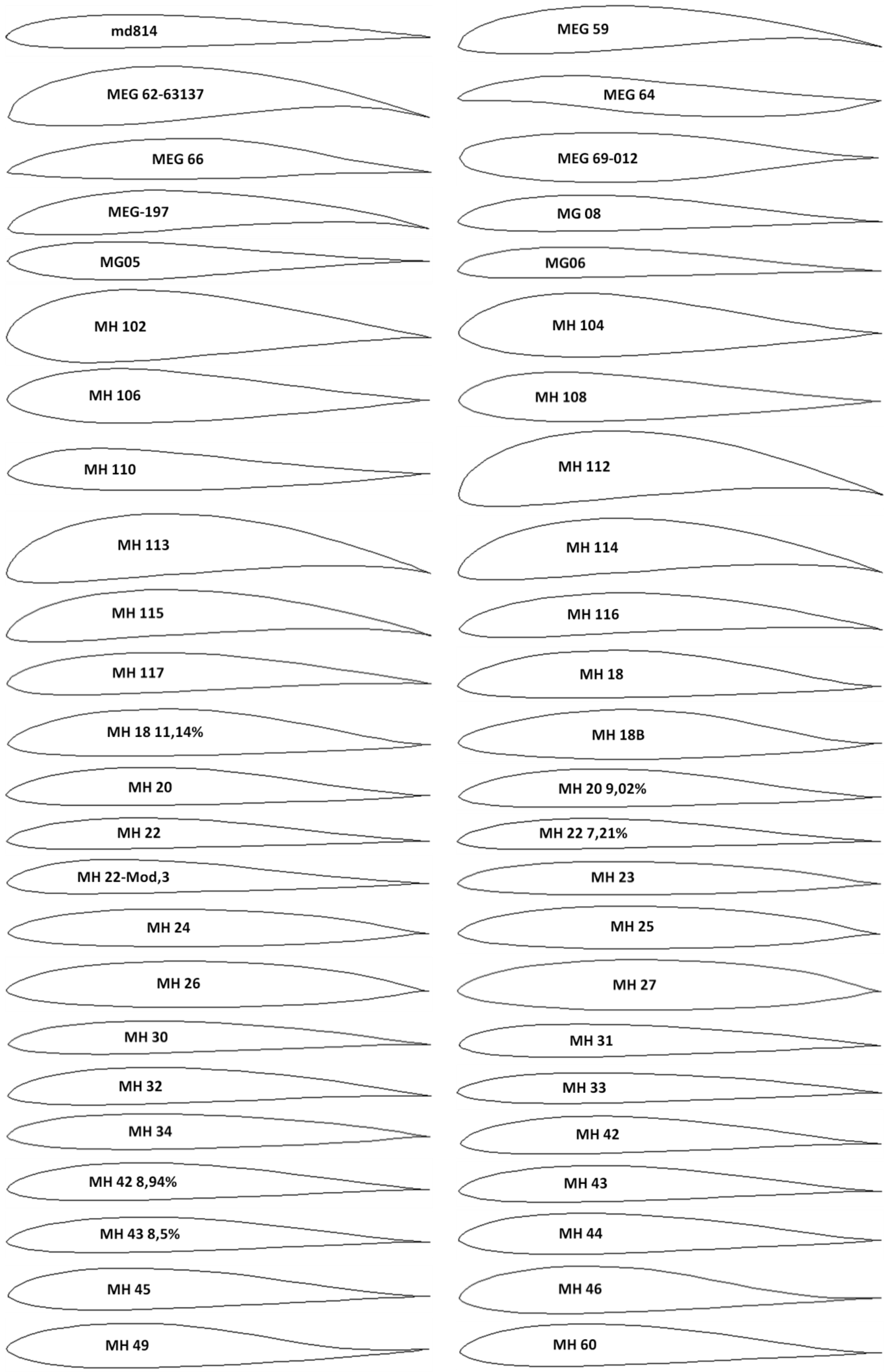

md814
MEG 59
MEG 62-63137
MEG 64
MEG 66
MEG 69-012
MEG-197
MG 08
MG05
MG06
MH 102
MH 104
MH 106
MH 108
MH 110
MH 112
MH 113
MH 114
MH 115
MH 116
MH 117
MH 18
MH 18 11,14%
MH 18B
MH 20
MH 20 9,02%
MH 22
MH 22 7,21%
MH 22-Mod,3
MH 23
MH 24
MH 25
MH 26
MH 27
MH 30
MH 31
MH 32
MH 33
MH 34
MH 42
MH 42 8,94%
MH 43
MH 43 8,5%
MH 44
MH 45
MH 46
MH 49
MH 60

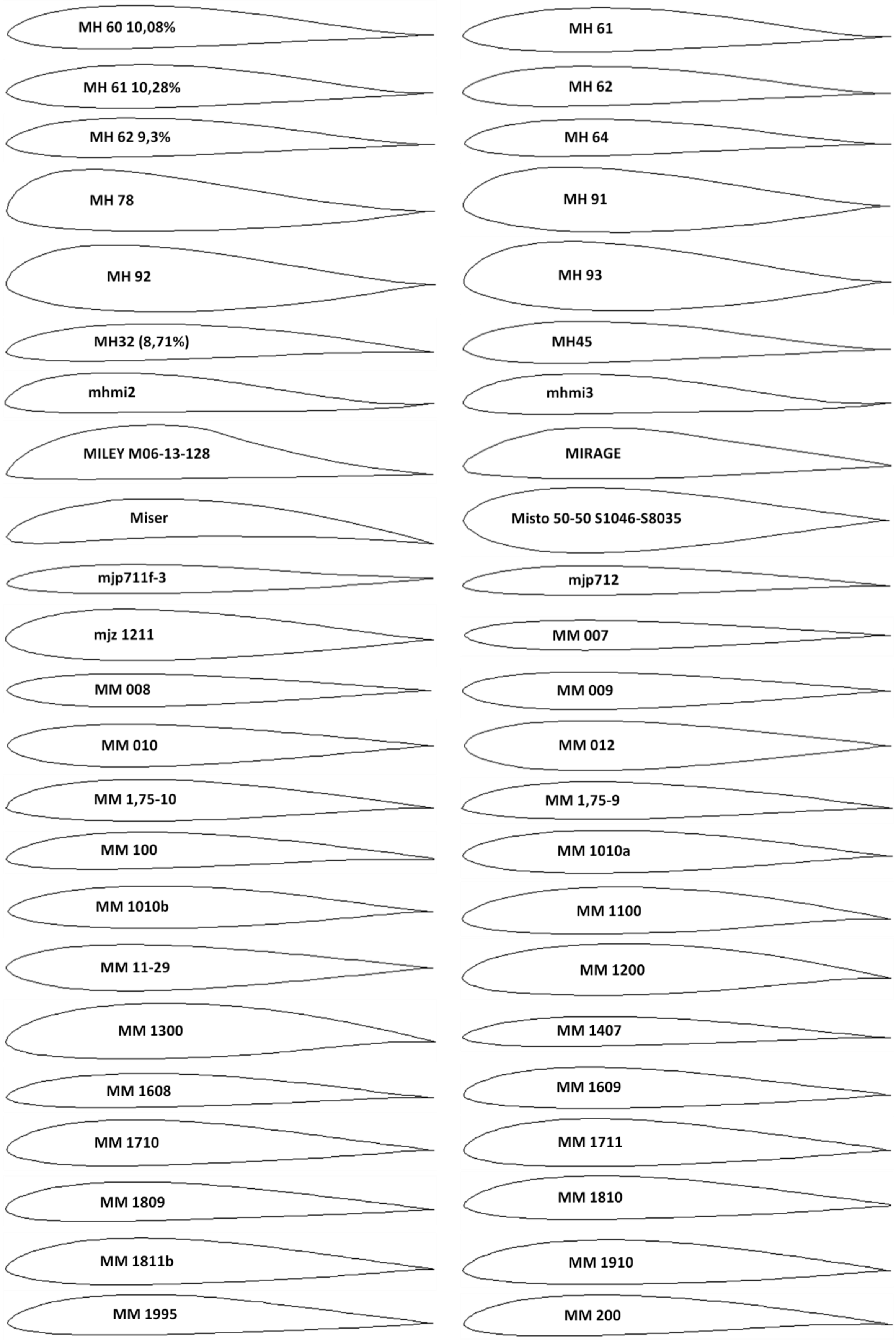

MH 60 10,08%
MH 61
MH 61 10,28%
MH 62
MH 62 9,3%
MH 64
MH 78
MH 91
MH 92
MH 93
MH32 (8,71%)
MH45
mhmi2
mhmi3
MILEY M06-13-128
MIRAGE
Miser
Misto 50-50 S1046-S8035
mjp711f-3
mjp712
mjz 1211
MM 007
MM 008
MM 009
MM 010
MM 012
MM 1,75-10
MM 1,75-9
MM 100
MM 1010a
MM 1010b
MM 1100
MM 11-29
MM 1200
MM 1300
MM 1407
MM 1608
MM 1609
MM 1710
MM 1711
MM 1809
MM 1810
MM 1811b
MM 1910
MM 1995
MM 200

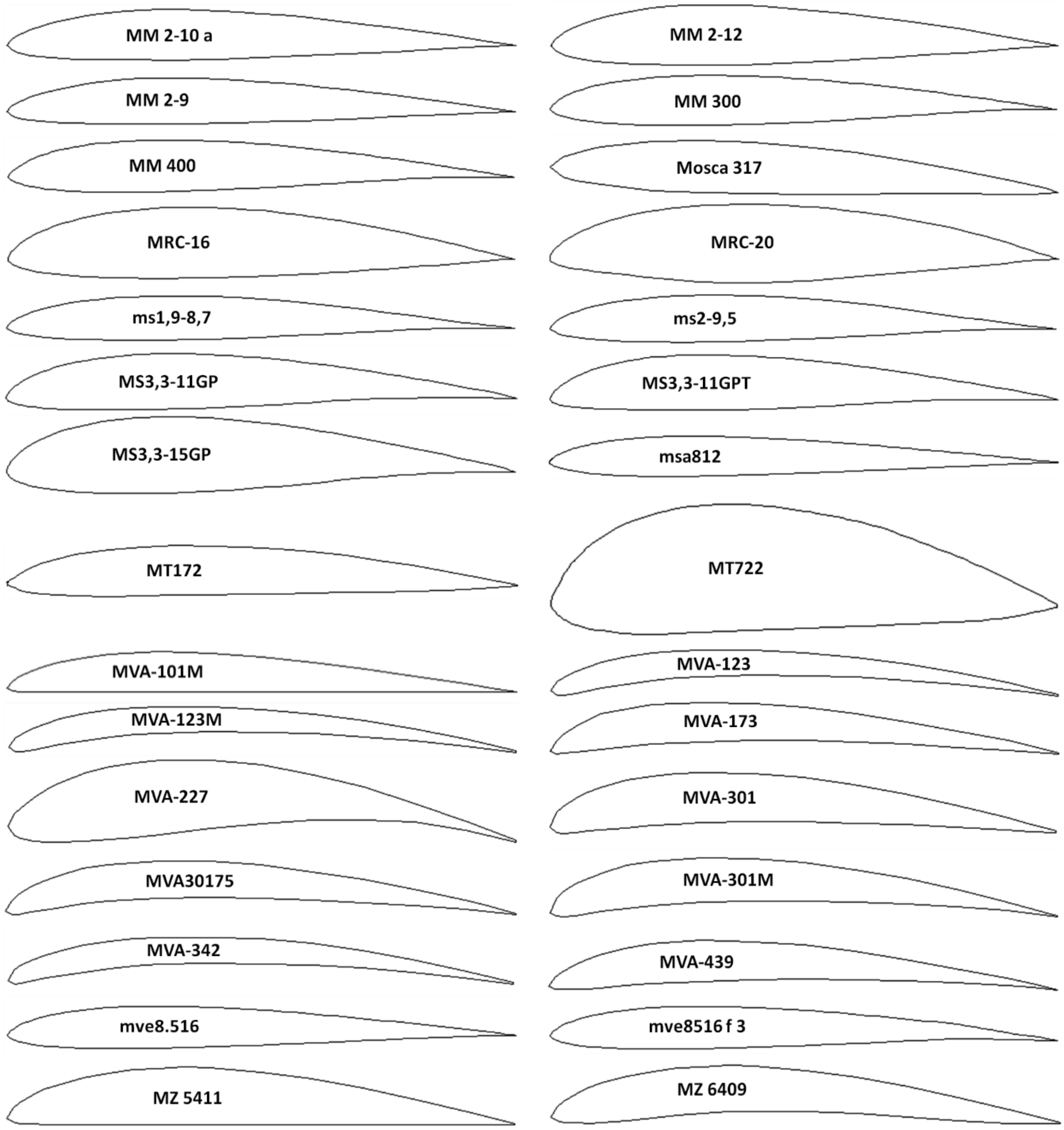

Results and discussion

The calculated pressure contours on the surfaces of the airfoils at the different angles of attack are presented in the Figs. 1-146. The calculated values on the scale can be represented as the basic values when comparing the pressure drop under conditions of changing the angle of attack of the airfoils.

146 airfoils of the airplane wings were considered. All airfoils are asymmetrical, with the exception of the Martin M 1, MG05 and Misto 50-50 S1046-S8035, which are symmetrical.

Aerodynamic characteristics depend on the geometry of the airfoil of the airplane wing. The maximum thickness along the chord is observed for the Marsden (27.88%), the minimum thickness along the chord is observed for the MVA-123 (5.3%) of the considered airfoils. The curved airfoils potentially have better aerodynamic characteristics. The camber of the MVA-227 airfoil is 11.65% relative to the chord length, which is the highest ratio among all the studied airfoils. The value of the radius of the leading edge of the airfoil affects the drag, i.e. the flight speed of the airplane. The smallest and largest leading edge radii of 0.1276% and 7.7426% were determined for the MM 1.75-9 and Marsden airfoils, respectively. The trailing edge thickness for the most airfoils is 0%. The maximum thickness of the trailing edge (0.728%) was identified for the MT722 airfoil.

Let us consider in detail the change in pressure on the surfaces of several proposed airfoils under conditions of changing the angle of attack: MARSKE MONARCH, Martin M 1, MATWIES6, MEG 64, MH 27, MILEY M06-13-128, MT722 and MVA-227.

The MARSKE MONARCH airfoil is characterized by a twofold increase in the drag coefficient during the airplane descent, compared with the airplane climb. A small bulge on the upper surface of the airfoil, formed at the place of thickening, leads to the formation of negative pressure.

The streamlined geometric shape of the Martin M 1 airfoil with a thickening in the middle ensures the formation of uniform negative pressure of the small value on the upper and lower surfaces in conditions of horizontal flight of the airplane. During maneuvers, the airplane wing is subjected to almost the same pressure values on the upper and lower surfaces, depending on the angle of attack.

The concave lower surface of the MATWIES6 airfoil forms the area of positive pressure during horizontal flight of the airplane. During the airplane climb, the camber of the airfoil increases the lifting force of the wing, and during the airplane descent, the pressure difference on the surfaces becomes minimal.

The MEG 64 airfoil, due to its specific geometric shape in the cross section, provides the formation of variable positive and negative pressures on edges and surfaces at different angles of attack. The action of pressures of the small values on this airfoil is noted.

The barrel shape of the MH 27 airfoil, like the Martin M 1 airfoil, ensures the formation of low negative pressure on the surfaces at the angle of attack of 0 degrees. Maximum pressure is concentrated on the leading edge and part of the upper or lower surfaces mating with it during maneuvers.

The MILEY M06-13-128 airfoil, at the angle of attack of 15 degrees, experiences the greater drag than at the angle of attack of -15 degrees. Maximum negative pressure on the airfoil occurs during the airplane climb.

The MT722 airfoil is characterized by increasing the negative pressure value by two times on the leading edge during the airplane descent in the atmosphere. The low aerodynamic characteristics of the airplane wing are determined by the small pressure difference on the upper and lower surfaces.

Based on the calculated pressure contours obtained on the MVA-227 airfoil, the occurrence of the large lifting force due to the significant pressure difference on the wing surfaces is confirmed.

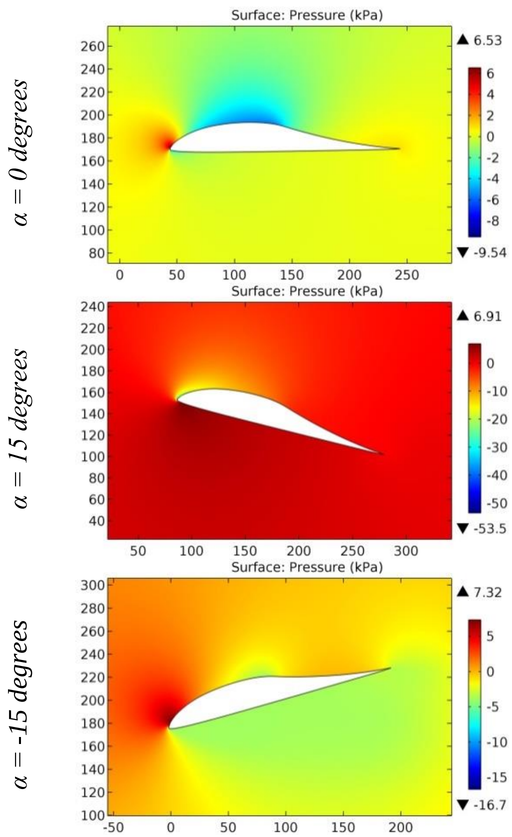

Figure 1. The pressure contours on the surfaces of the M06-13-1 airfoil.

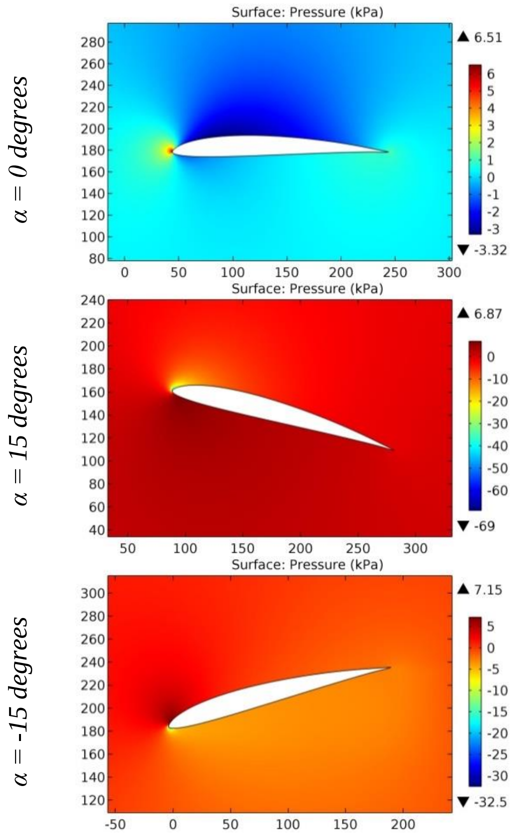

Figure 2. The pressure contours on the surfaces of the M3 - HB396 airfoil.

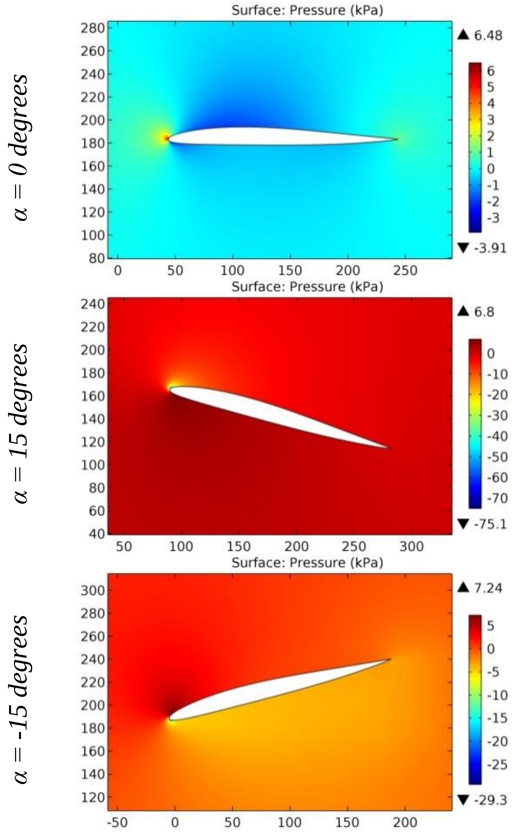

Figure 3. The pressure contours on the surfaces of the M6 (65%) airfoil.

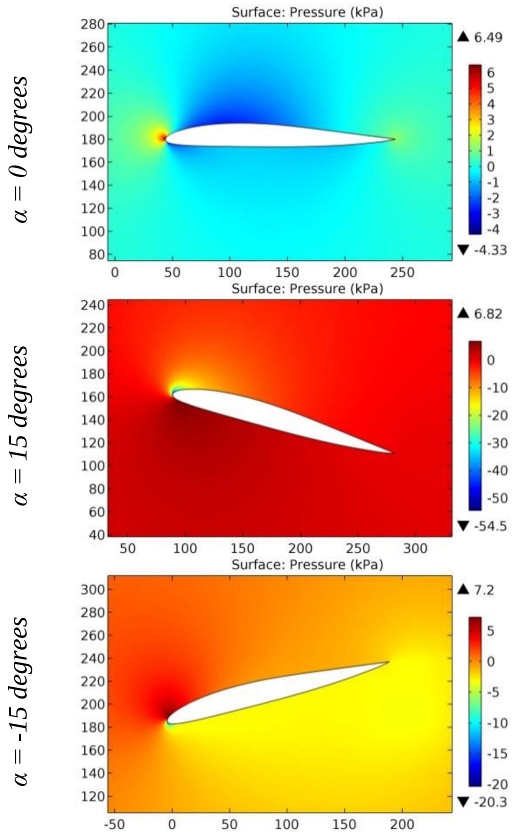

Figure 4. The pressure contours on the surfaces of the M6 (85%) airfoil.

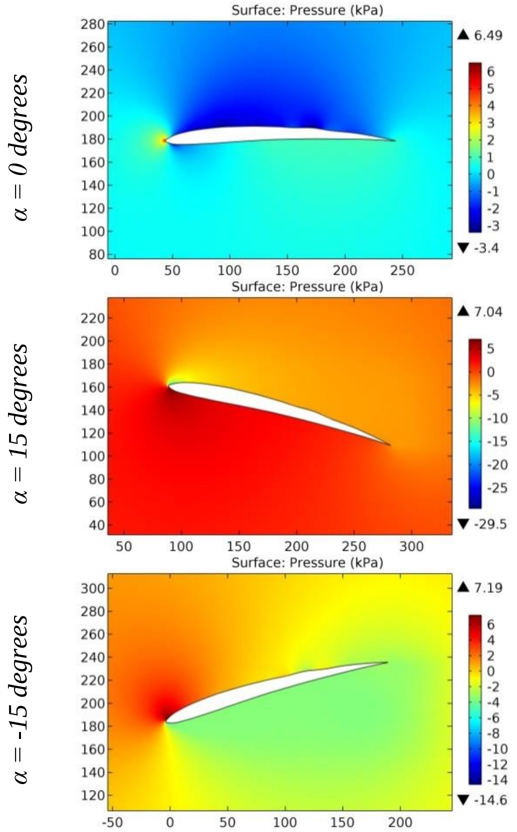

Figure 5. The pressure contours on the surfaces of the MA409 (original) airfoil.

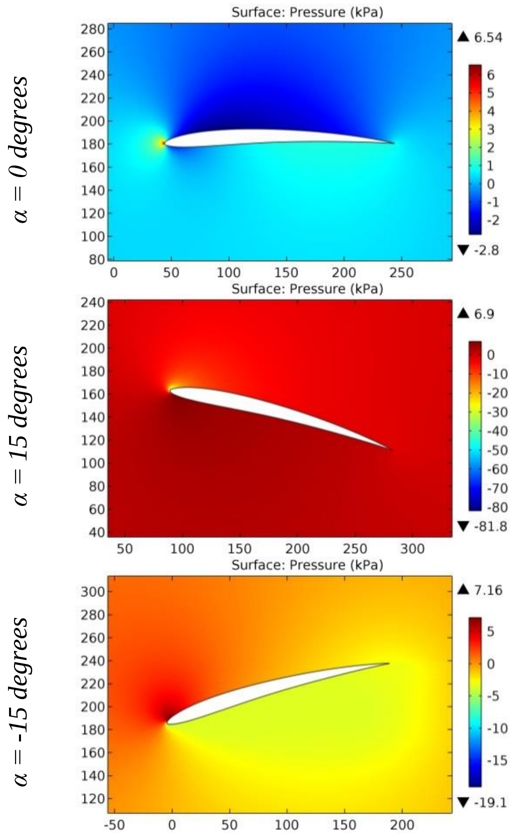

Figure 6. The pressure contours on the surfaces of the MA409 (smoothed) airfoil.

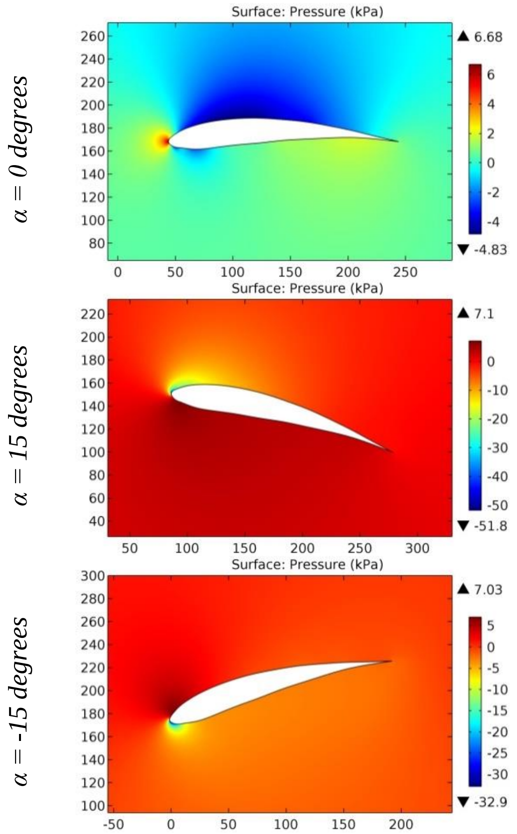

Figure 7. The pressure contours on the surfaces of the Marquardt airfoil.

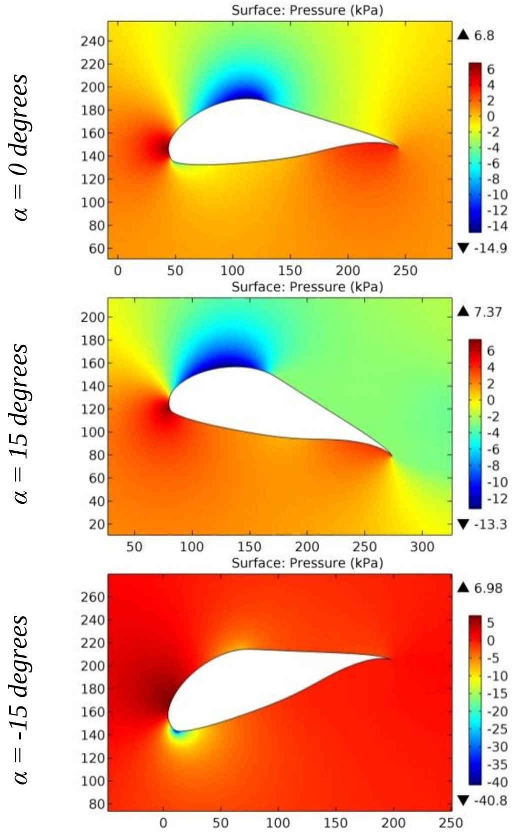

Figure 8. The pressure contours on the surfaces of the Marsden airfoil.

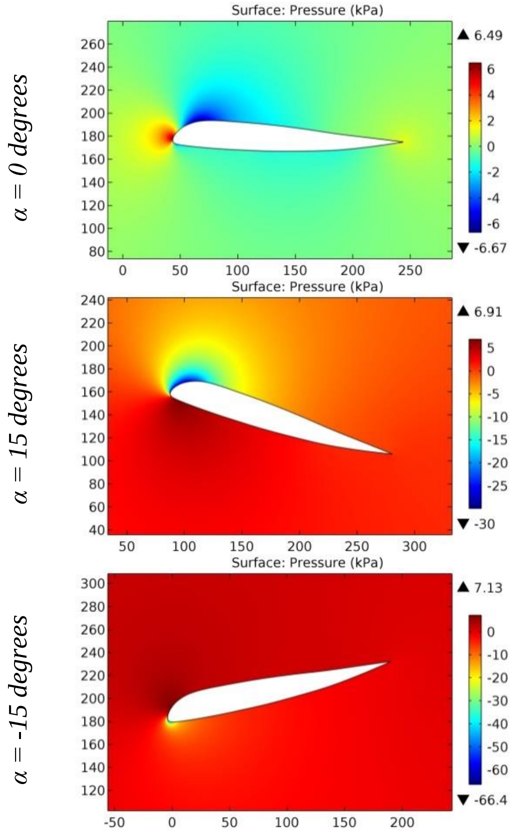

Figure 9. The pressure contours on the surfaces of the MARSKE MONARCH airfoil.

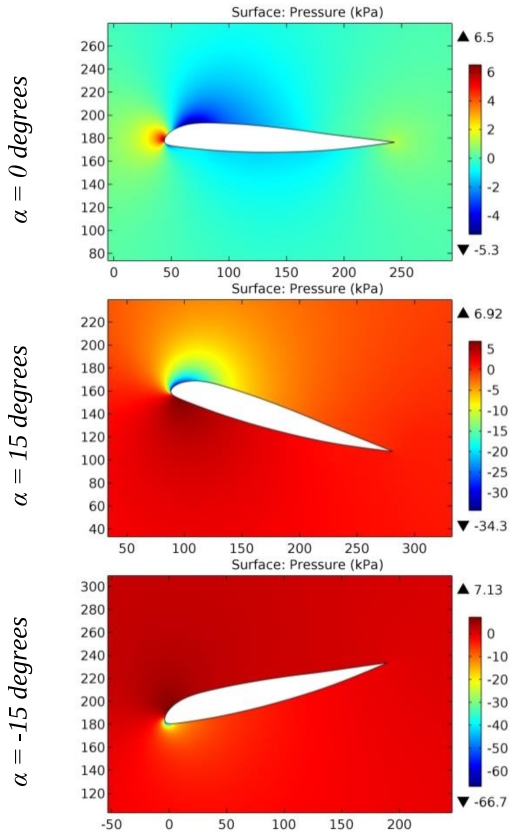

Figure 10. The pressure contours on the surfaces of the MARSKE PIONEER IA airfoil.

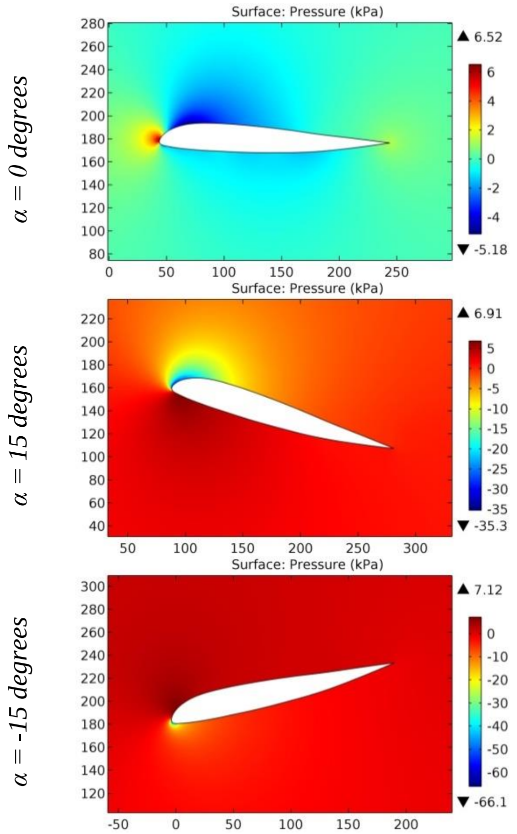

Figure 11. The pressure contours on the surfaces of the MARSKE PIONEER IID ROOT airfoil.

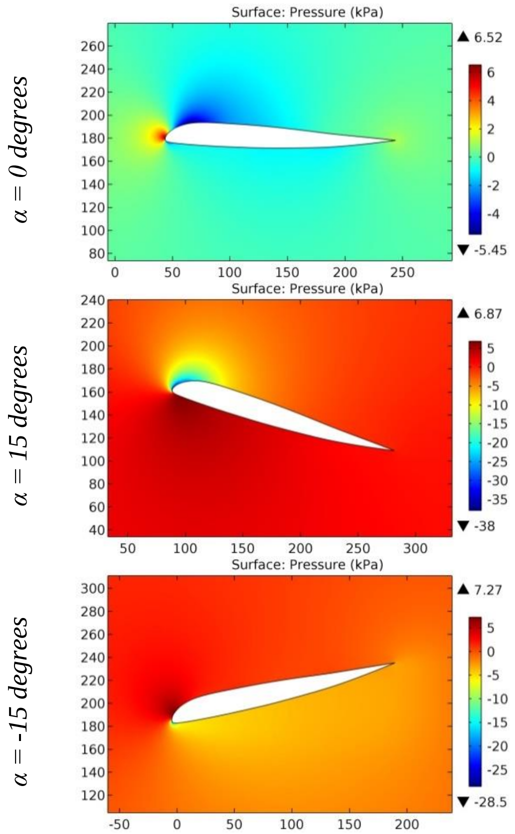

Figure 12. The pressure contours on the surfaces of the MARSKE PIONEER IID TIP airfoil.

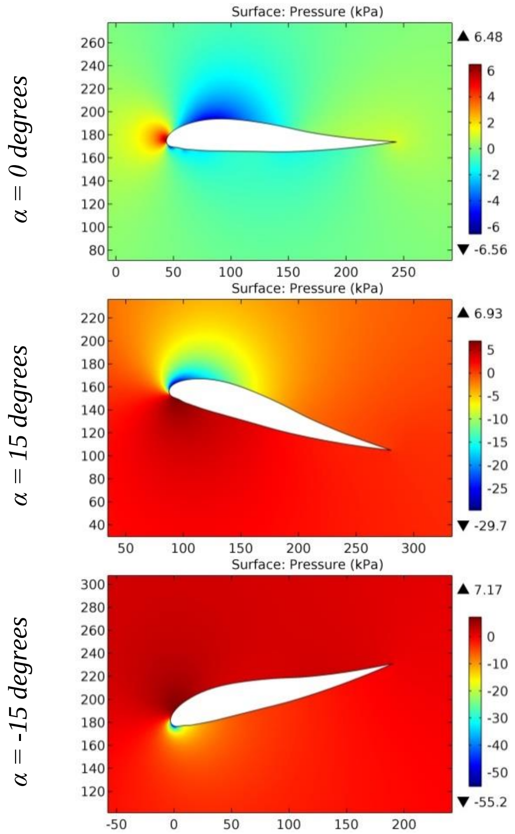

Figure 13. The pressure contours on the surfaces of the MARSKE XM-1D airfoil.

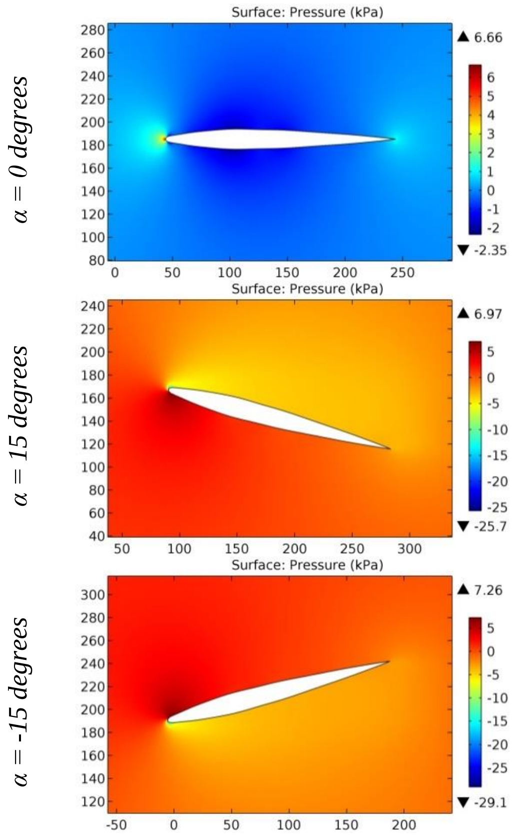

Figure 14. The pressure contours on the surfaces of the Martin M 1 airfoil.

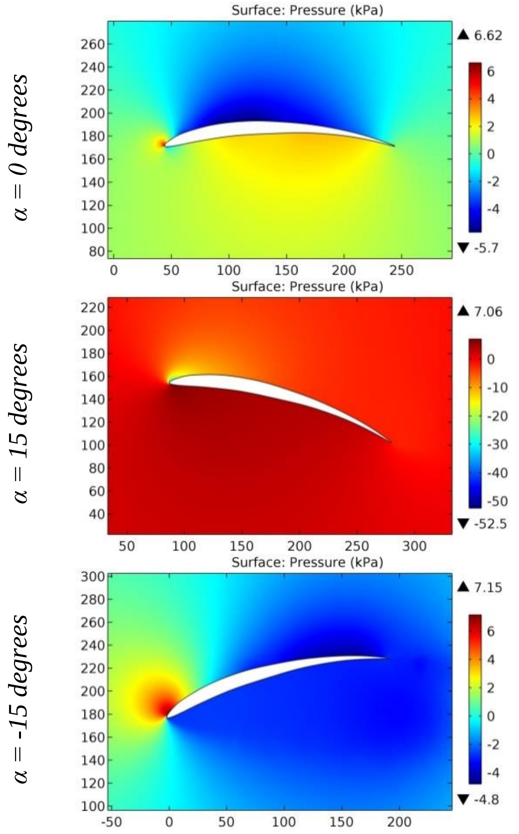

Figure 15. The pressure contours on the surfaces of the MATWIES6 airfoil.

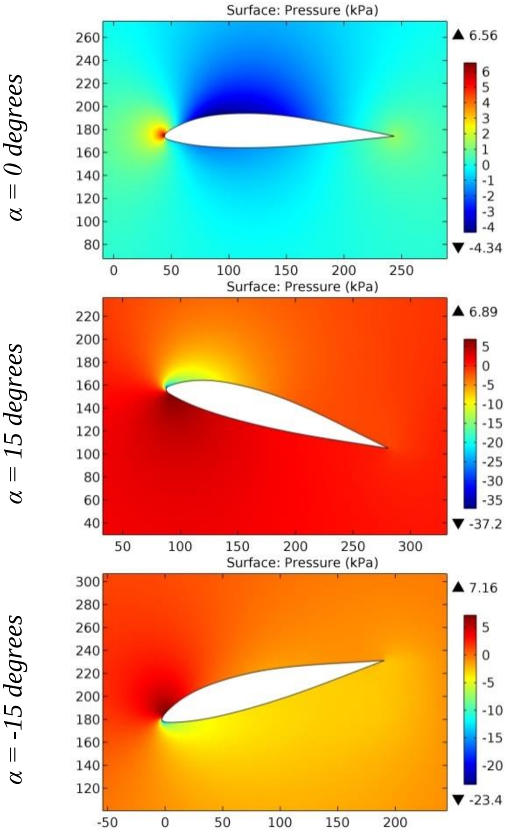

Figure 16. The pressure contours on the surfaces of the MB253515 airfoil.

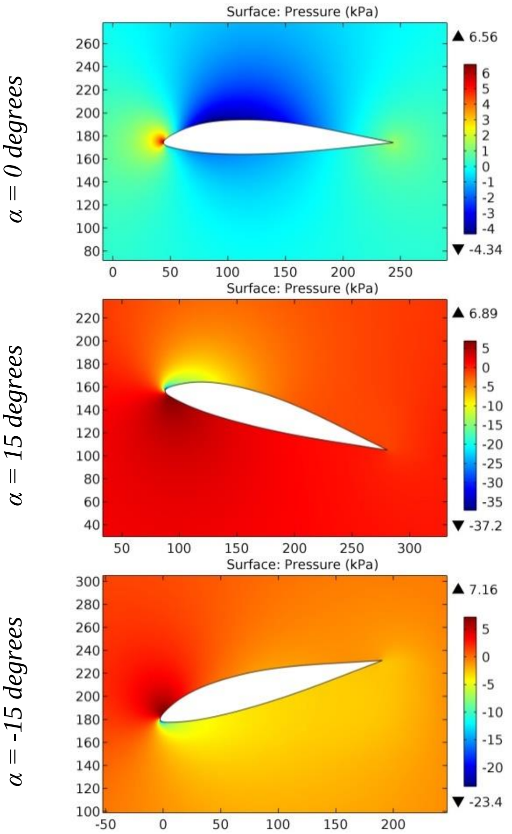

Figure 17. The pressure contours on the surfaces of the MB253515 15,0% smoothed airfoil.

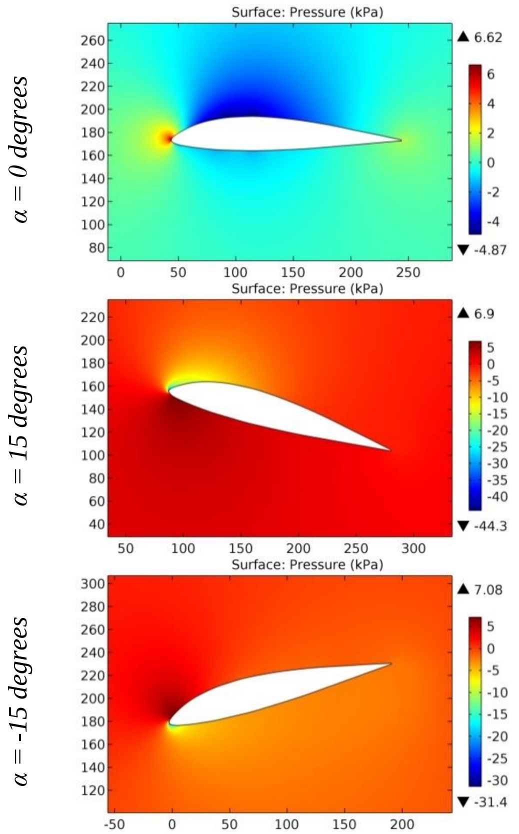

Figure 18. The pressure contours on the surfaces of the MB303515 airfoil.

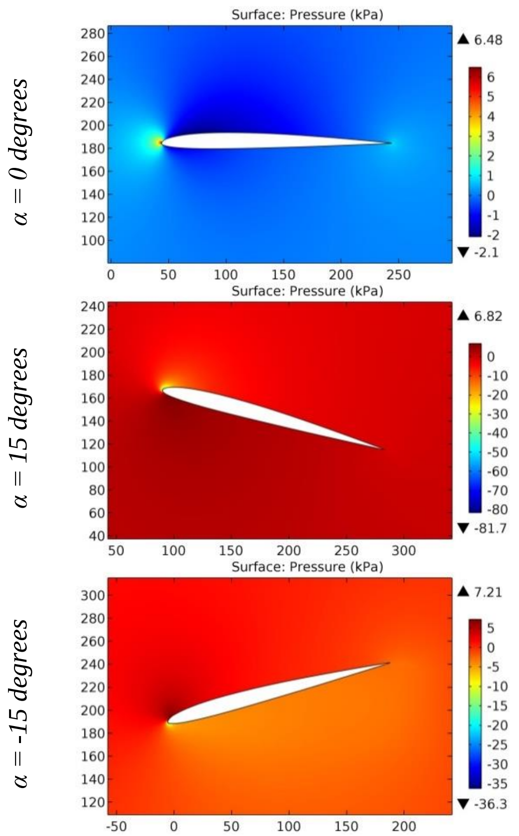

Figure 19. The pressure contours on the surfaces of the mb7136 airfoil.

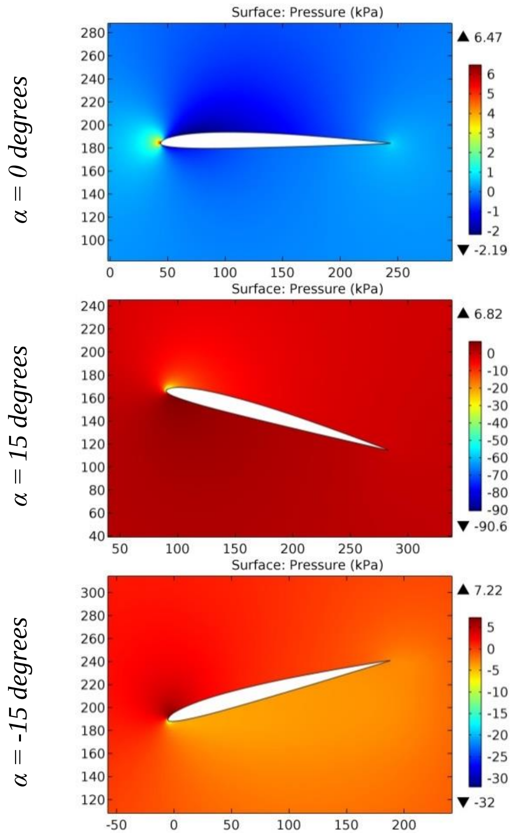

Figure 20. The pressure contours on the surfaces of the mb714 airfoil.

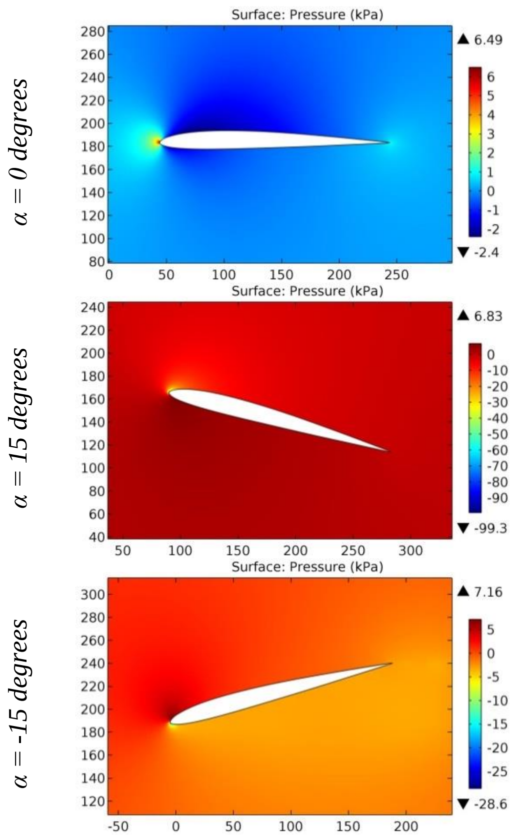

Figure 21. The pressure contours on the surfaces of the mc813 airfoil.

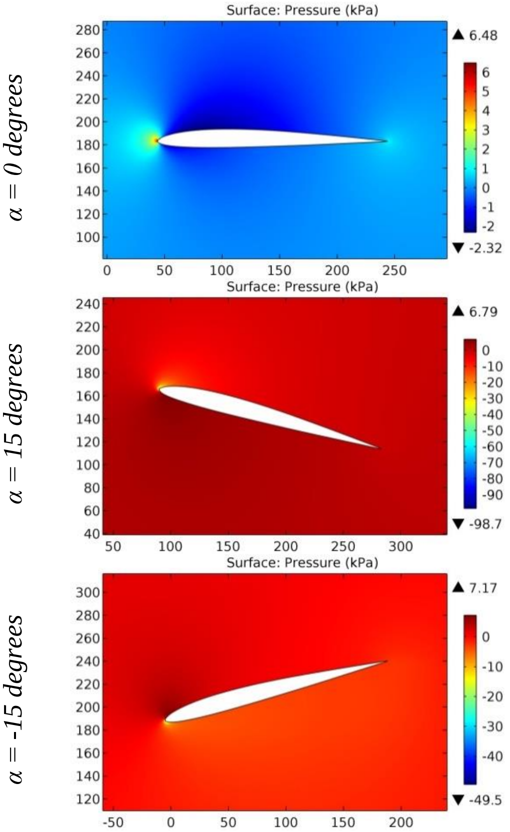

Figure 22. The pressure contours on the surfaces of the md8135 airfoil.

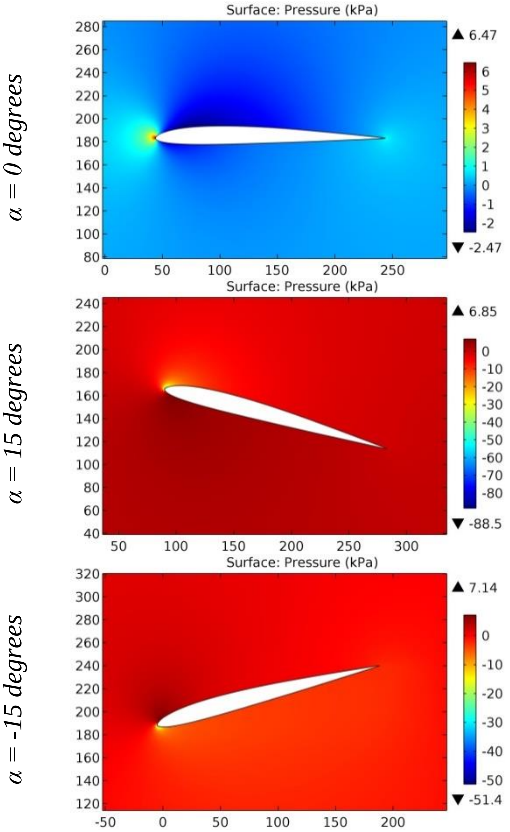

Figure 23. The pressure contours on the surfaces of the md814 airfoil.

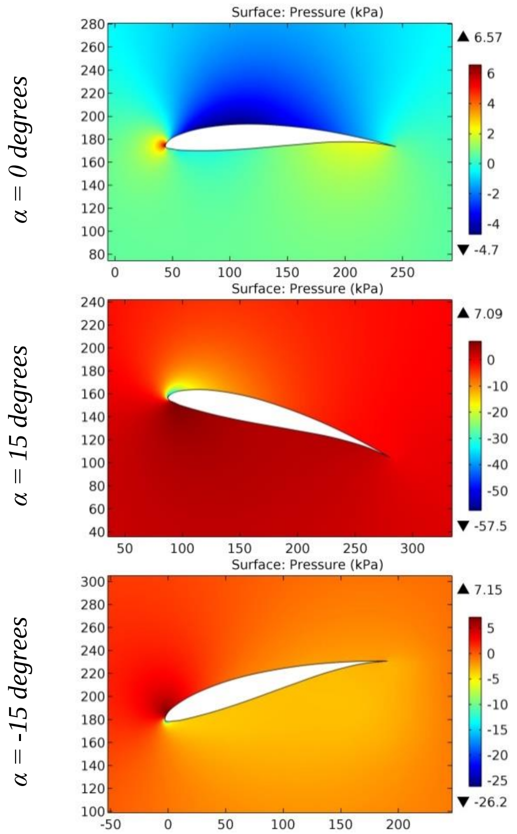

Figure 24. The pressure contours on the surfaces of the MEG 59 airfoil.

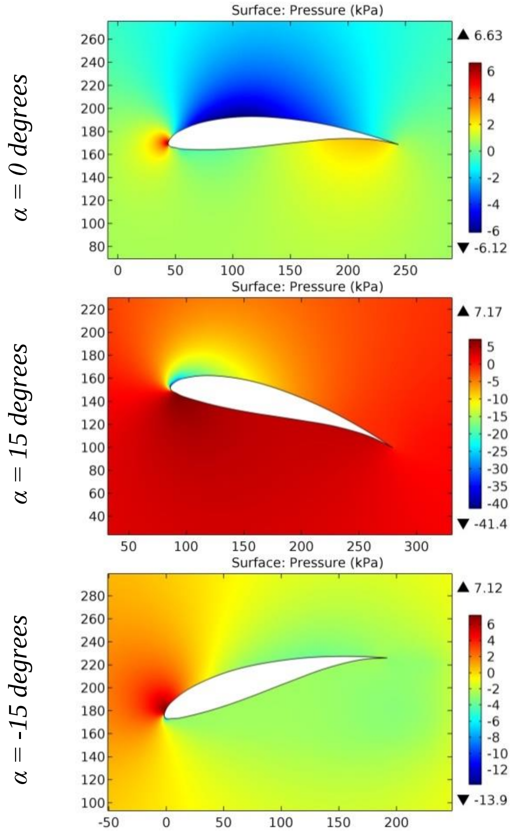

Figure 25. The pressure contours on the surfaces of the MEG 62-63137 airfoil.

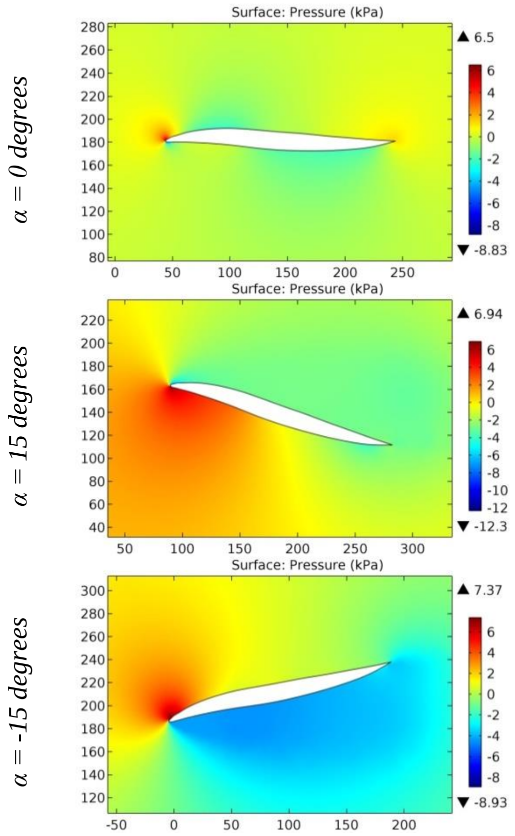

Figure 26. The pressure contours on the surfaces of the MEG 64 airfoil.

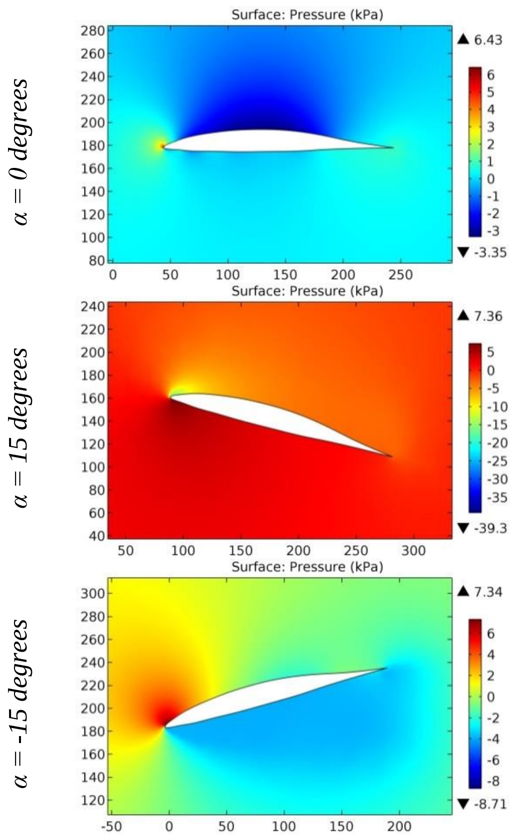

Figure 27. The pressure contours on the surfaces of the MEG 66 airfoil.

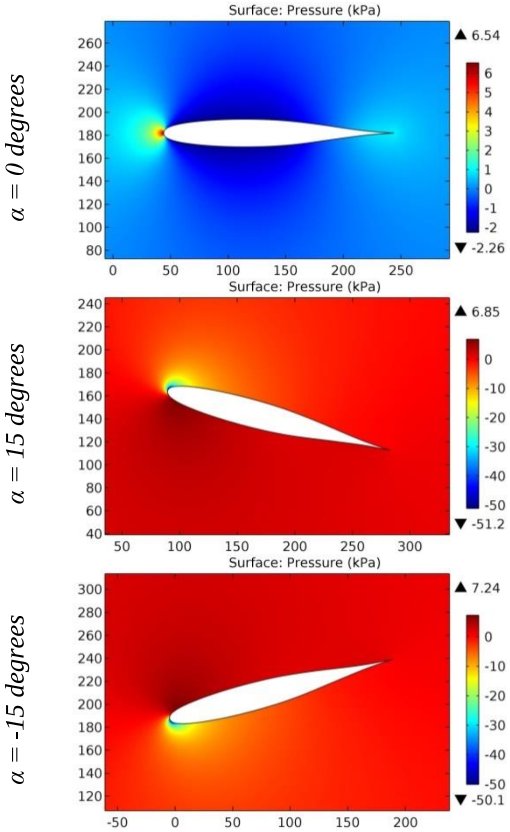

Figure 28. The pressure contours on the surfaces of the MEG 69-012 airfoil.

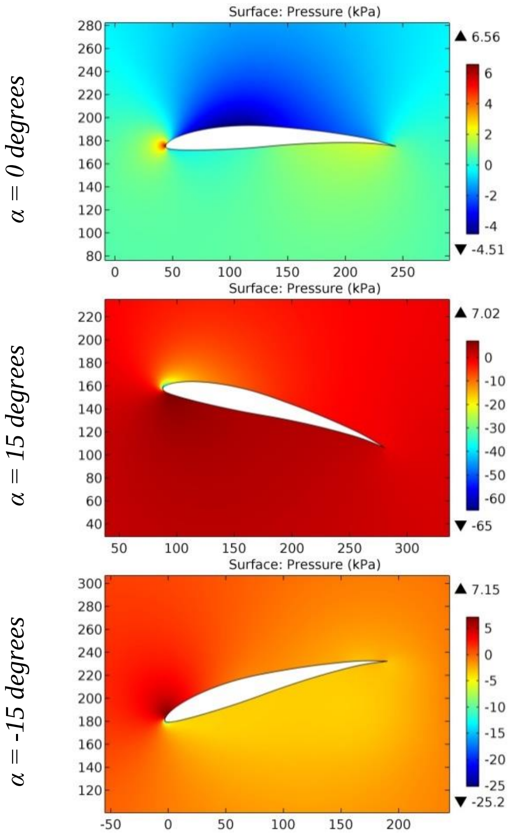

Figure 29. The pressure contours on the surfaces of the MEG-197 airfoil.

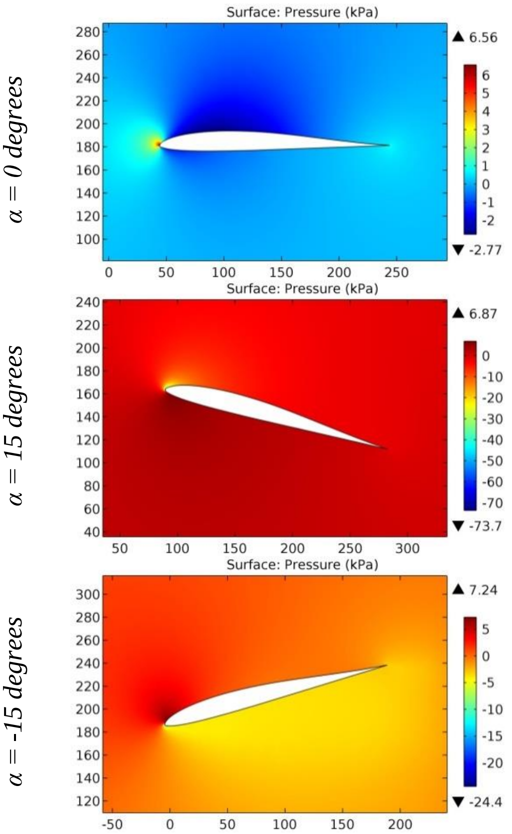

Figure 30. The pressure contours on the surfaces of the MG 08 airfoil.

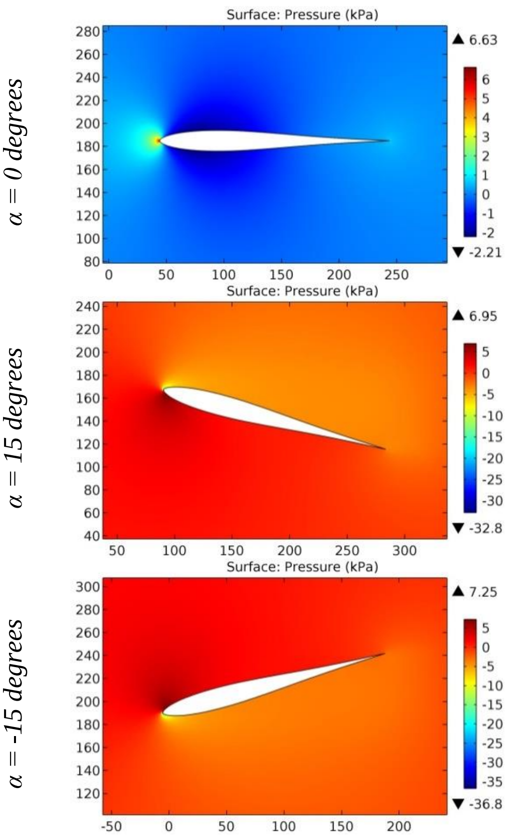

Figure 31. The pressure contours on the surfaces of the MG05 airfoil.

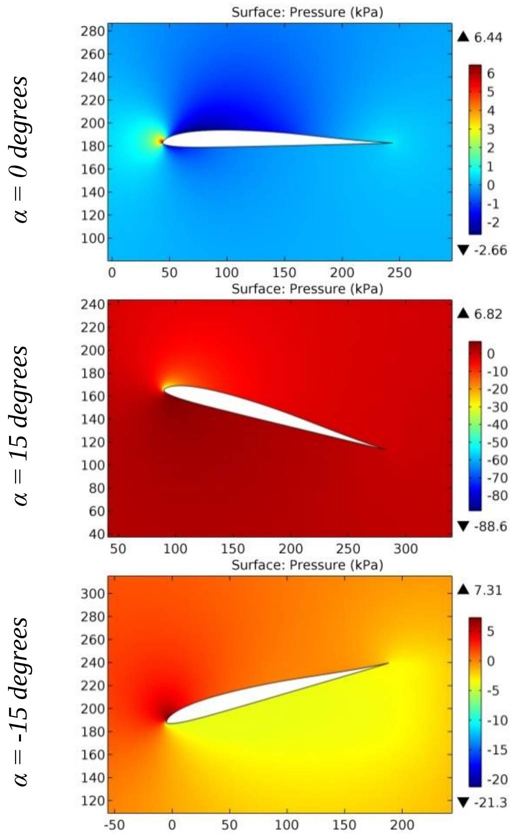

Figure 32. The pressure contours on the surfaces of the MG06 airfoil.

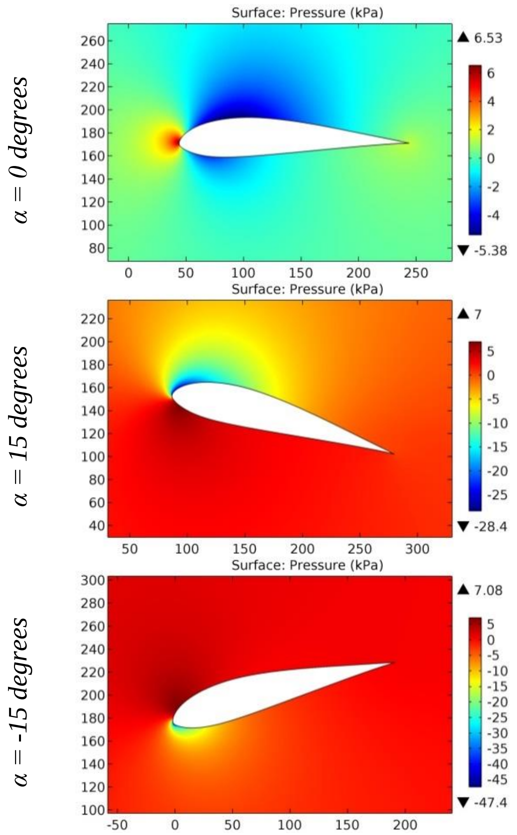

Figure 33. The pressure contours on the surfaces of the MH 102 airfoil.

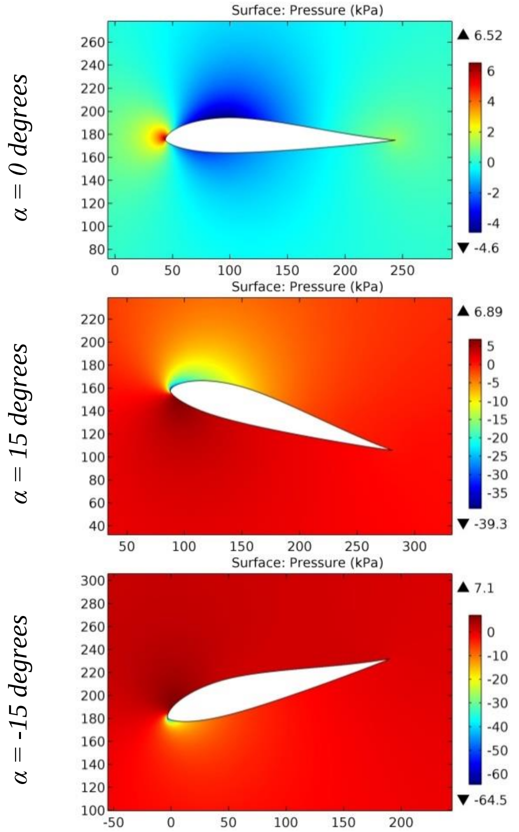

Figure 34. The pressure contours on the surfaces of the MH 104 airfoil.

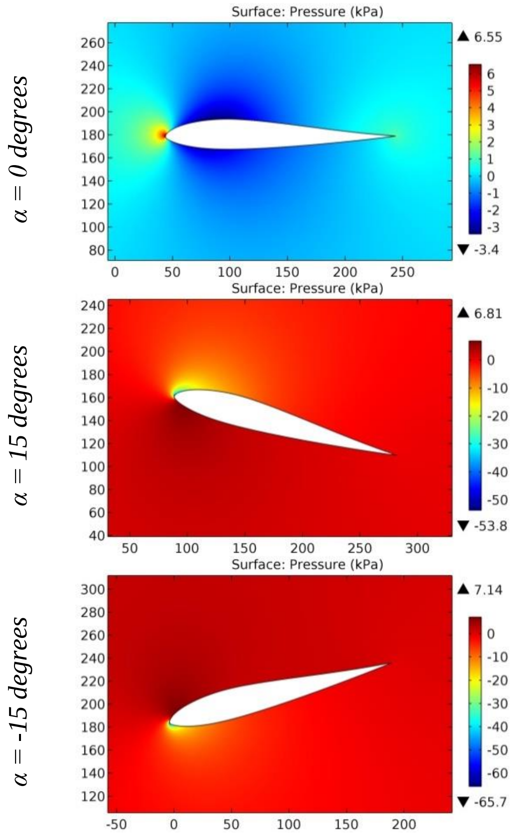

Figure 35. The pressure contours on the surfaces of the MH 106 airfoil.

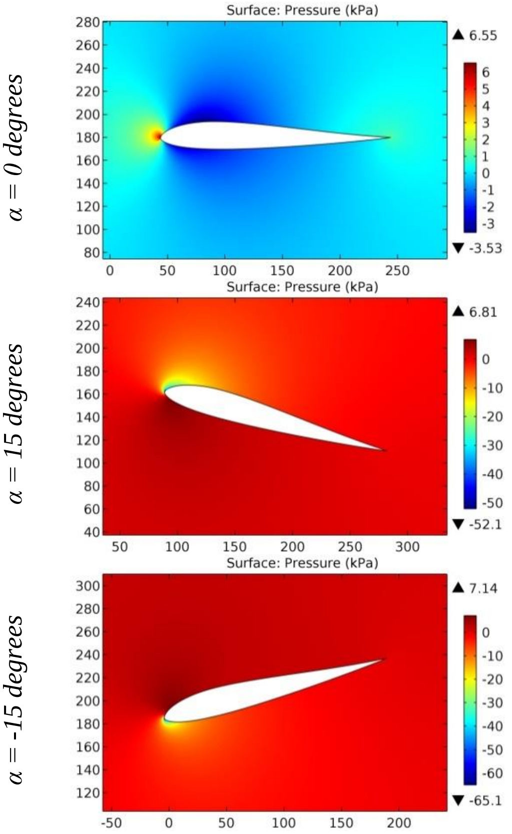

Figure 36. The pressure contours on the surfaces of the MH 108 airfoil.

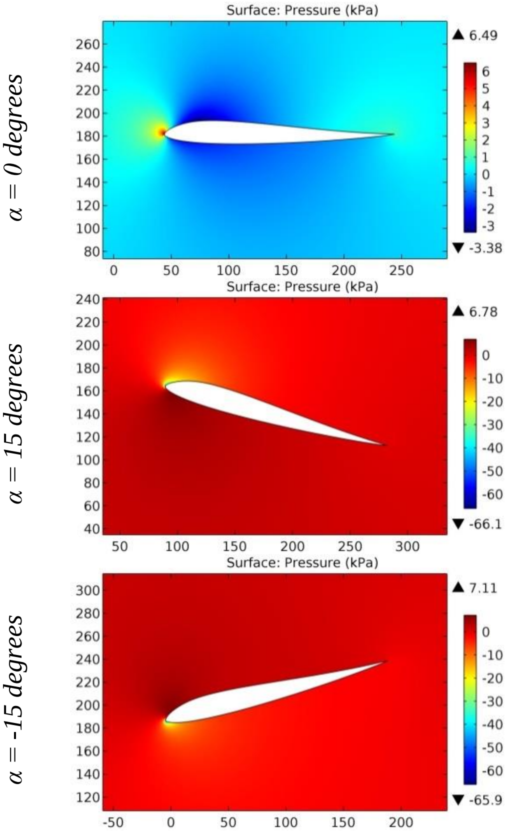

Figure 37. The pressure contours on the surfaces of the MH 110 airfoil.

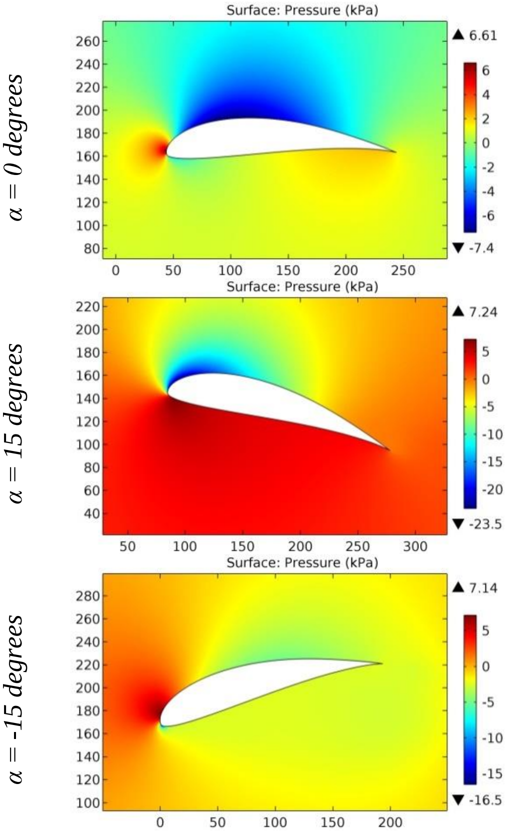

Figure 38. The pressure contours on the surfaces of the MH 112 airfoil.

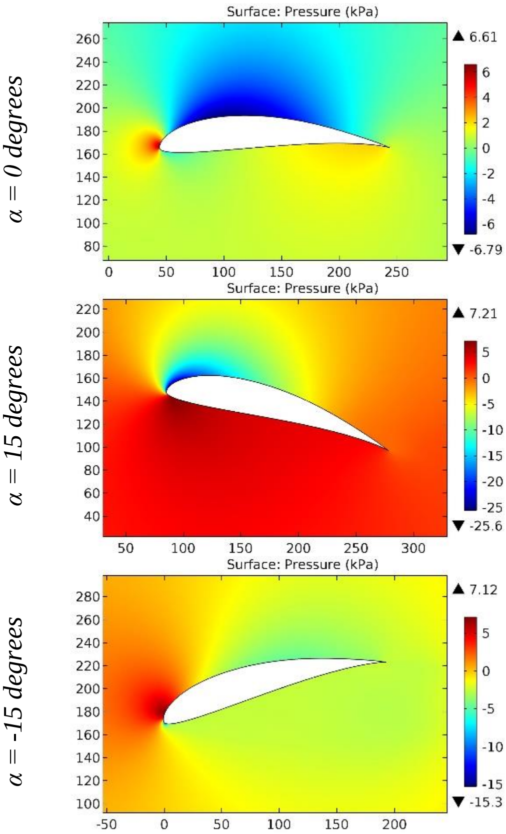

Figure 39. The pressure contours on the surfaces of the MH 113 airfoil.

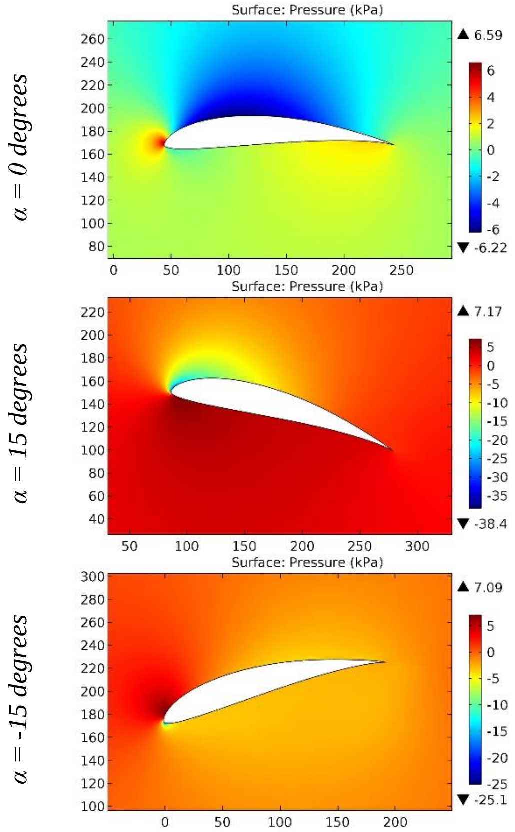

Figure 40. The pressure contours on the surfaces of the MH 114 airfoil.

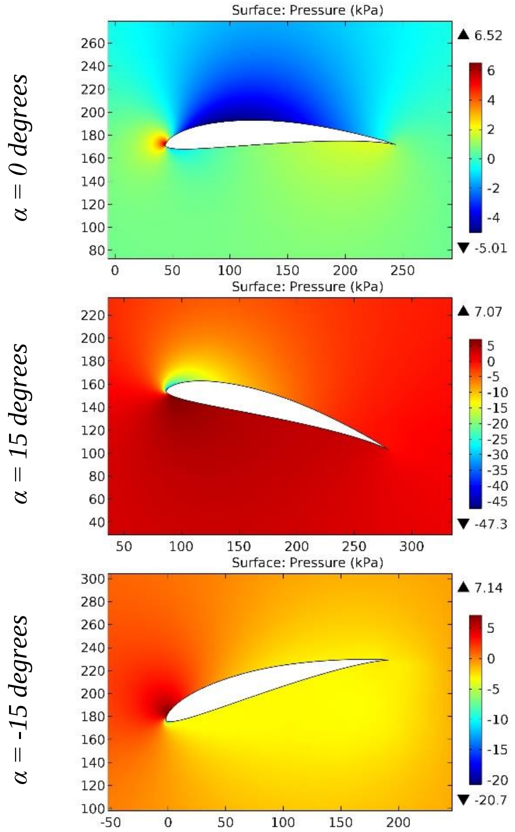

Figure 41. The pressure contours on the surfaces of the MH 115 airfoil.

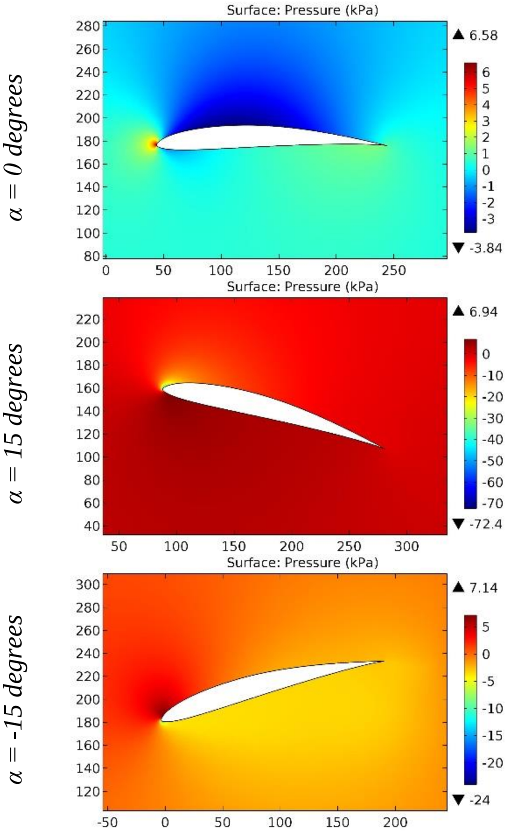

Figure 42. The pressure contours on the surfaces of the MH 116 airfoil.

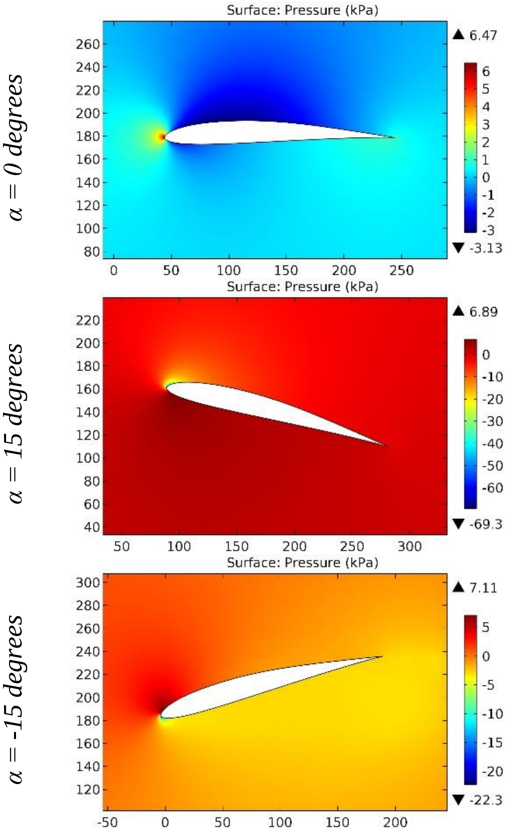

Figure 43. The pressure contours on the surfaces of the MH 117 airfoil.

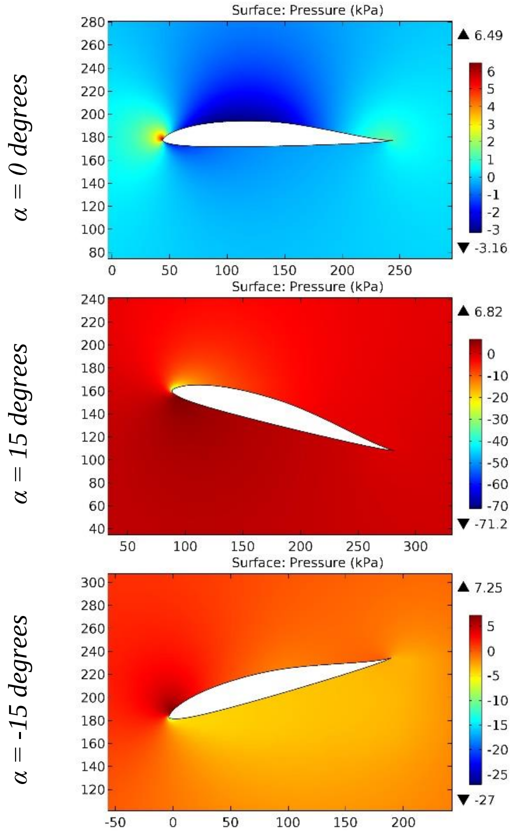

Figure 44. The pressure contours on the surfaces of the MH 18 airfoil.

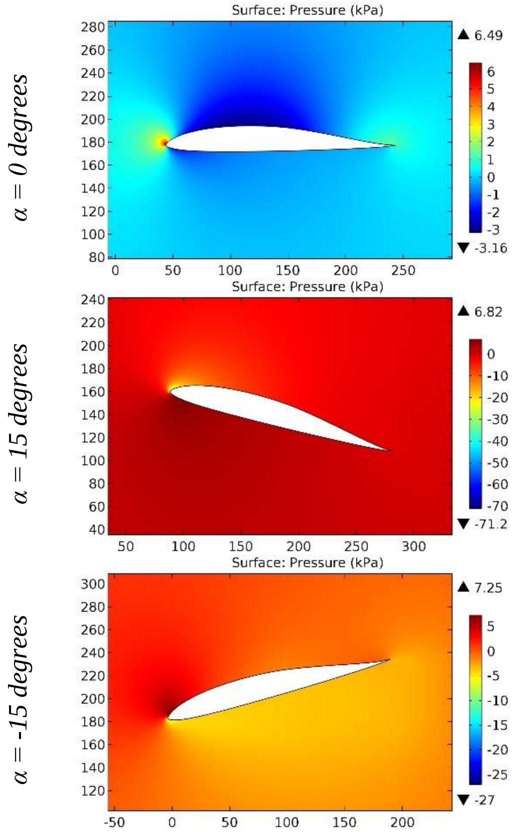

Figure 45. The pressure contours on the surfaces of the MH 18 11,14% airfoil.

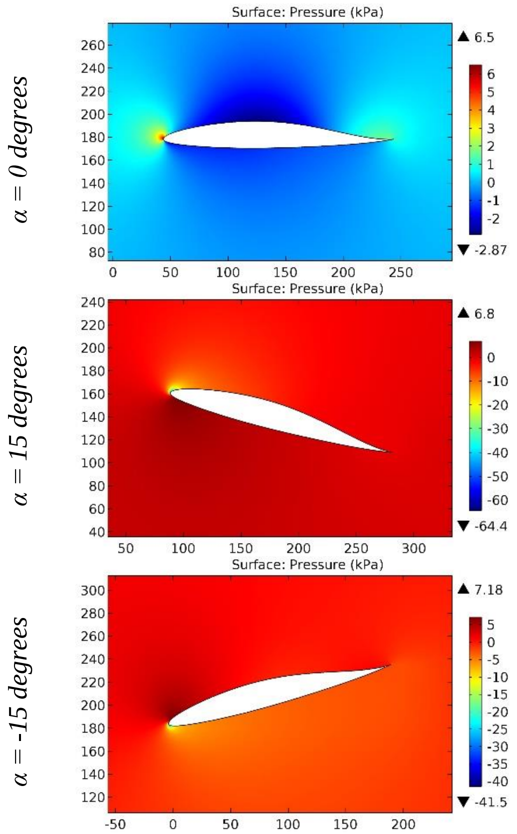

Figure 46. The pressure contours on the surfaces of the MH 18B airfoil.

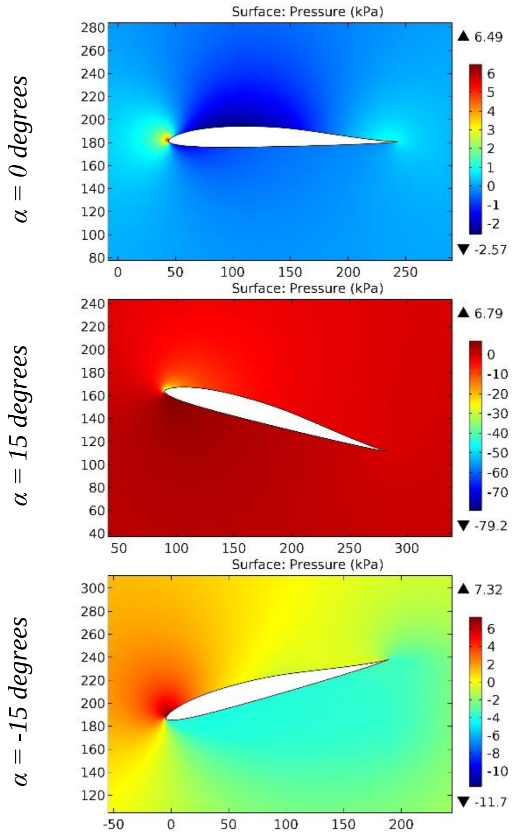

Figure 47. The pressure contours on the surfaces of the MH 20 airfoil.

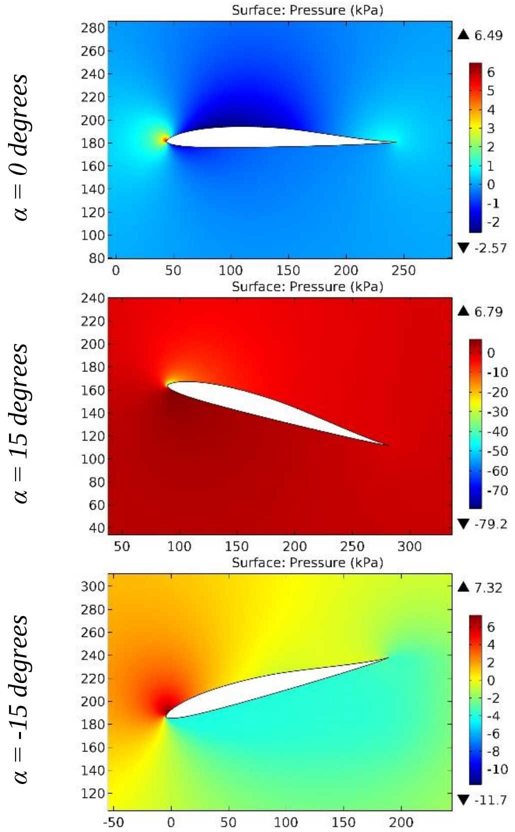

Figure 48. The pressure contours on the surfaces of the MH 20 9,02% airfoil.

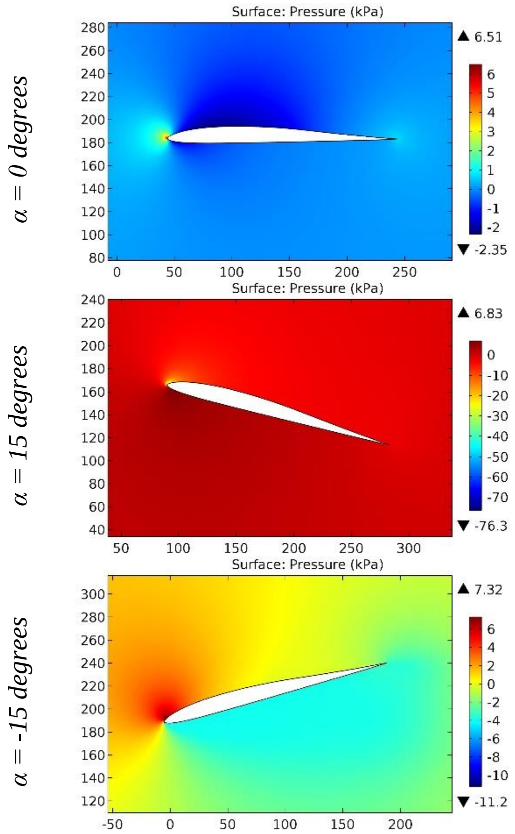

Figure 49. The pressure contours on the surfaces of the MH 22 airfoil.

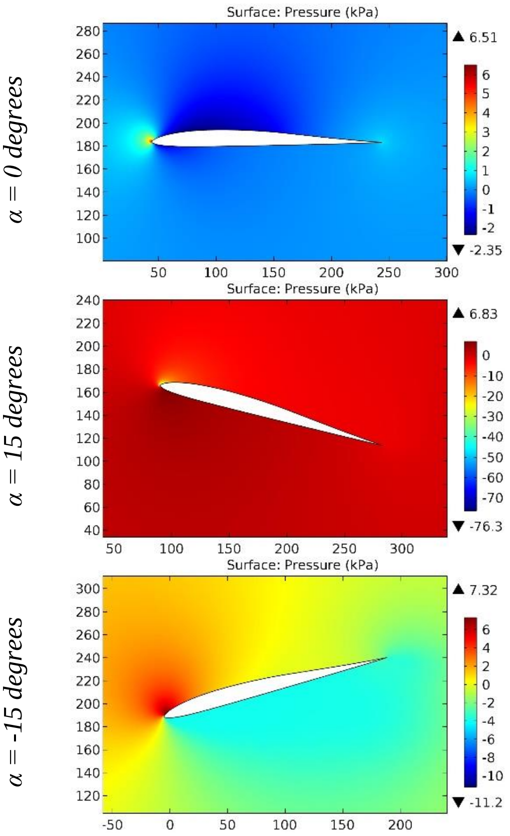

Figure 50. The pressure contours on the surfaces of the MH 22 7,21% airfoil.

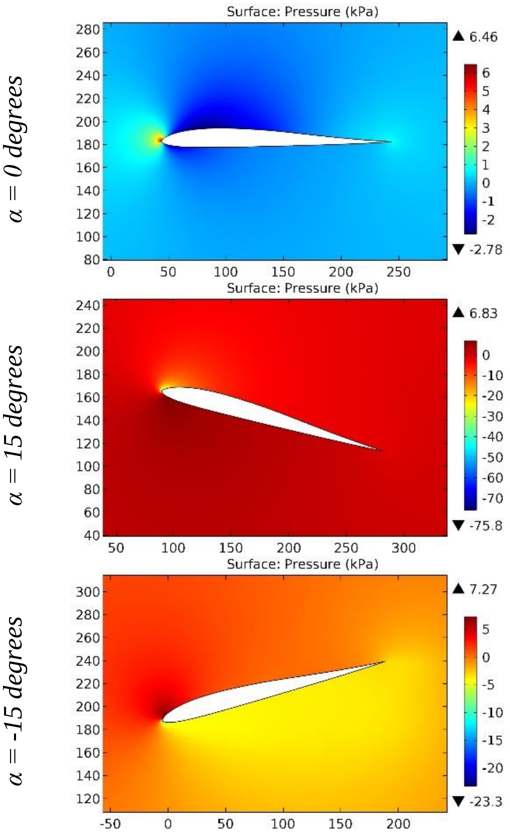

Figure 51. The pressure contours on the surfaces of the MH 22-Mod,3 airfoil.

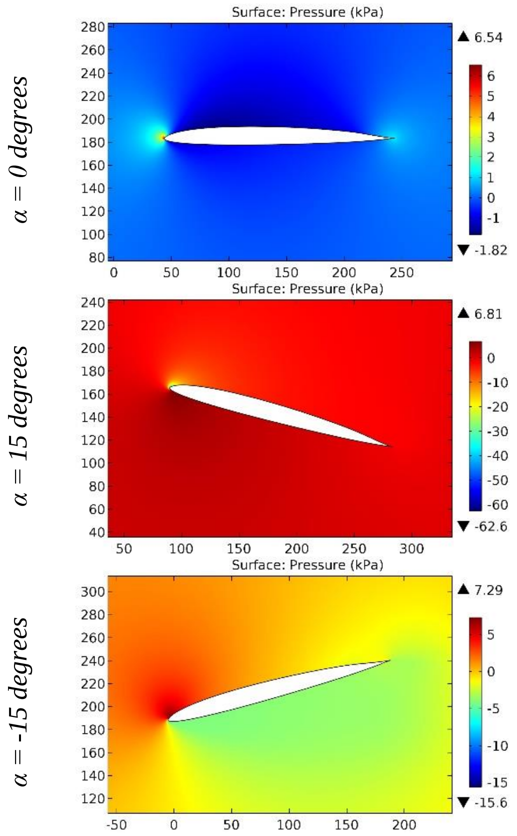

Figure 52. The pressure contours on the surfaces of the MH 23 airfoil.

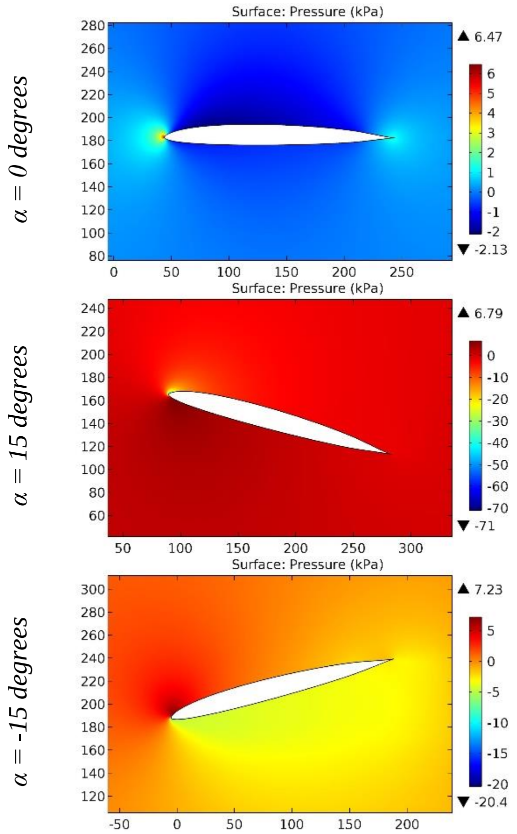

Figure 53. The pressure contours on the surfaces of the MH 24 airfoil.

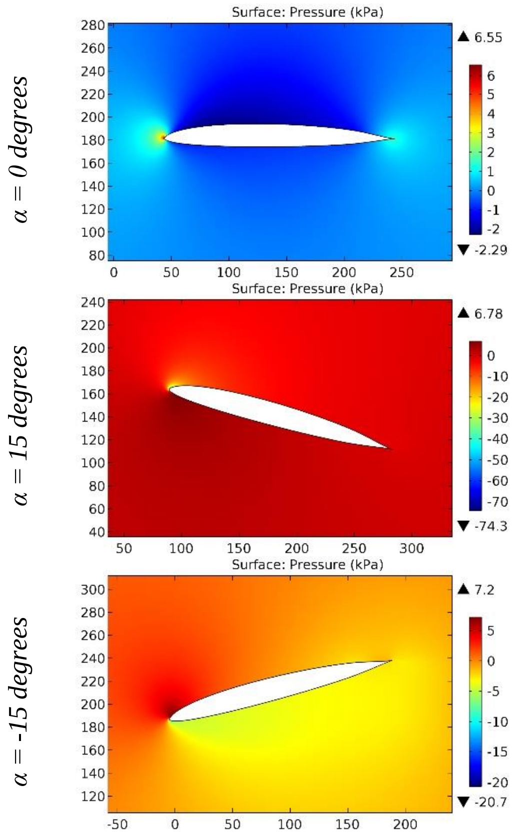

Figure 54. The pressure contours on the surfaces of the MH 25 airfoil.

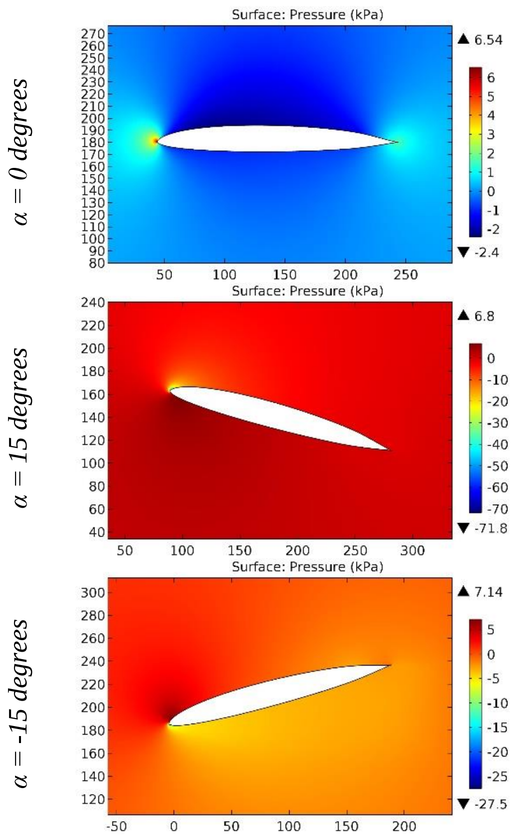

Figure 55. The pressure contours on the surfaces of the MH 26 airfoil.

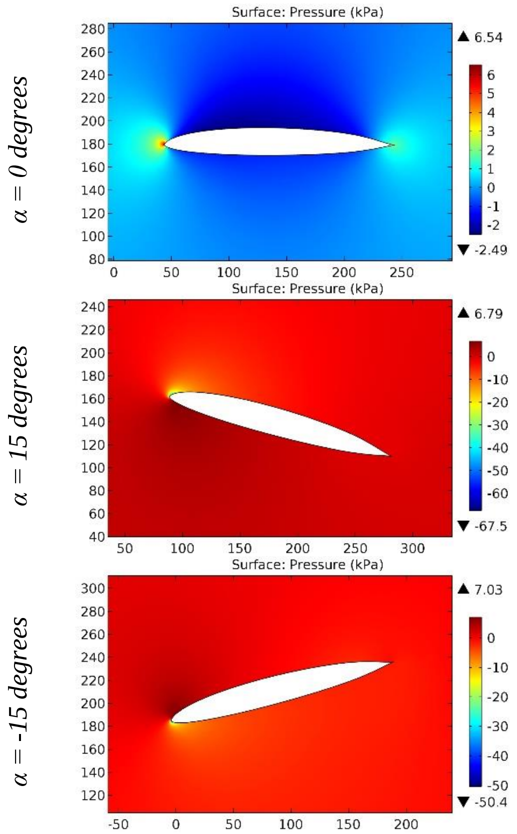

Figure 56. The pressure contours on the surfaces of the MH 27 airfoil.

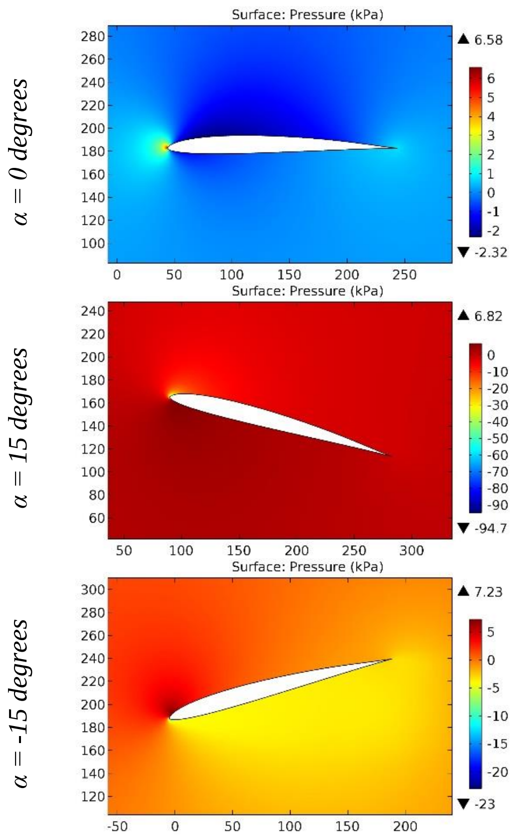

Figure 57. The pressure contours on the surfaces of the MH 30 airfoil.

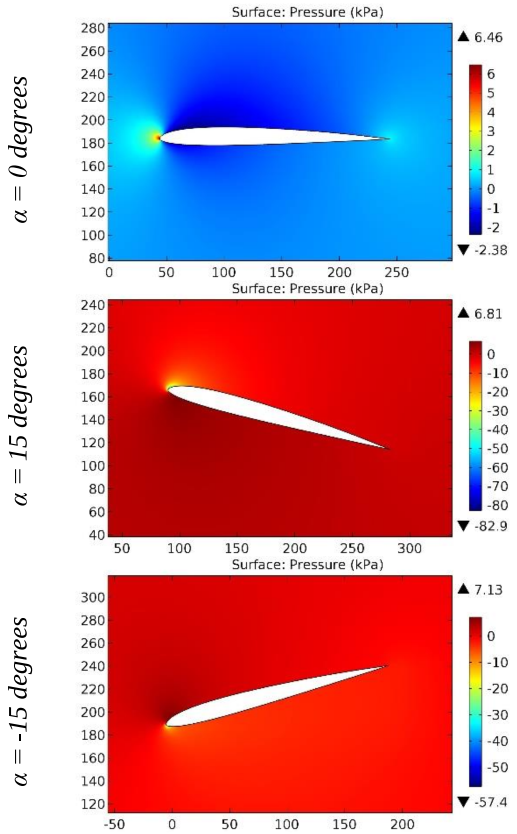

Figure 58. The pressure contours on the surfaces of the MH 31 airfoil.

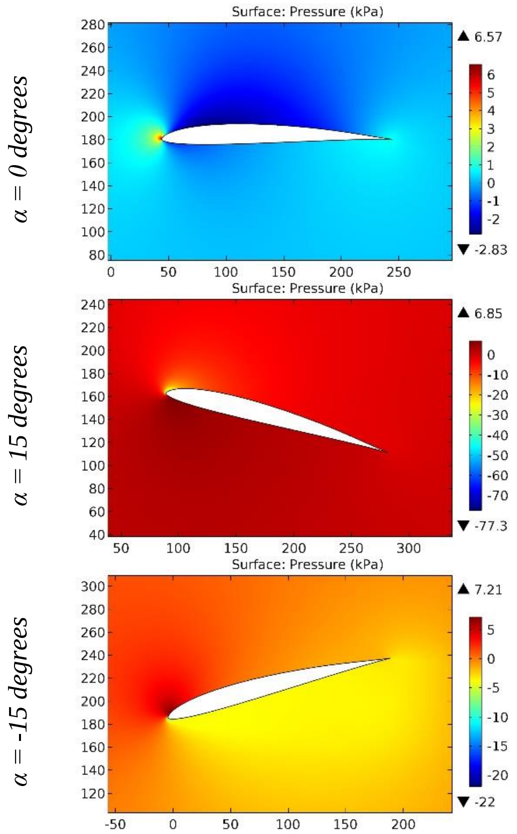

Figure 59. The pressure contours on the surfaces of the MH 32 airfoil.

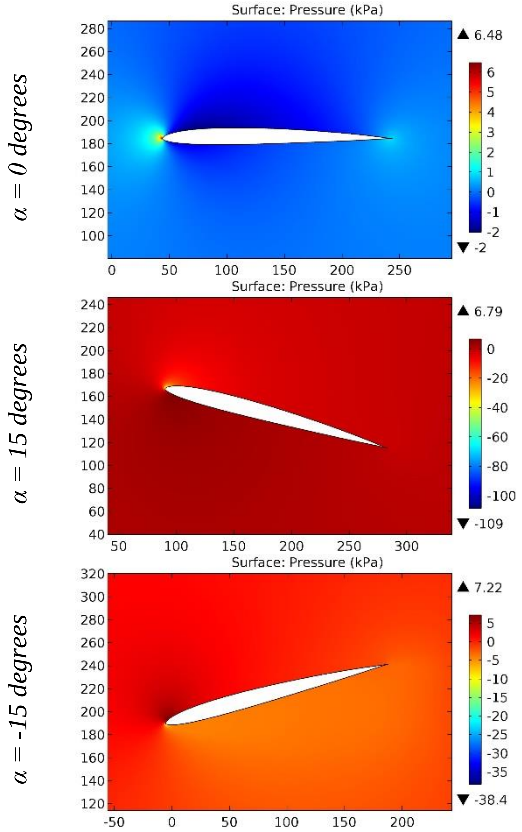

Figure 60. The pressure contours on the surfaces of the MH 33 airfoil.

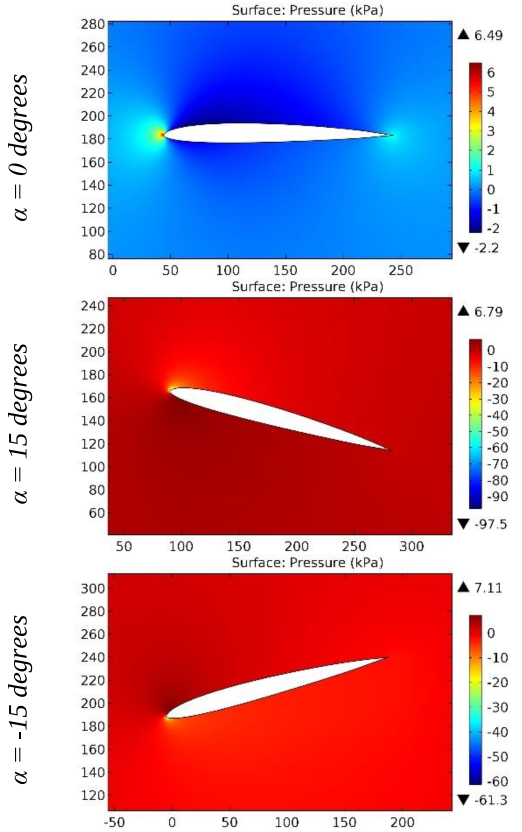

Figure 61. The pressure contours on the surfaces of the MH 34 airfoil.

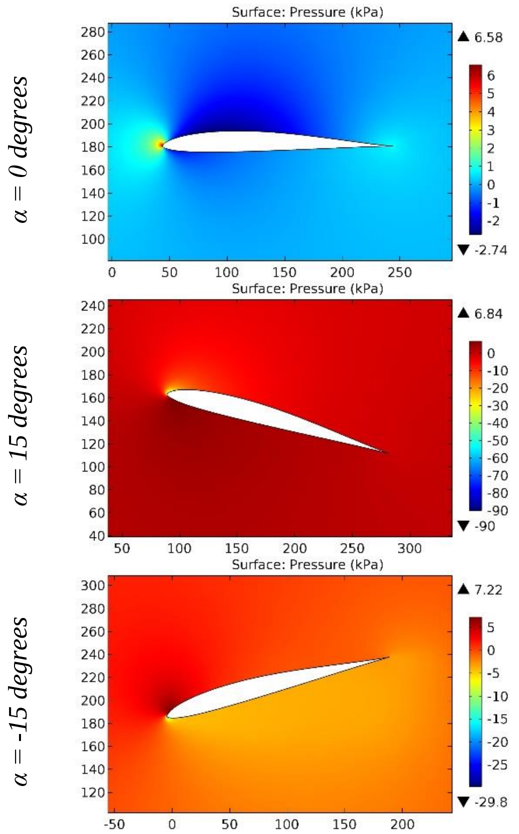

Figure 62. The pressure contours on the surfaces of the MH 42 airfoil.

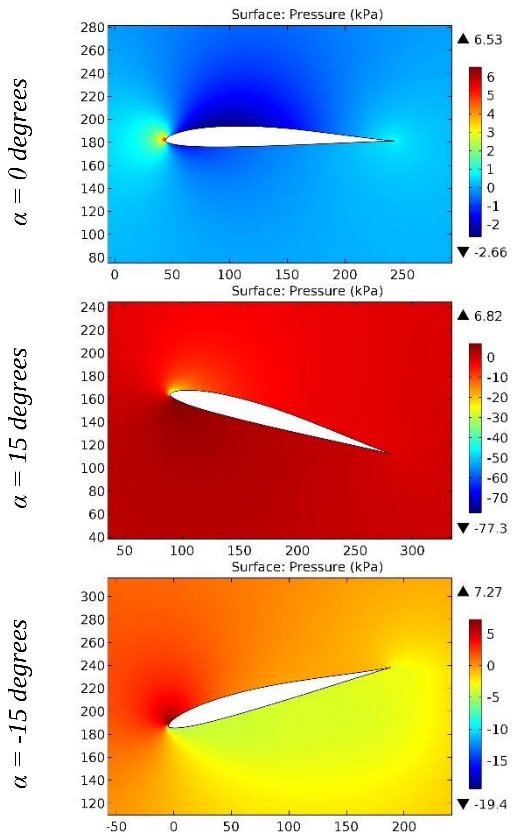

Figure 63. The pressure contours on the surfaces of the MH 42 8,94% airfoil.

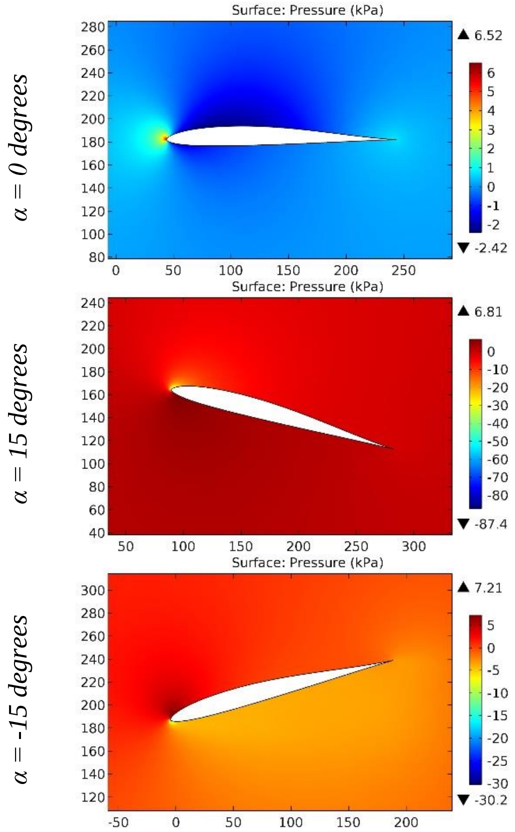

Figure 64. The pressure contours on the surfaces of the MH 43 airfoil.

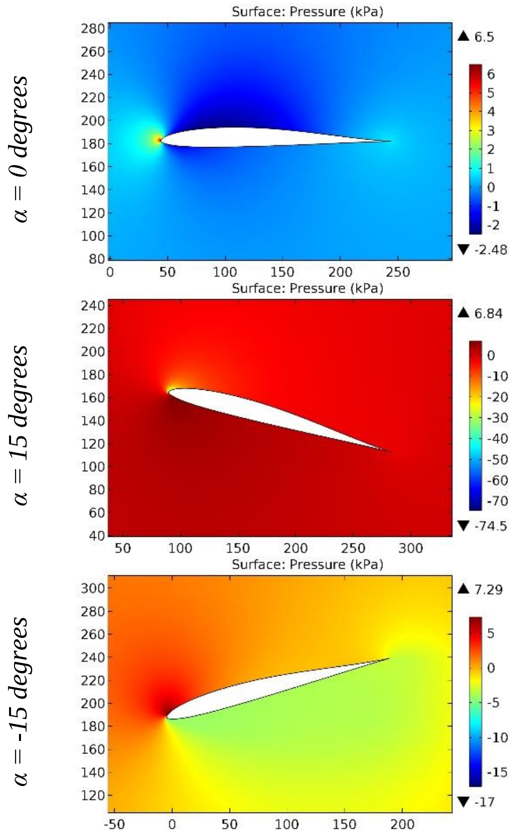

Figure 65. The pressure contours on the surfaces of the MH 43 8,5% airfoil.

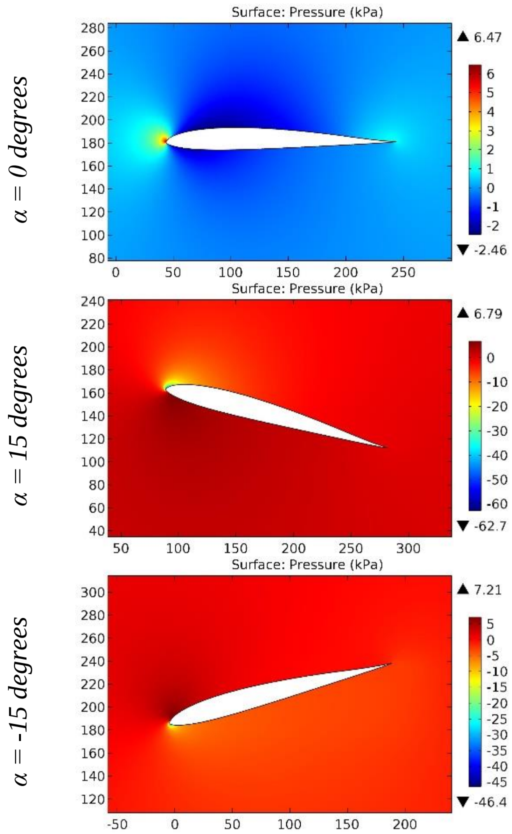

Figure 66. The pressure contours on the surfaces of the MH 44 airfoil.

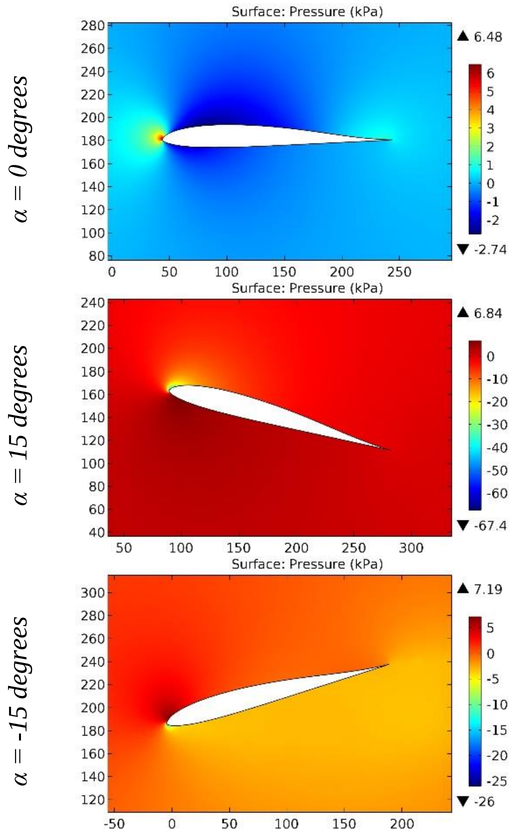

Figure 67. The pressure contours on the surfaces of the MH 45 airfoil.

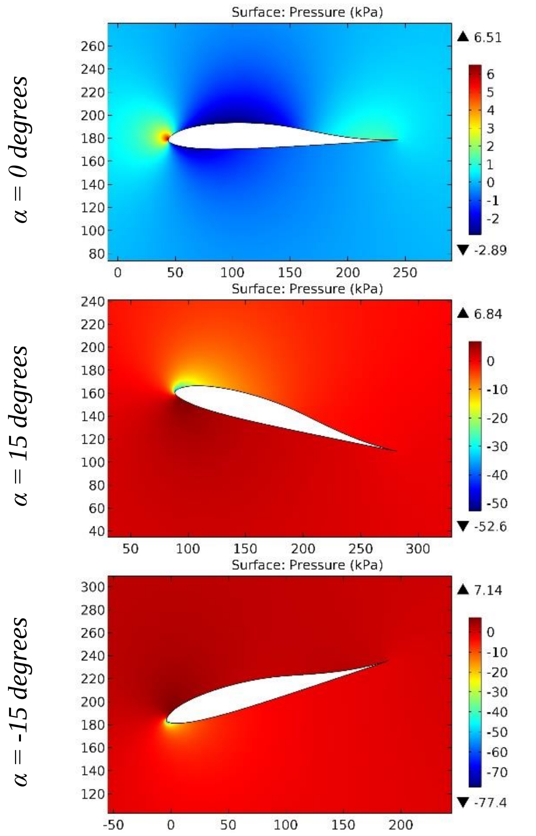

Figure 68. The pressure contours on the surfaces of the MH 46 airfoil.

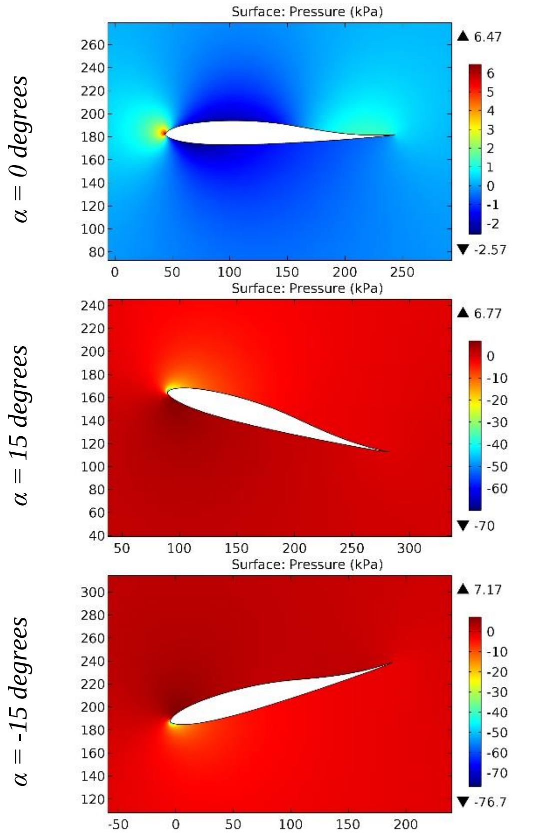

Figure 69. The pressure contours on the surfaces of the MH 49 airfoil.

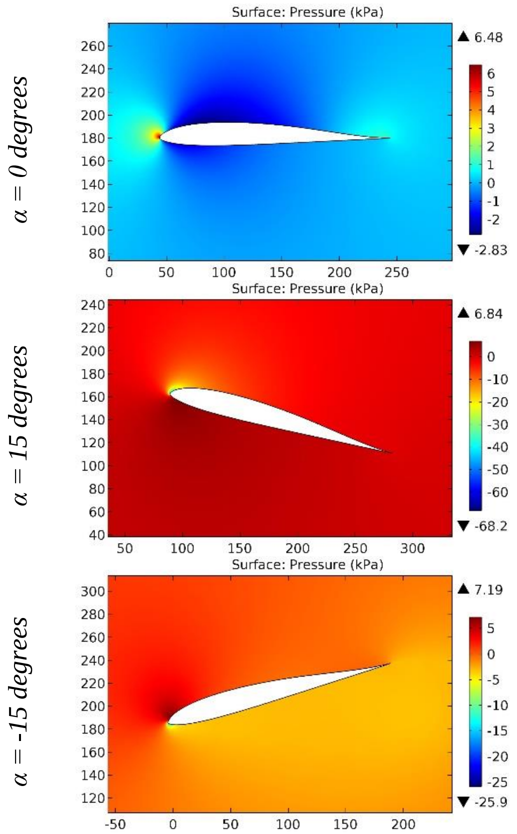

Figure 70. The pressure contours on the surfaces of the MH 60 airfoil.

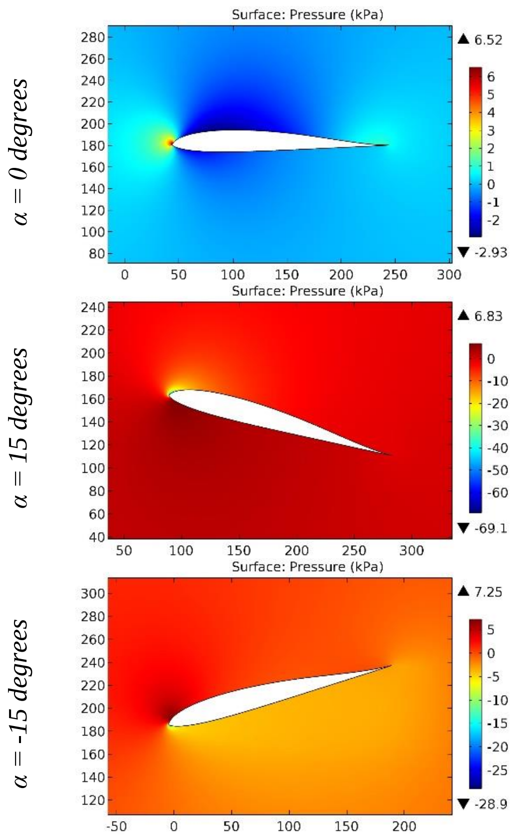

Figure 71. The pressure contours on the surfaces of the MH 60 10,08% airfoil.

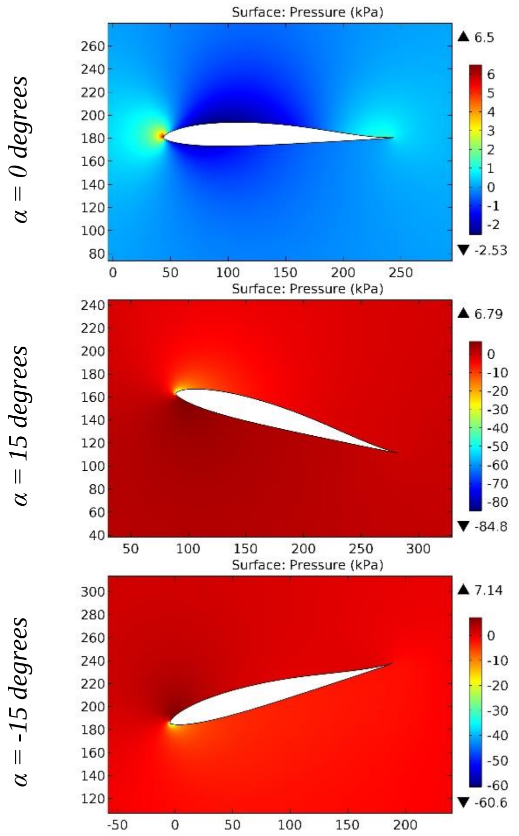

Figure 72. The pressure contours on the surfaces of the MH 61 airfoil.

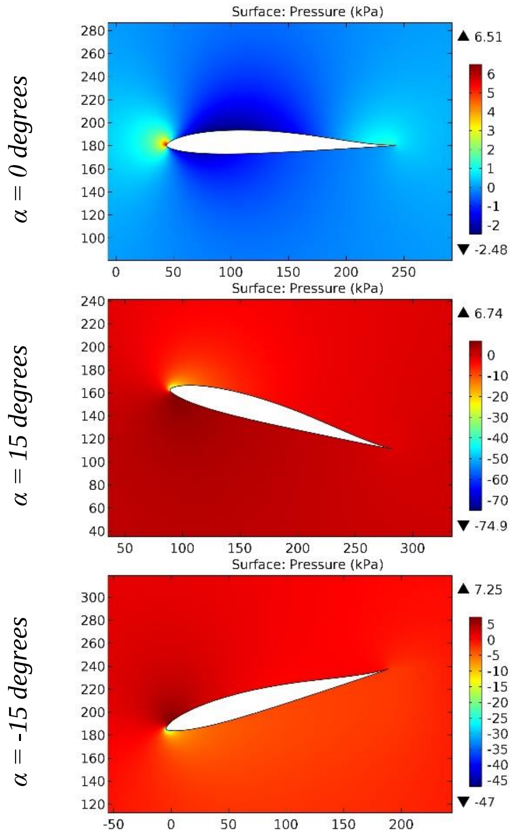

Figure 73. The pressure contours on the surfaces of the MH 61 10,28% airfoil.

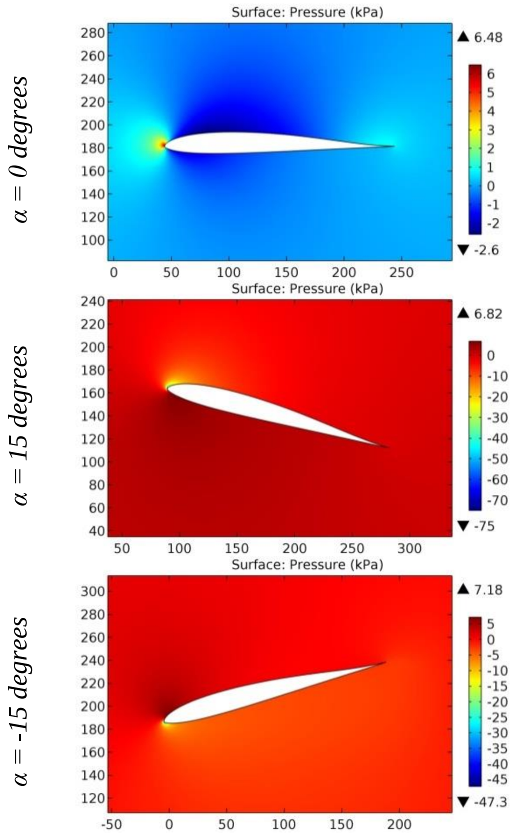

Figure 74. The pressure contours on the surfaces of the MH 62 airfoil.

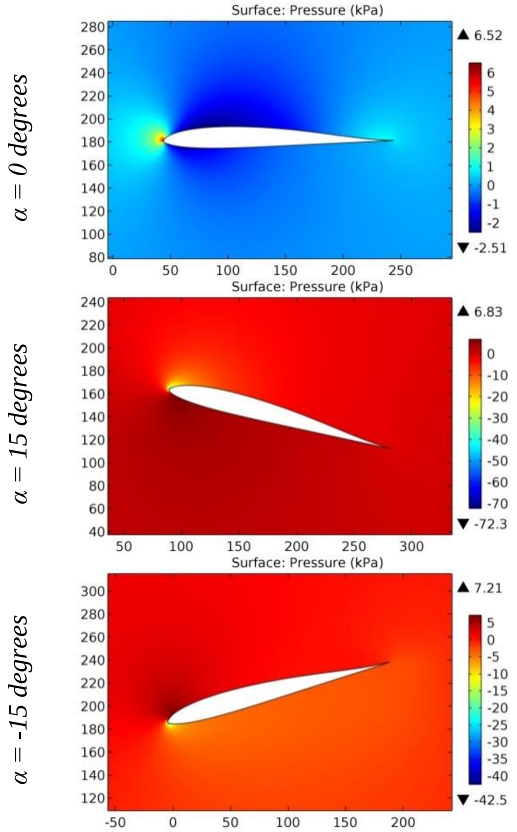

Figure 75. The pressure contours on the surfaces of the MH 62 9,3% airfoil.

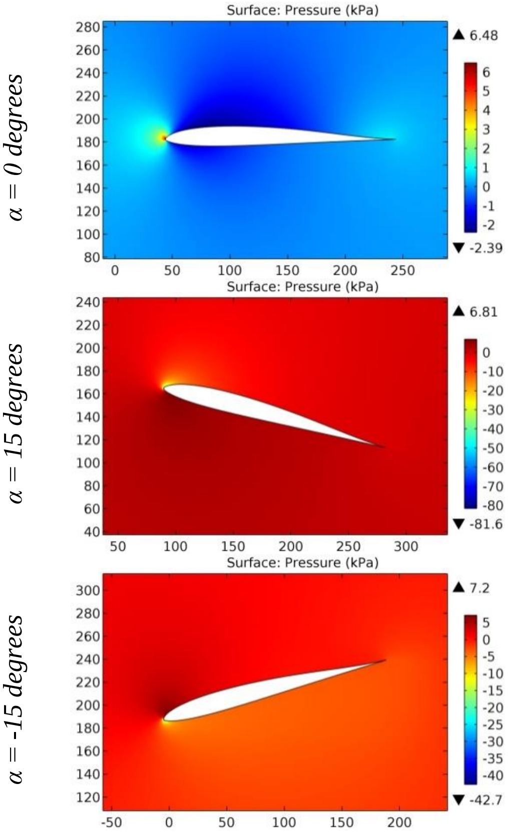

Figure 76. The pressure contours on the surfaces of the MH 64 airfoil.

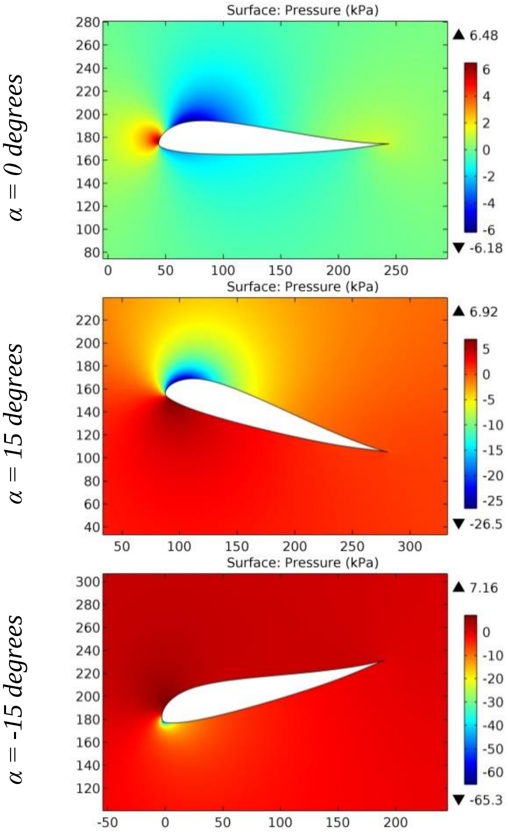

Figure 77. The pressure contours on the surfaces of the MH 78 airfoil.

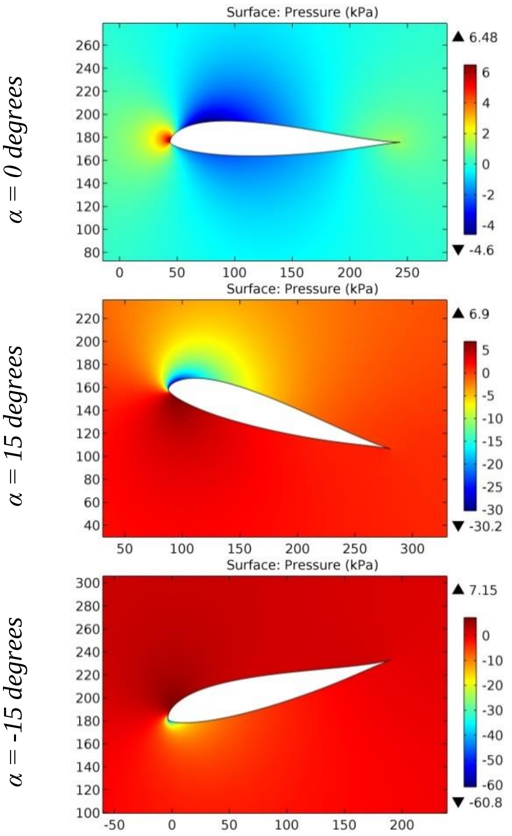

Figure 78. The pressure contours on the surfaces of the MH 91 airfoil.

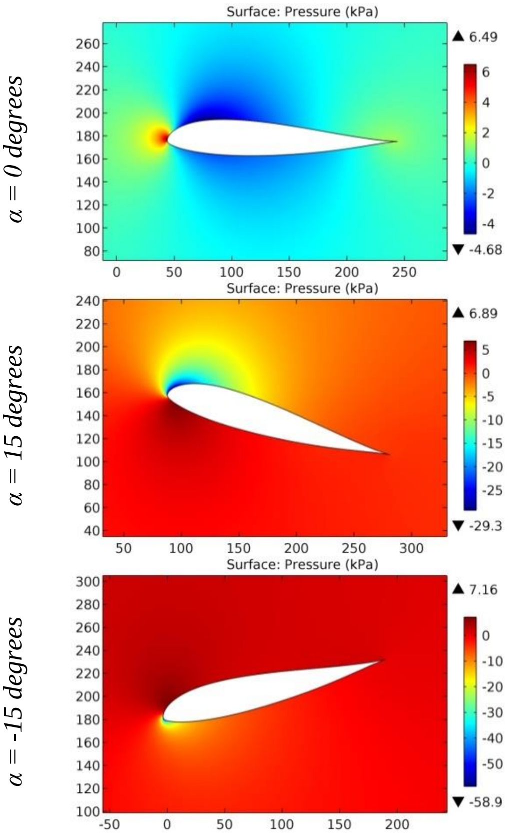

Figure 79. The pressure contours on the surfaces of the MH 92 airfoil.

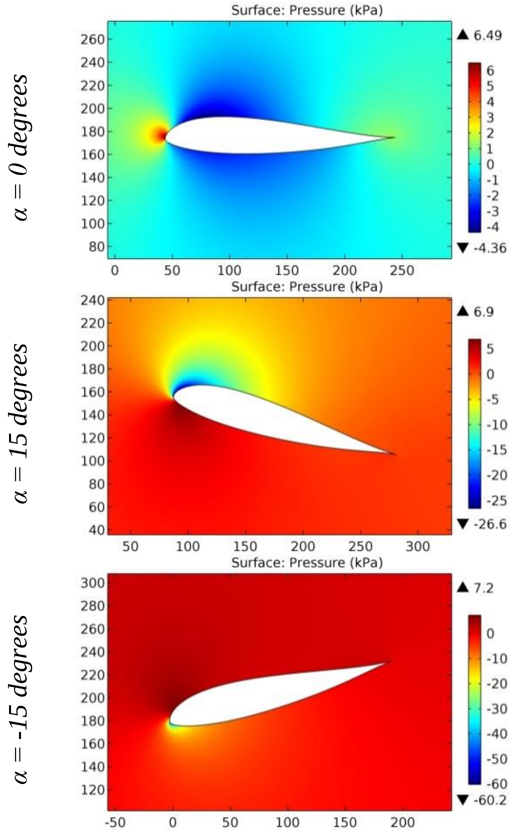

Figure 80. The pressure contours on the surfaces of the MH 93 airfoil.

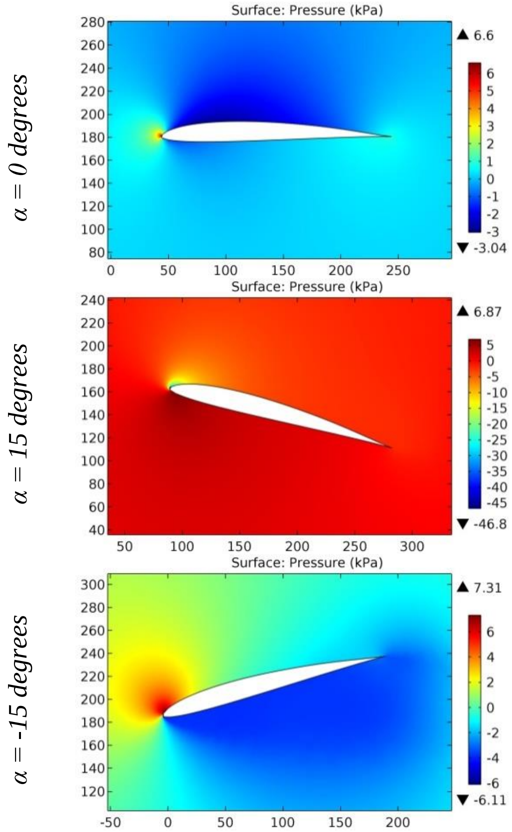

Figure 81. The pressure contours on the surfaces of the MH32 (8,71%) airfoil.

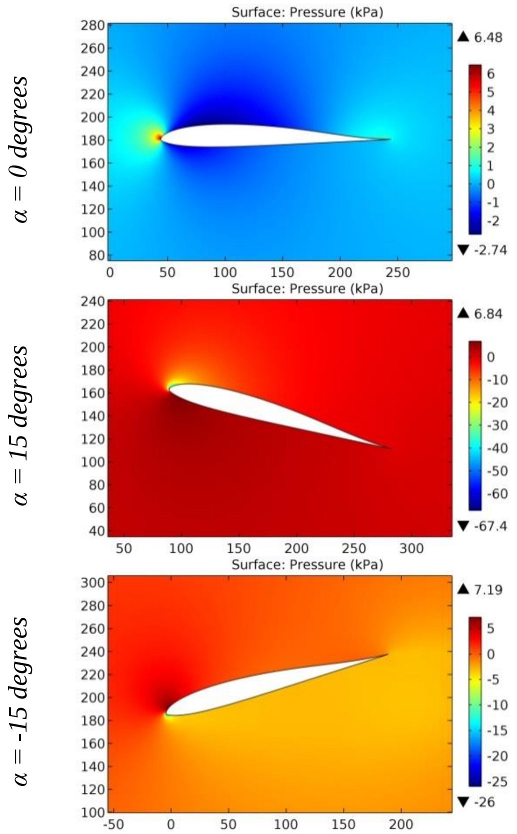

Figure 82. The pressure contours on the surfaces of the MH45 airfoil.

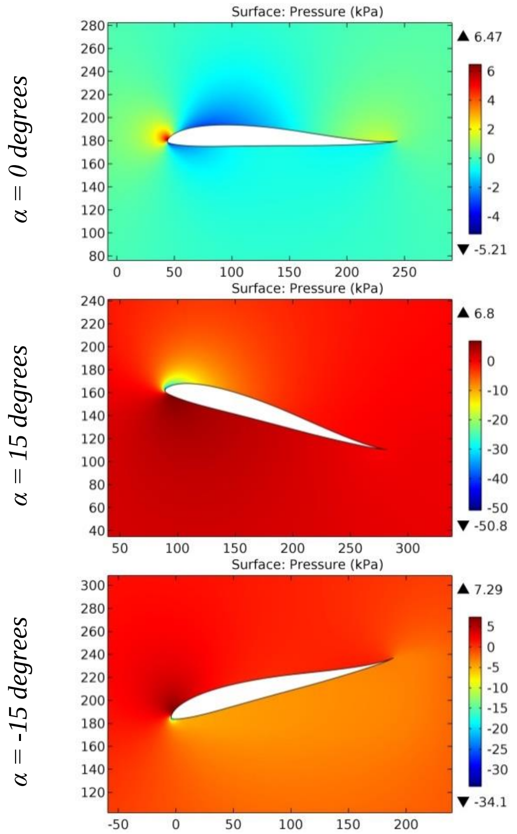

Figure 83. The pressure contours on the surfaces of the mhmi2 airfoil.

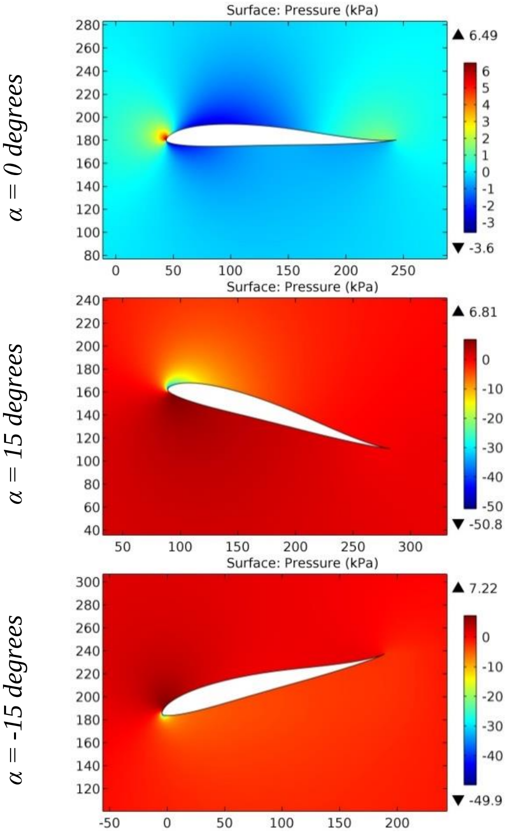

Figure 84. The pressure contours on the surfaces of the mhmi3 airfoil.

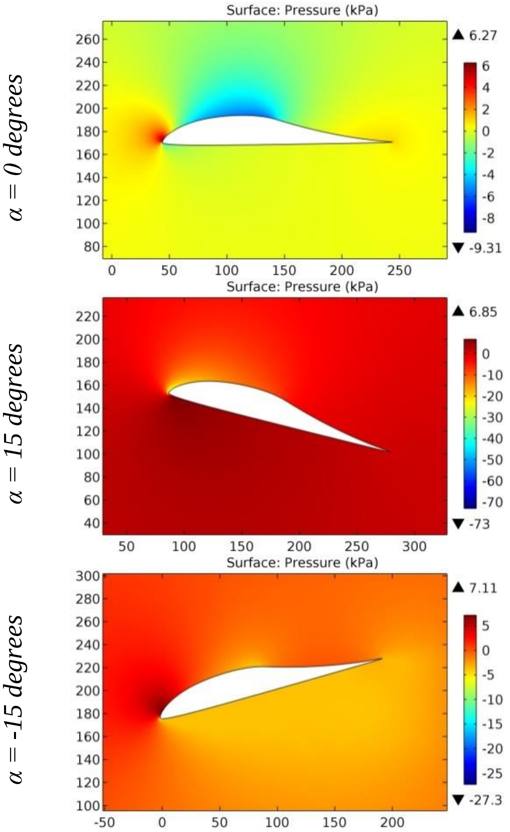

Figure 85. The pressure contours on the surfaces of the MILEY M06-13-128 airfoil.

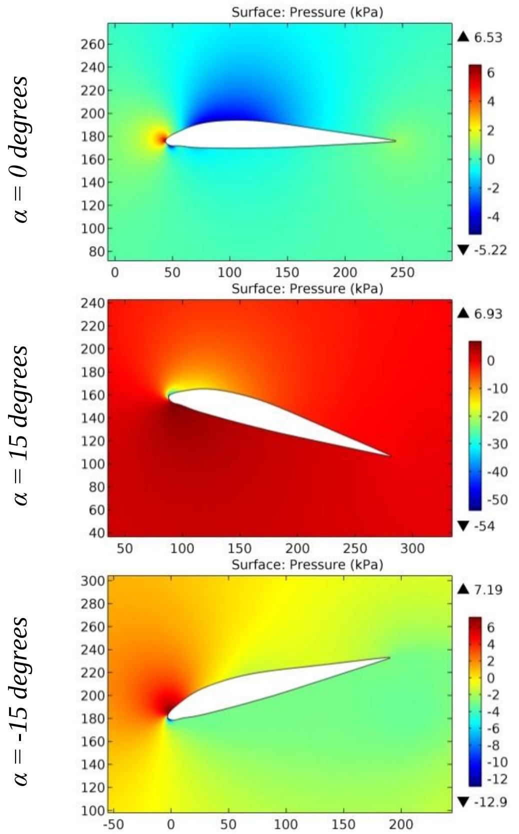

Figure 86. The pressure contours on the surfaces of the MIRAGE airfoil.

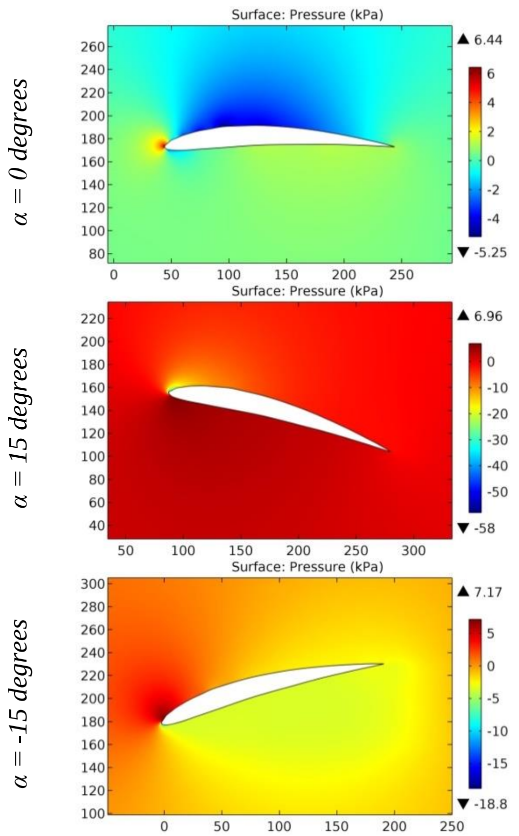

Figure 87. The pressure contours on the surfaces of the Miser airfoil.

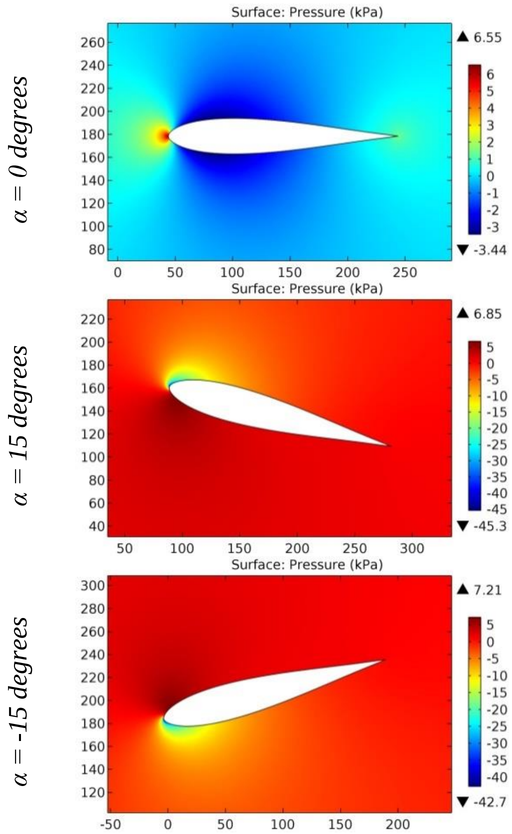

Figure 88. The pressure contours on the surfaces of the Misto 50-50 S1046-S8035 airfoil.

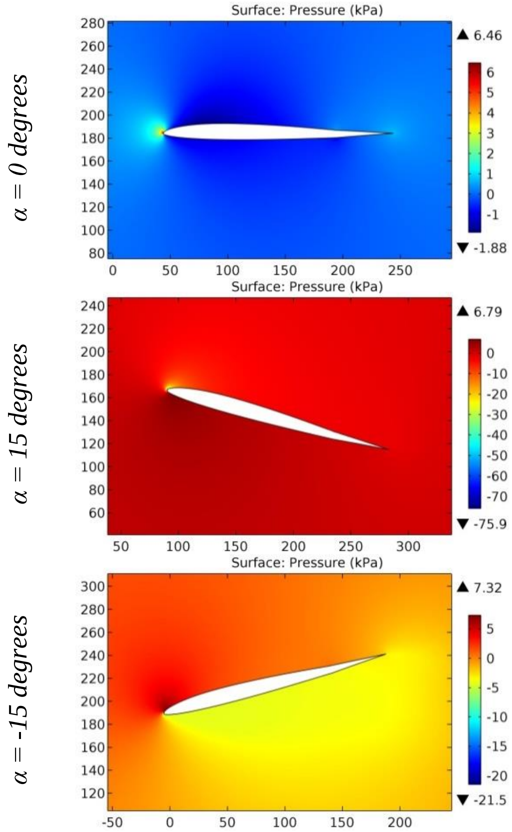

Figure 89. The pressure contours on the surfaces of the mjp711f-3 airfoil.

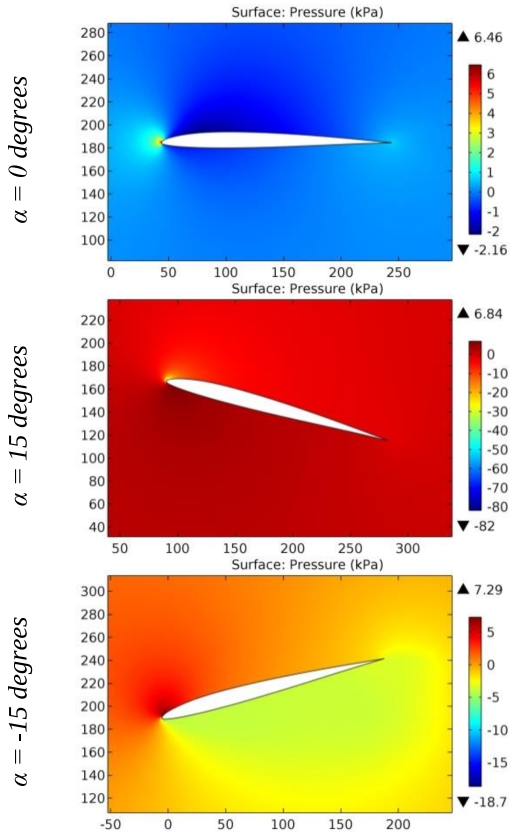

Figure 90. The pressure contours on the surfaces of the mjp712 airfoil.

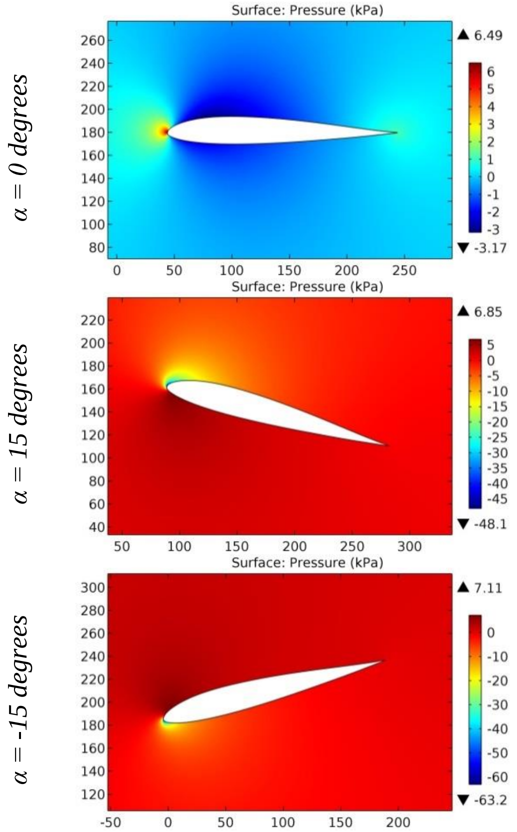

Figure 91. The pressure contours on the surfaces of the mjz 1211 airfoil.

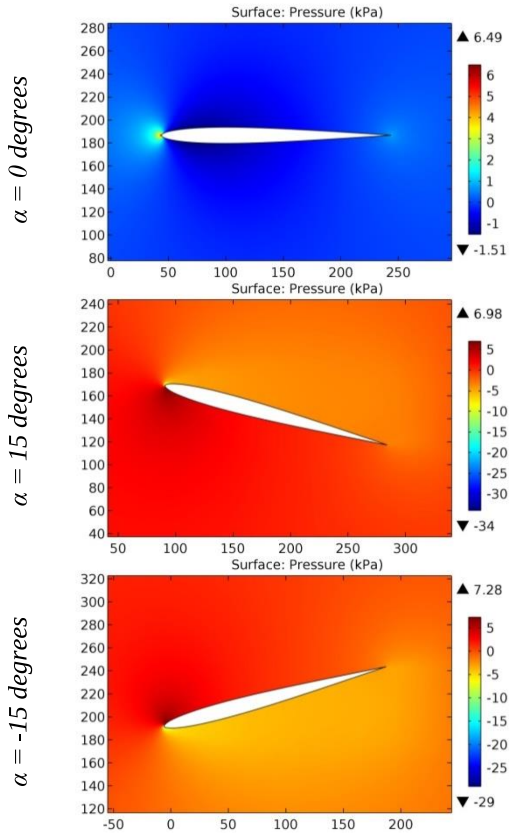

Figure 92. The pressure contours on the surfaces of the MM 007 airfoil.

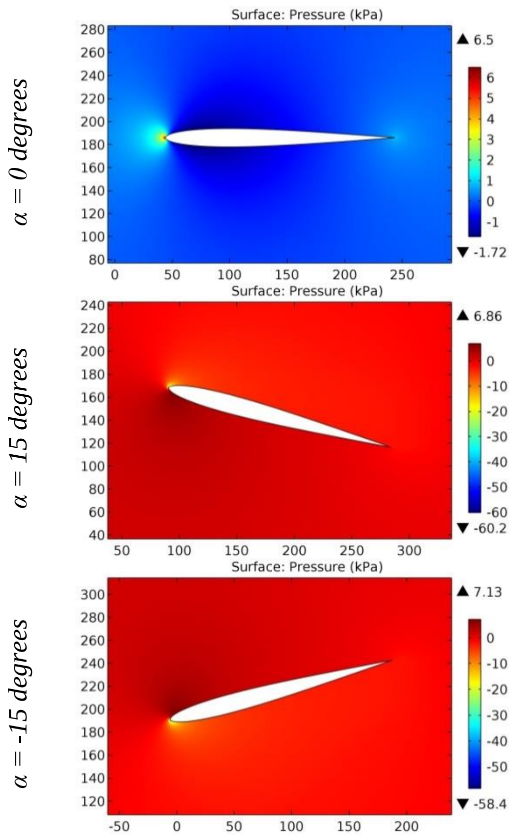

Figure 93. The pressure contours on the surfaces of the MM 008 airfoil.

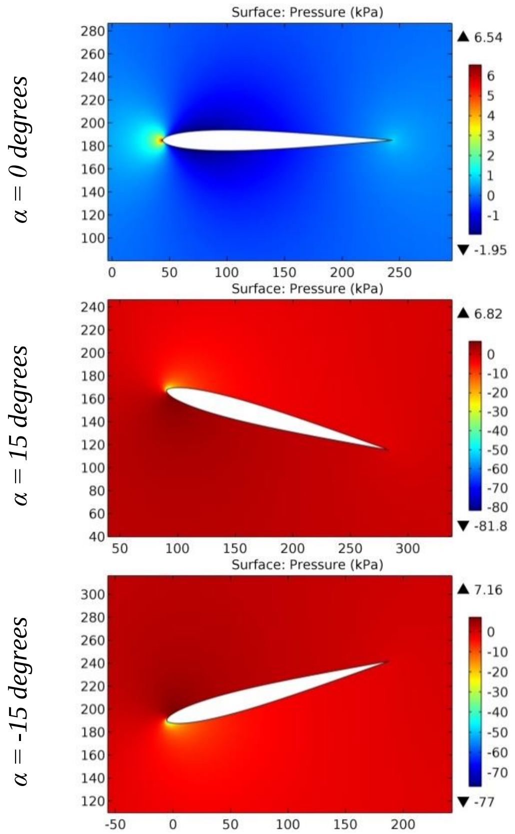

Figure 94. The pressure contours on the surfaces of the MM 009 airfoil.

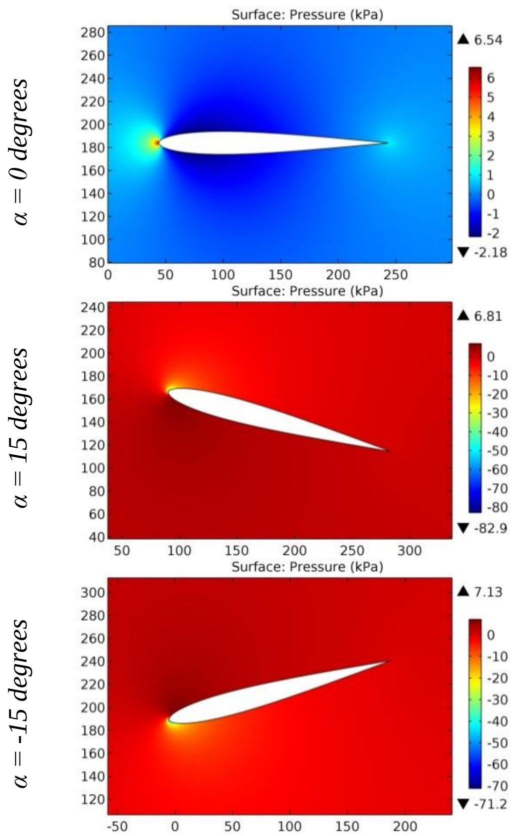

Figure 95. The pressure contours on the surfaces of the MM 010 airfoil.

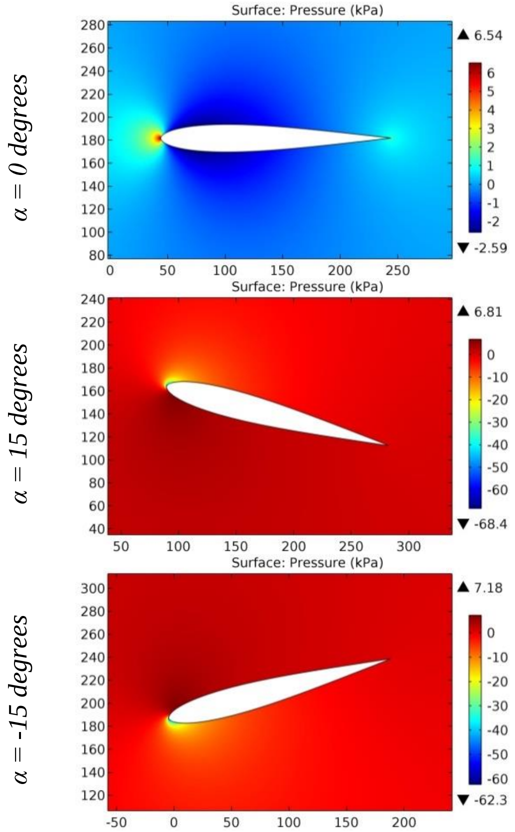

Figure 96. The pressure contours on the surfaces of the MM 012 airfoil.

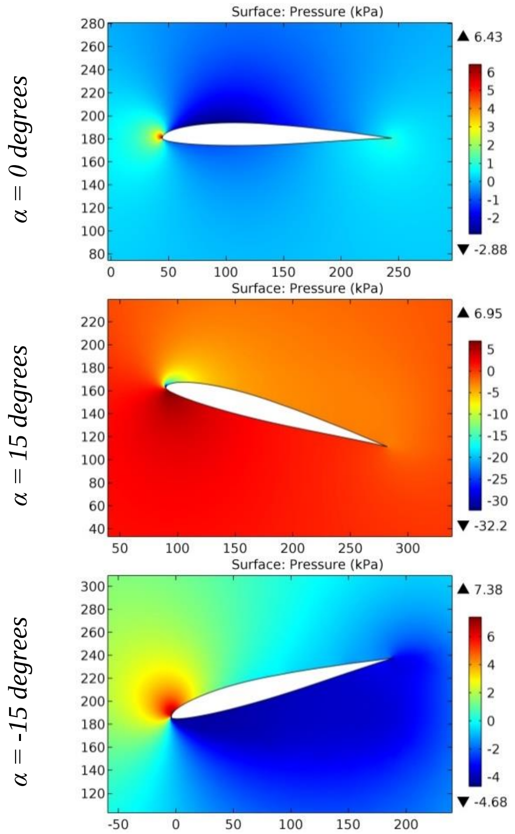

Figure 97. The pressure contours on the surfaces of the MM 1,75-10 airfoil.

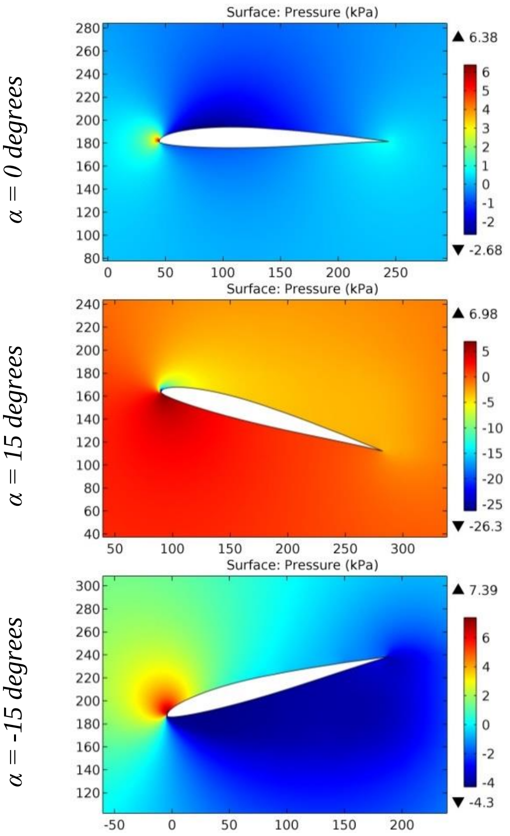

Figure 98. The pressure contours on the surfaces of the MM 1,75-9 airfoil.

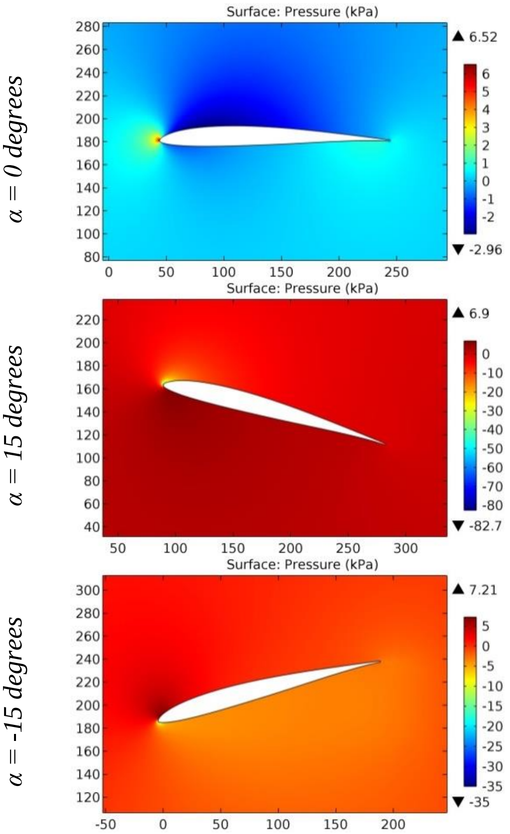

Figure 99. The pressure contours on the surfaces of the MM 100 airfoil.

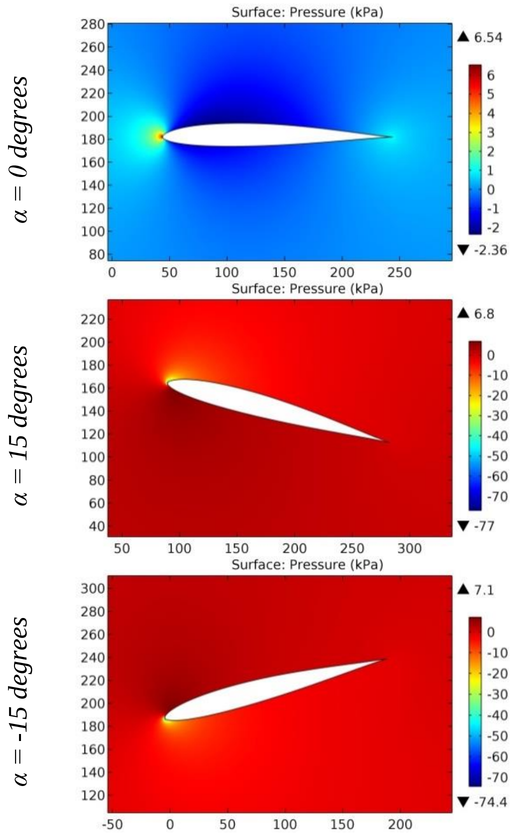

Figure 100. The pressure contours on the surfaces of the MM 1010a airfoil.

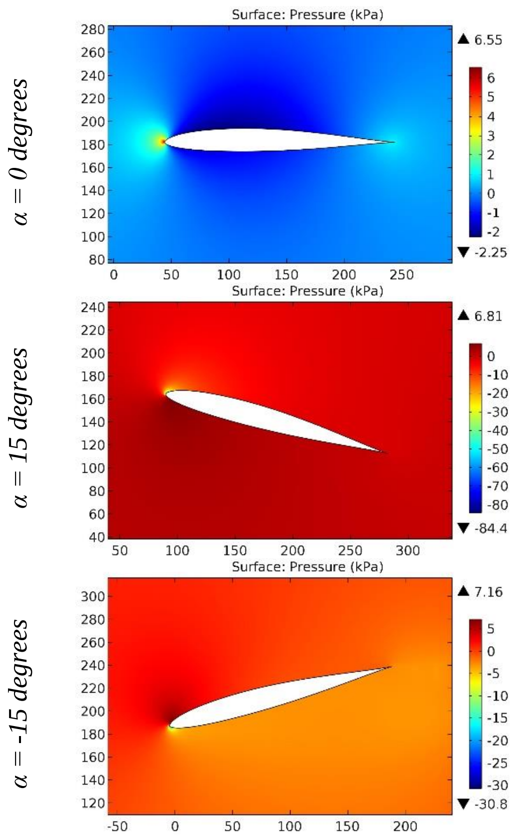

Figure 101. The pressure contours on the surfaces of the MM 1010b airfoil.

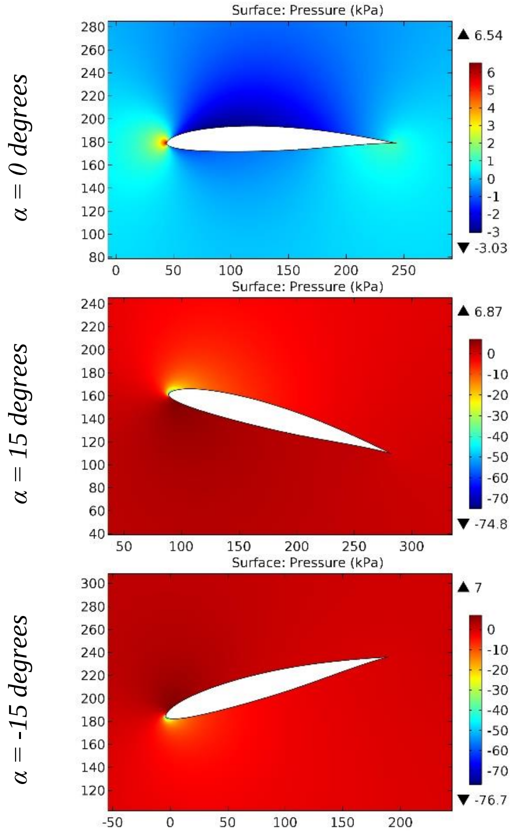

Figure 102. The pressure contours on the surfaces of the MM 1100 airfoil.

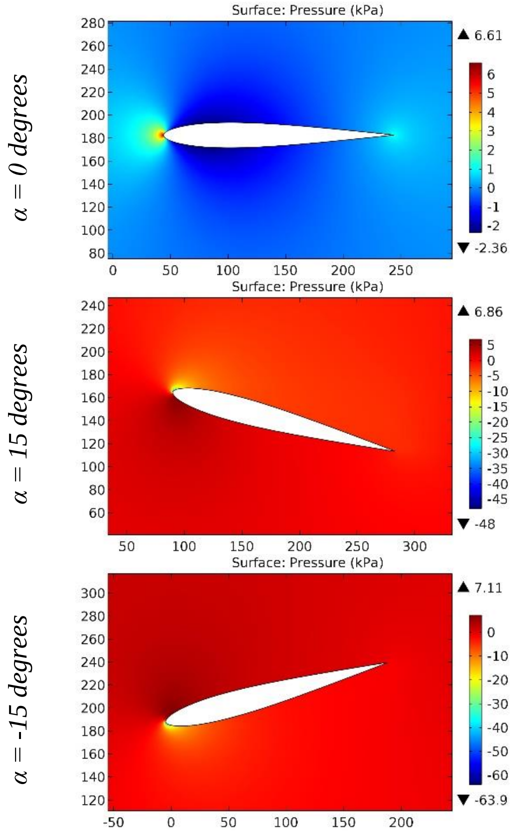

Figure 103. The pressure contours on the surfaces of the MM 11-29 airfoil.

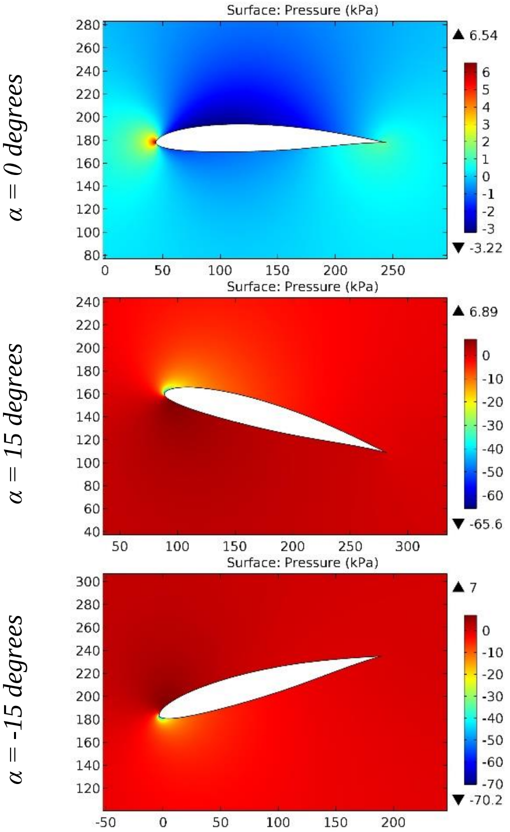

Figure 104. The pressure contours on the surfaces of the MM 1200 airfoil.

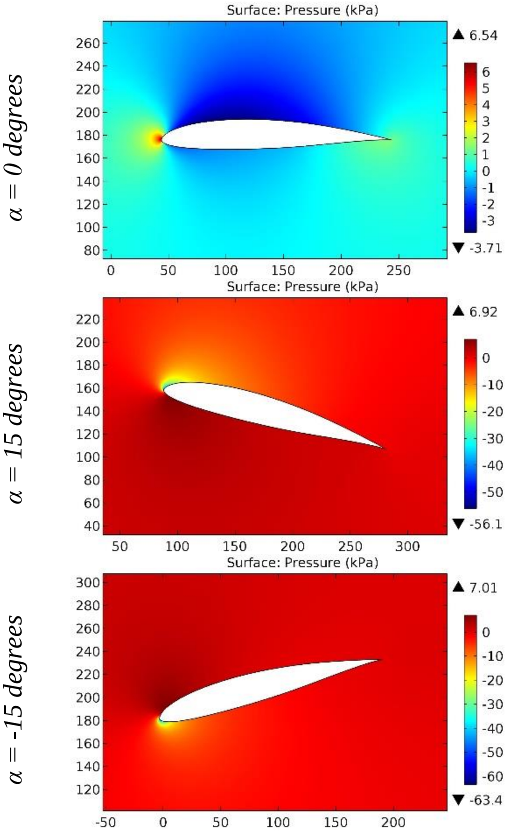

Figure 105. The pressure contours on the surfaces of the MM 1300 airfoil.

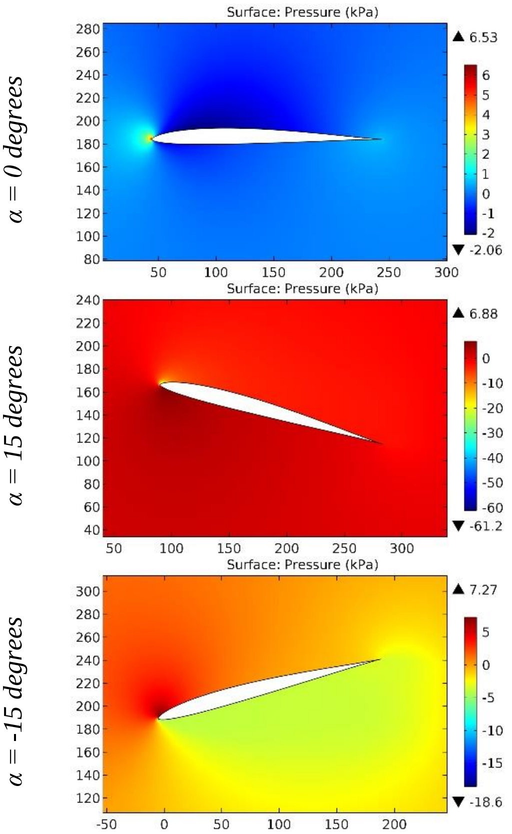

Figure 106. The pressure contours on the surfaces of the MM 1407 airfoil.

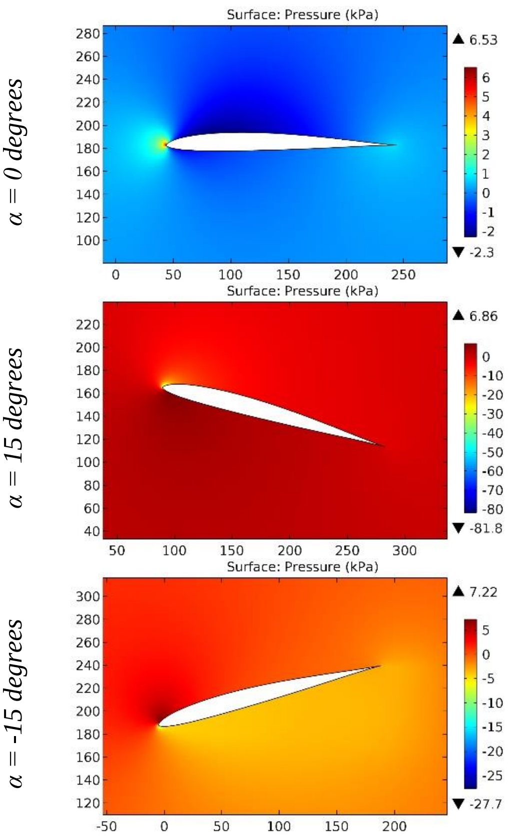

Figure 107. The pressure contours on the surfaces of the MM 1608 airfoil.

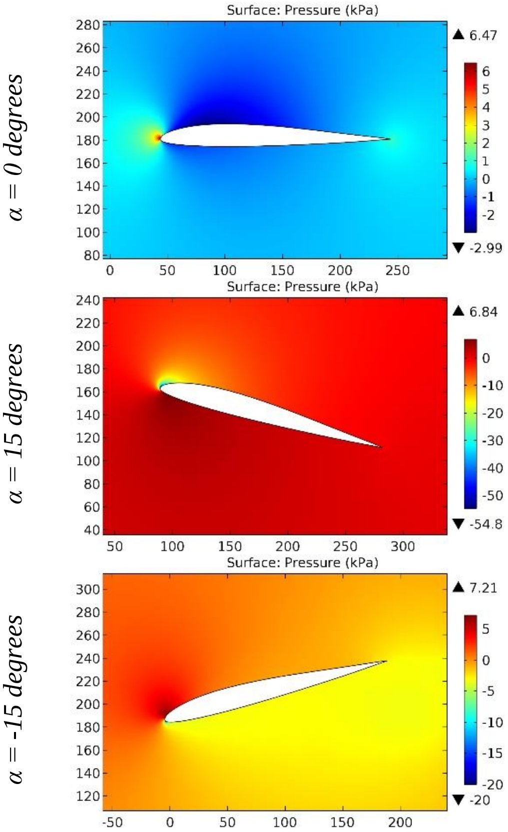

Figure 108. The pressure contours on the surfaces of the MM 1609 airfoil.

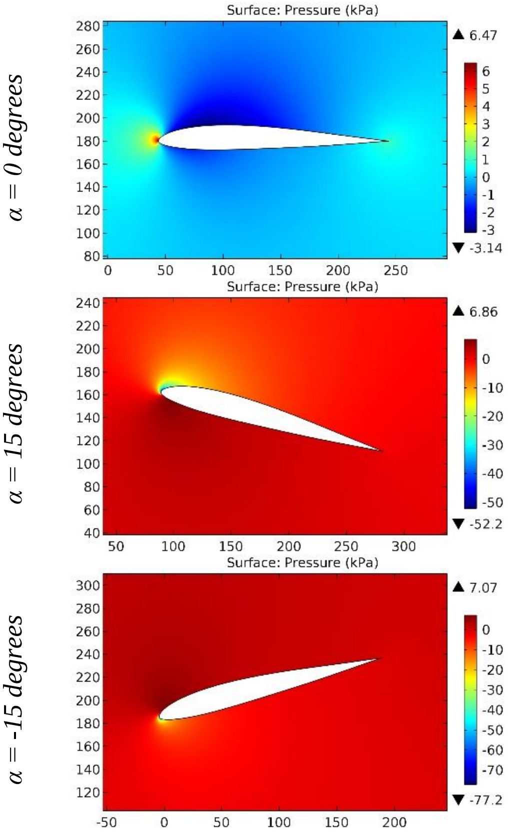

Figure 109. The pressure contours on the surfaces of the MM 1710 airfoil.

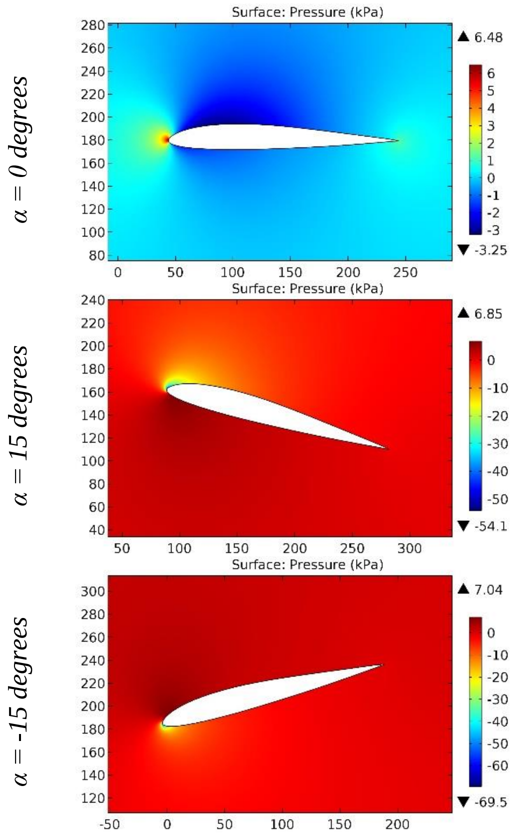

Figure 110. The pressure contours on the surfaces of the MM 1711 airfoil.

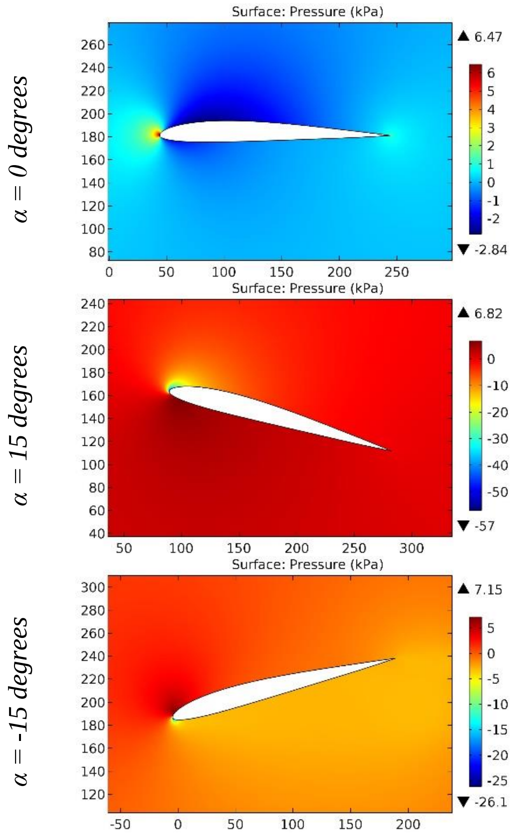

Figure 111. The pressure contours on the surfaces of the MM 1809 airfoil.

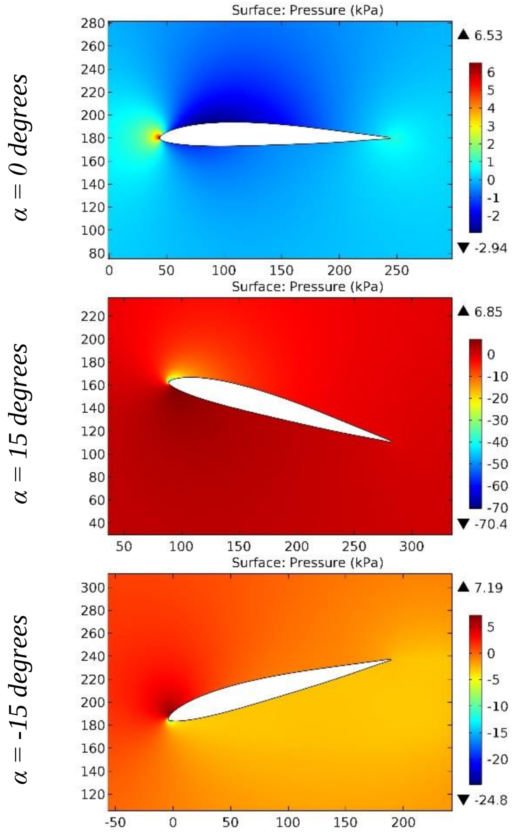

Figure 112. The pressure contours on the surfaces of the MM 1810 airfoil.

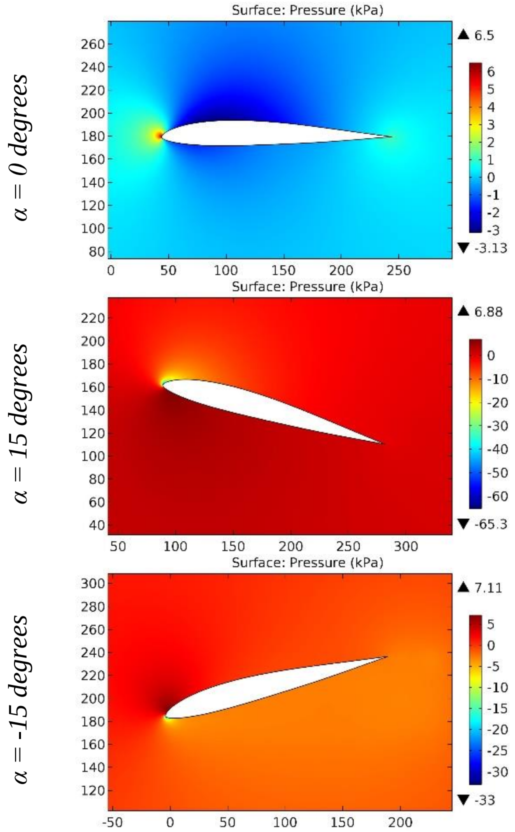

Figure 113. The pressure contours on the surfaces of the MM 1811b airfoil.

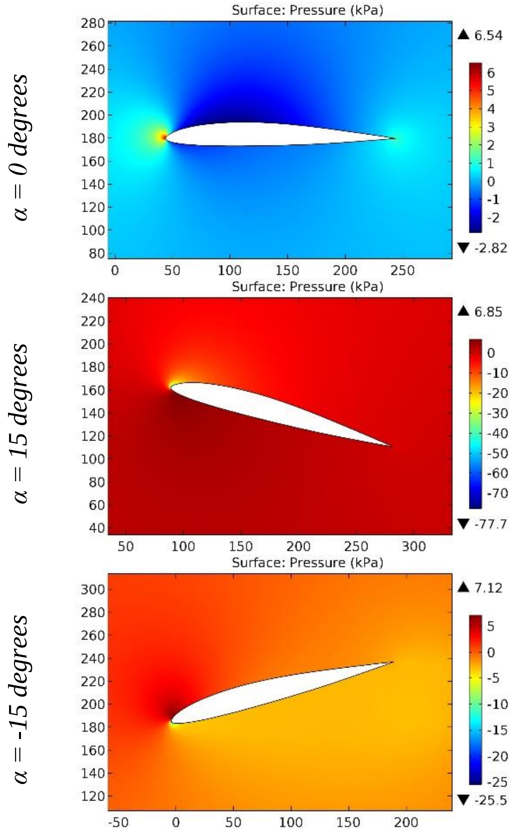

Figure 114. The pressure contours on the surfaces of the MM 1910 airfoil.

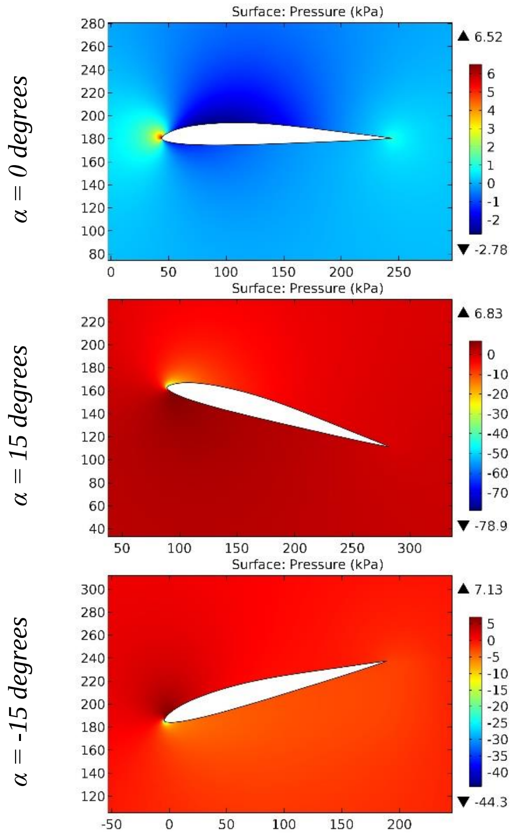

Figure 115. The pressure contours on the surfaces of the MM 1995 airfoil.

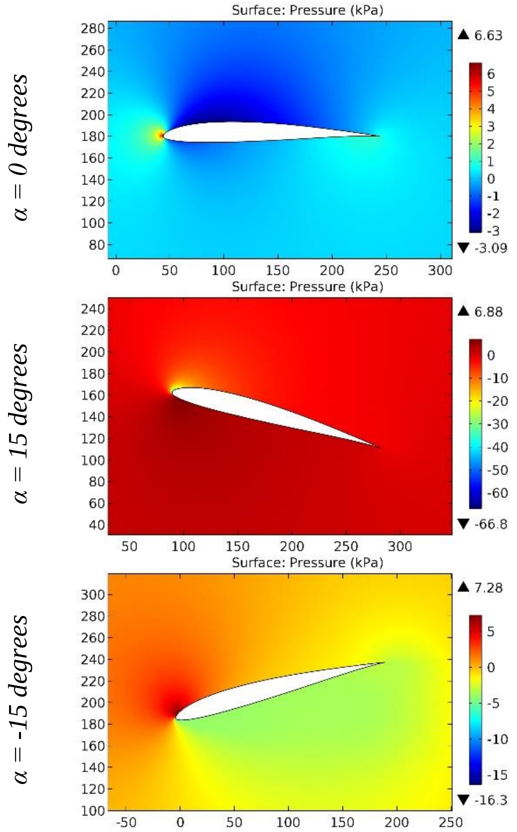

Figure 116. The pressure contours on the surfaces of the MM 200 airfoil.

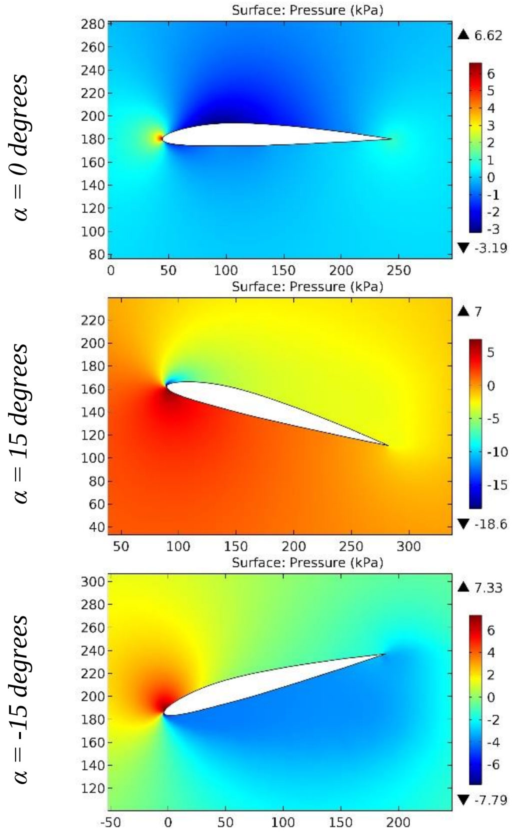

Figure 117. The pressure contours on the surfaces of the MM 2-10 a airfoil.

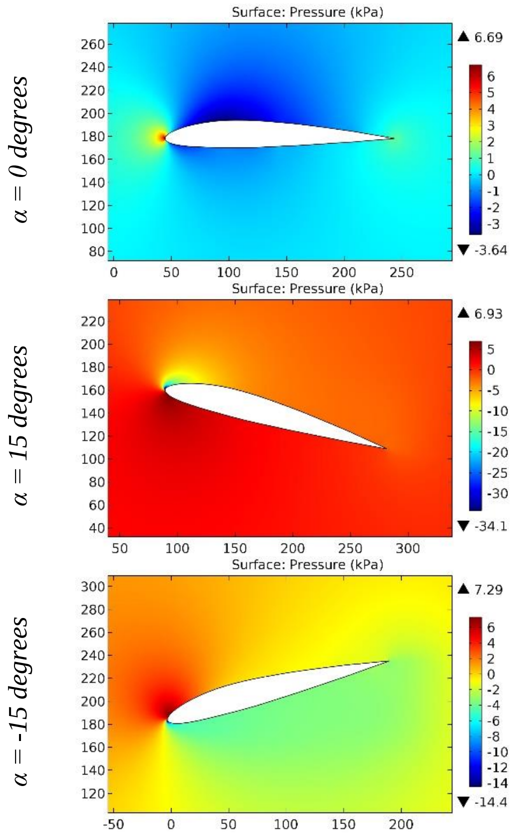

Figure 118. The pressure contours on the surfaces of the MM 2-12 airfoil.

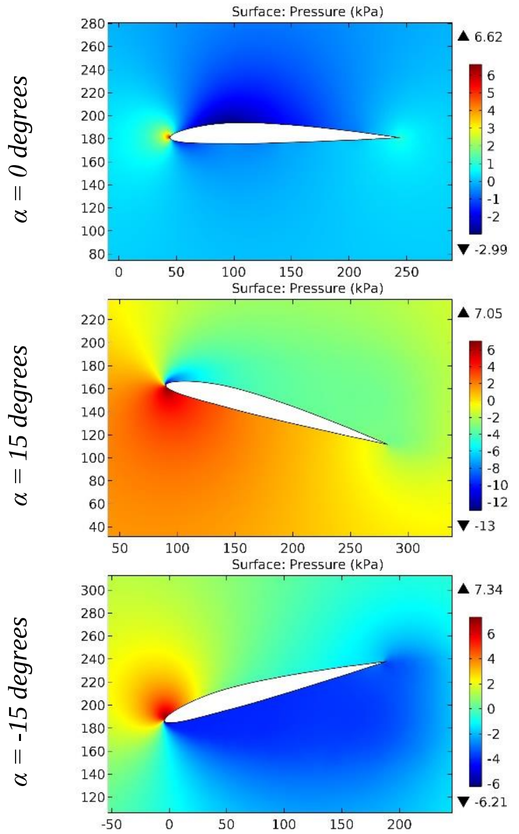

Figure 119. The pressure contours on the surfaces of the MM 2-9 airfoil.

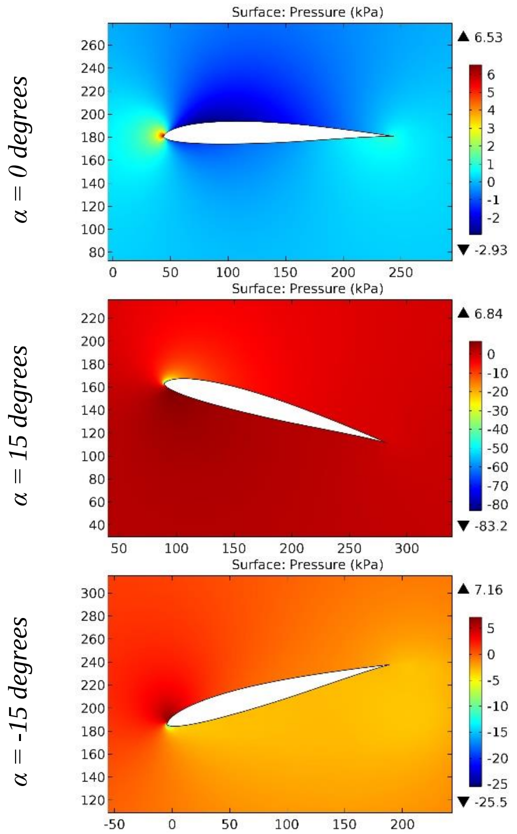

Figure 120. The pressure contours on the surfaces of the MM 300 airfoil.

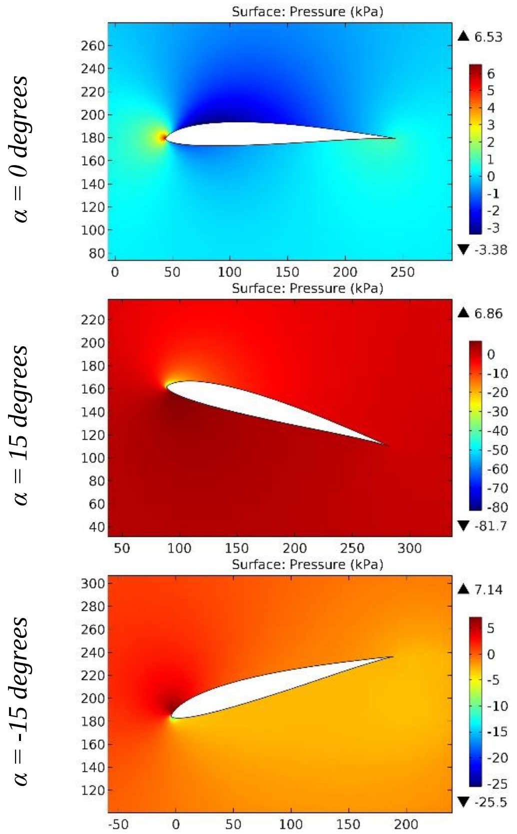

Figure 121. The pressure contours on the surfaces of the MM 400 airfoil.

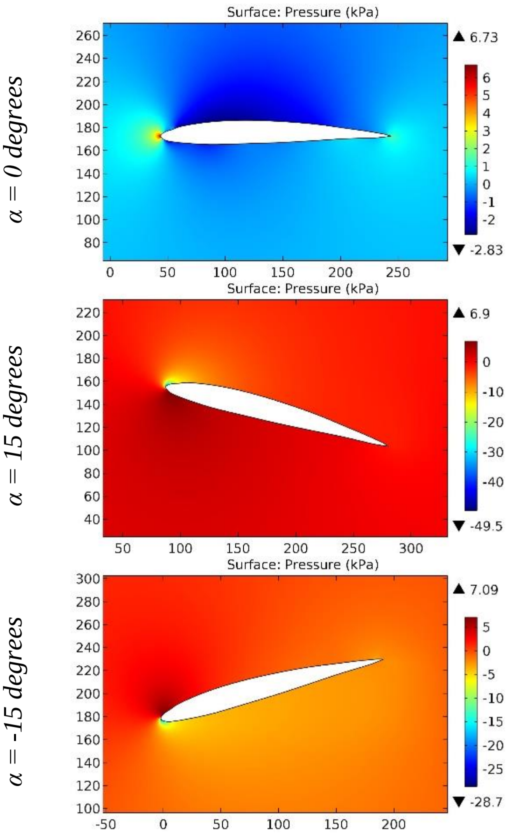

Figure 122. The pressure contours on the surfaces of the Mosca 317 airfoil.

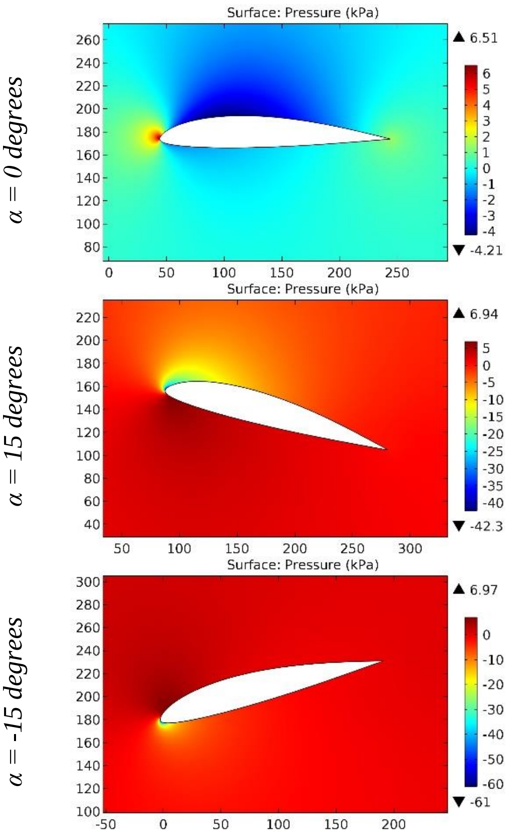

Figure 123. The pressure contours on the surfaces of the MRC-16 airfoil.

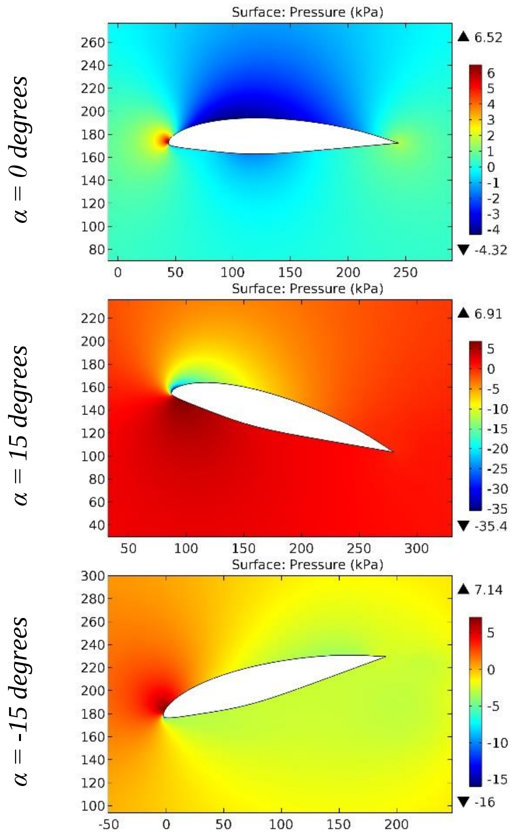

Figure 124. The pressure contours on the surfaces of the MRC-20 airfoil.

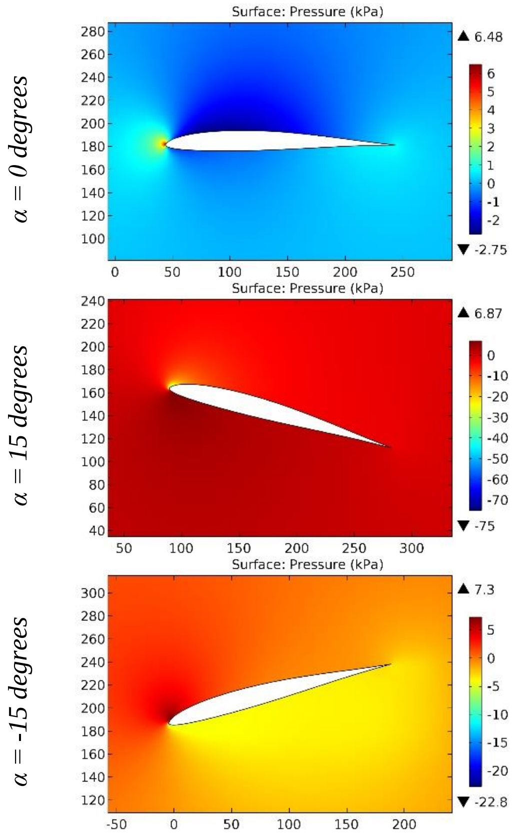

Figure 125. The pressure contours on the surfaces of the ms1,9-8,7 airfoil.

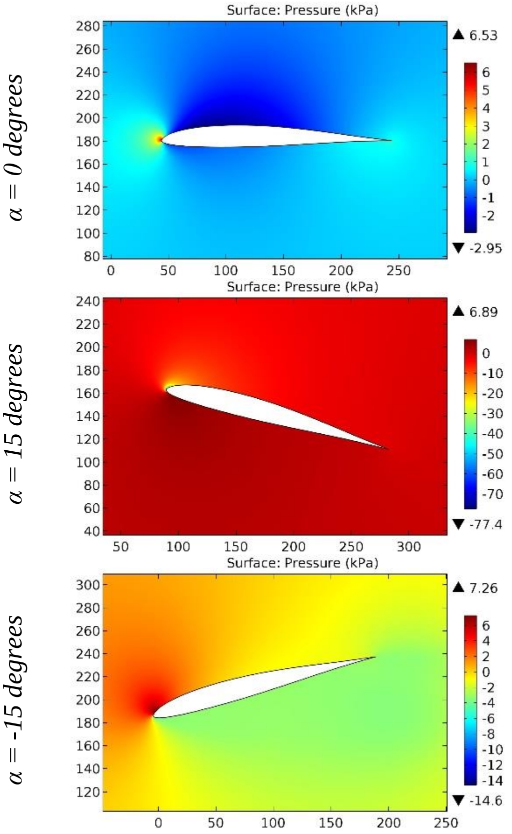

Figure 126. The pressure contours on the surfaces of the ms2-9,5 airfoil.

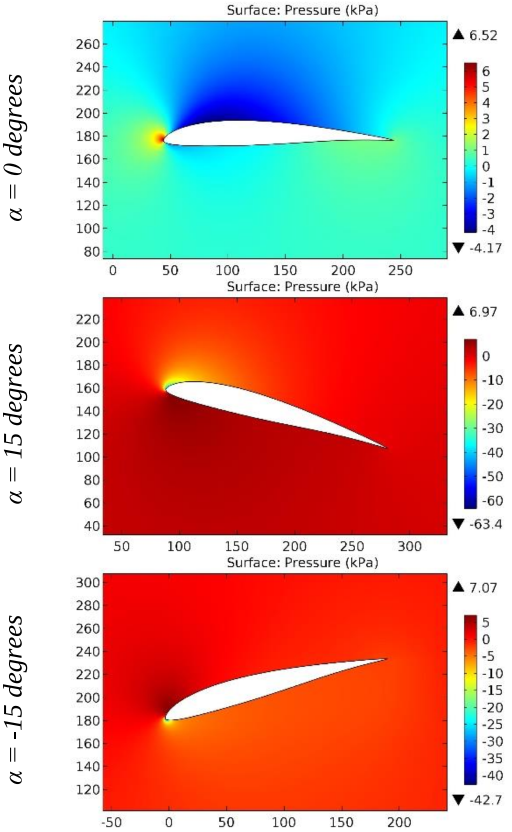

Figure 127. The pressure contours on the surfaces of the MS3,3-11GP airfoil.

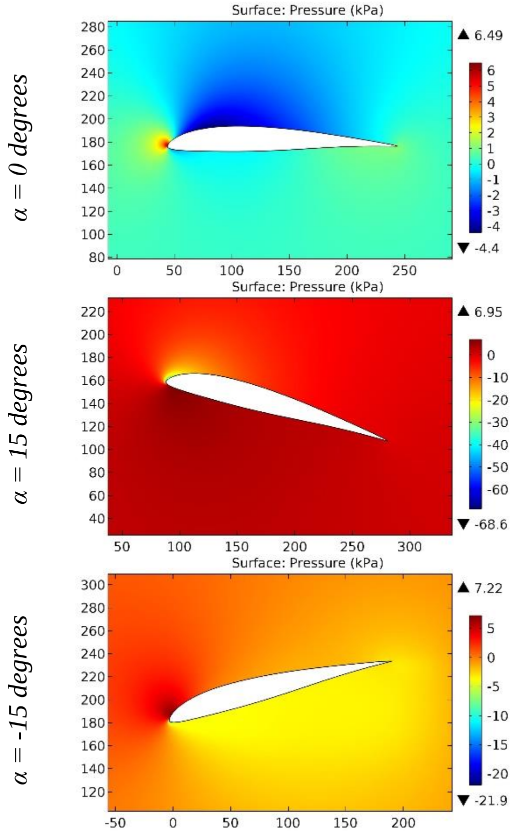

Figure 128. The pressure contours on the surfaces of the MS3,3-11GPT airfoil.

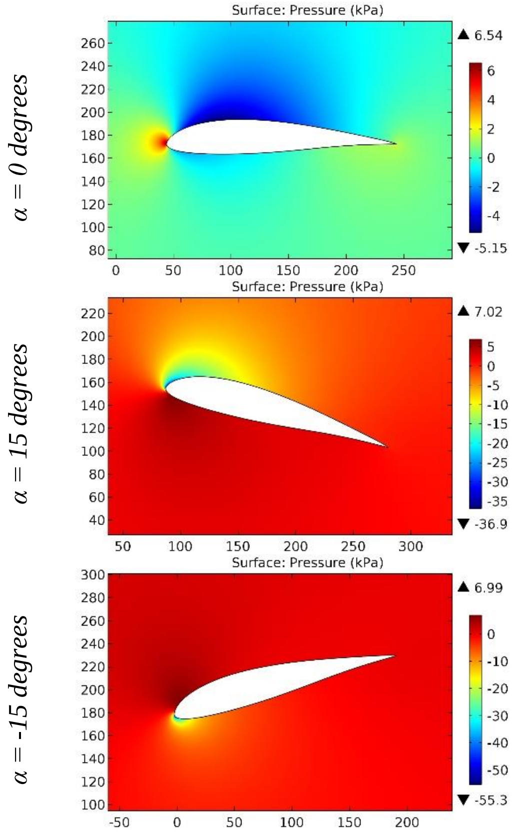

Figure 129. The pressure contours on the surfaces of the MS3,3-15GP airfoil.

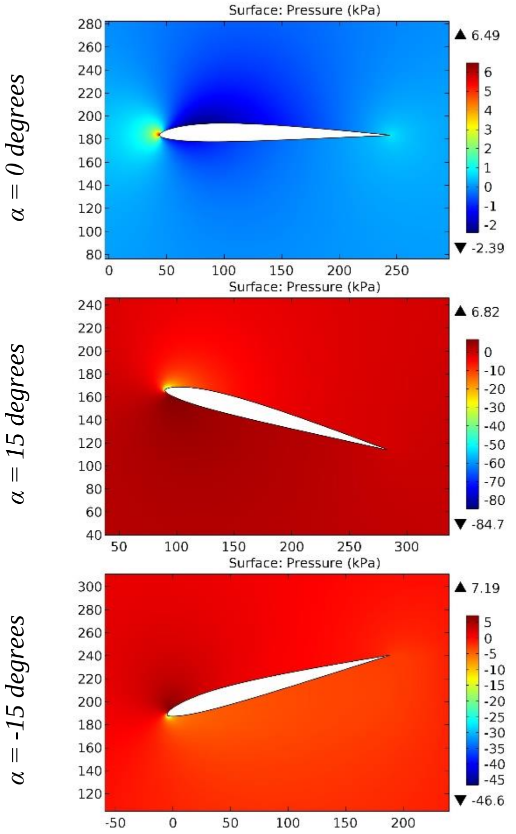

Figure 130. The pressure contours on the surfaces of the msa812 airfoil.

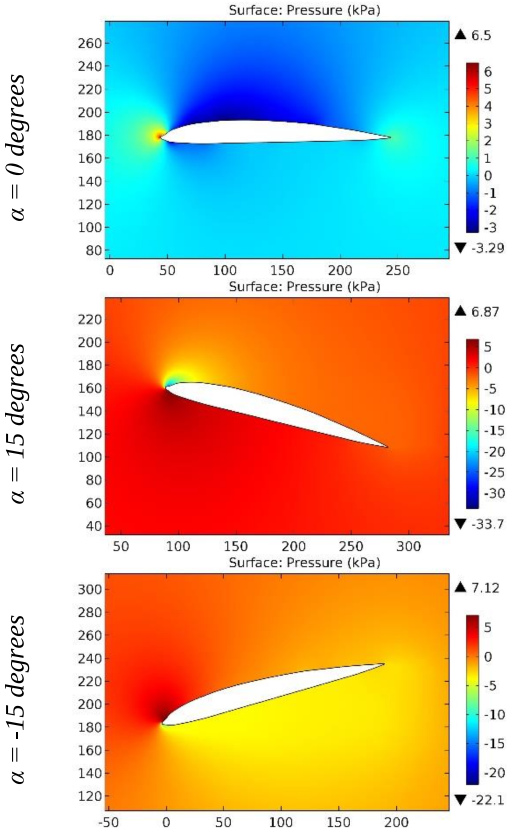

Figure 131. The pressure contours on the surfaces of the MT172 airfoil.

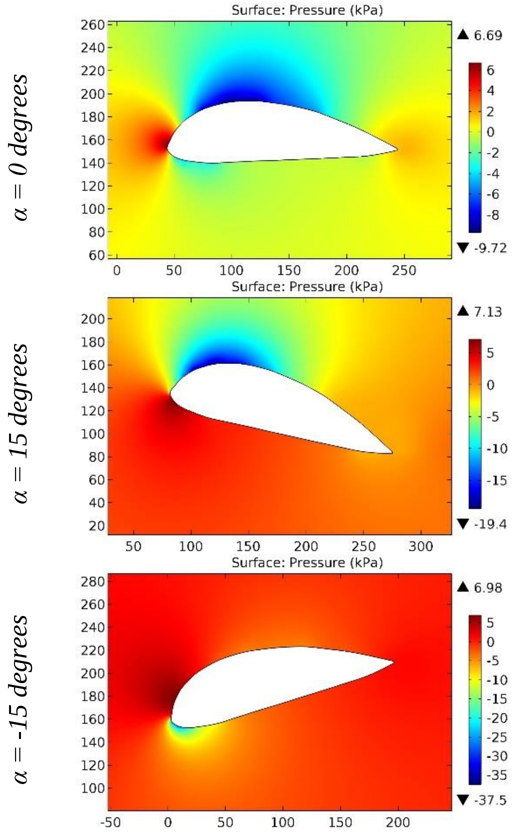

Figure 132. The pressure contours on the surfaces of the MT722 airfoil.

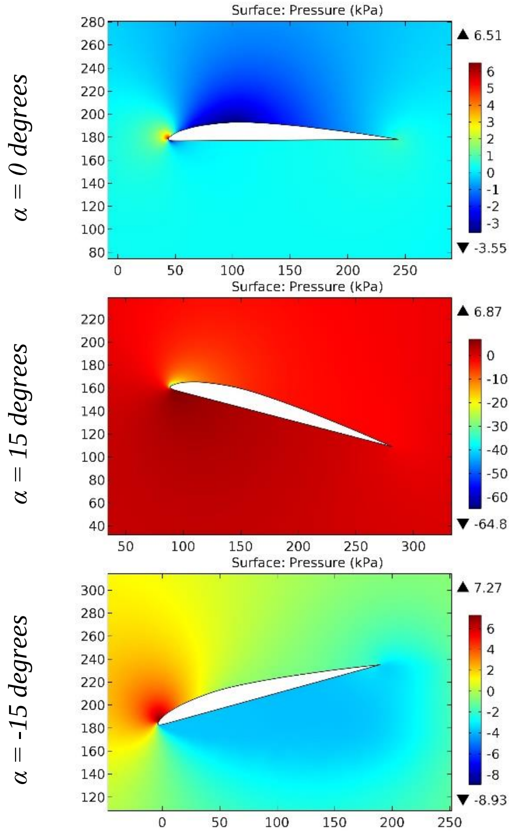

Figure 133. The pressure contours on the surfaces of the MVA-101M airfoil.

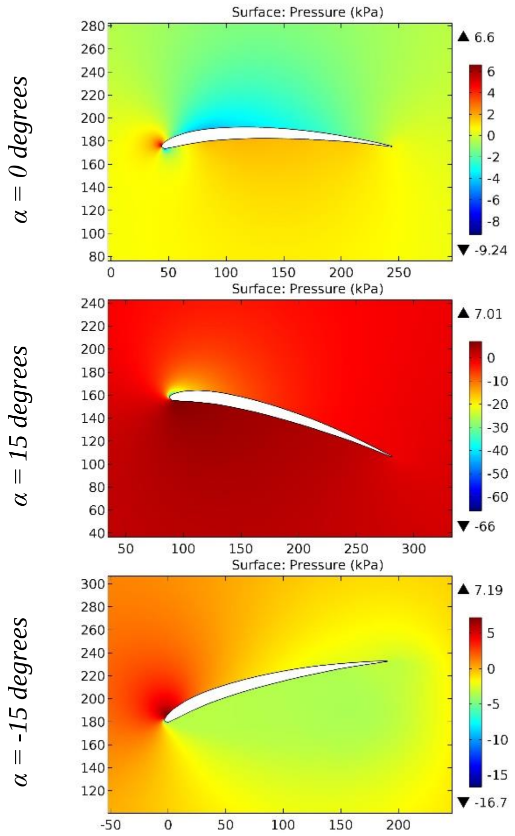

Figure 134. The pressure contours on the surfaces of the MVA-123 airfoil.

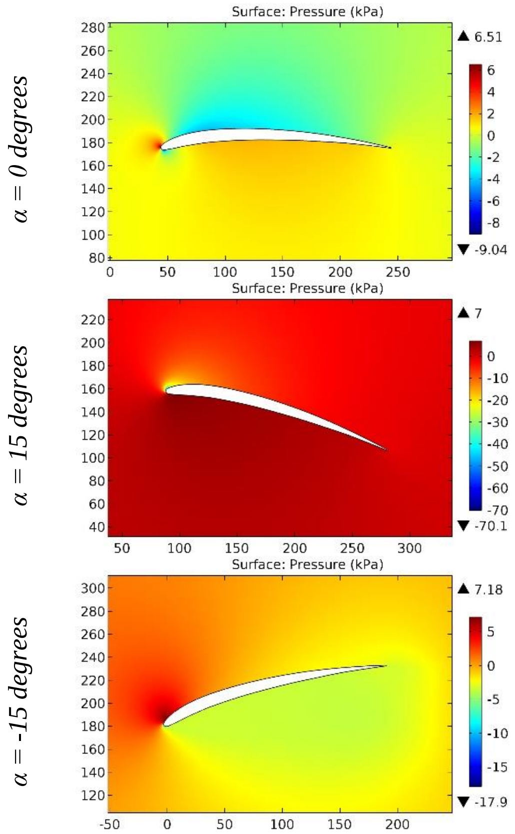

Figure 135. The pressure contours on the surfaces of the MVA-123M airfoil.

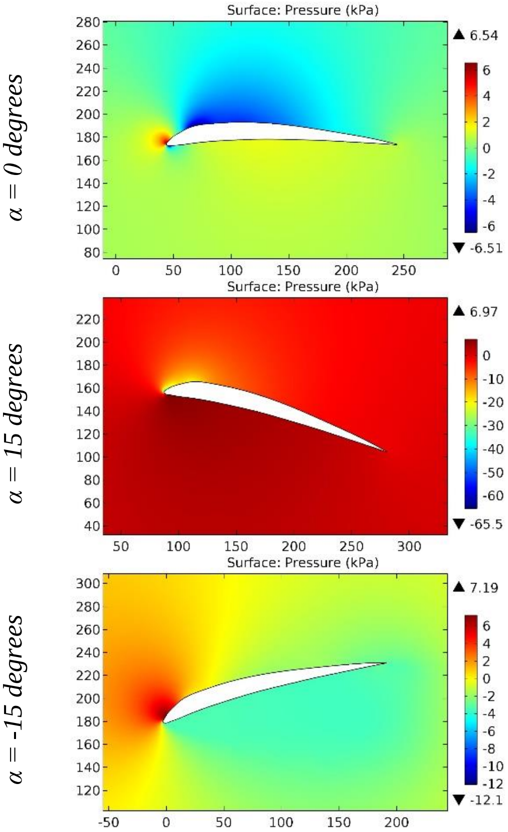

Figure 136. The pressure contours on the surfaces of the MVA-173 airfoil.

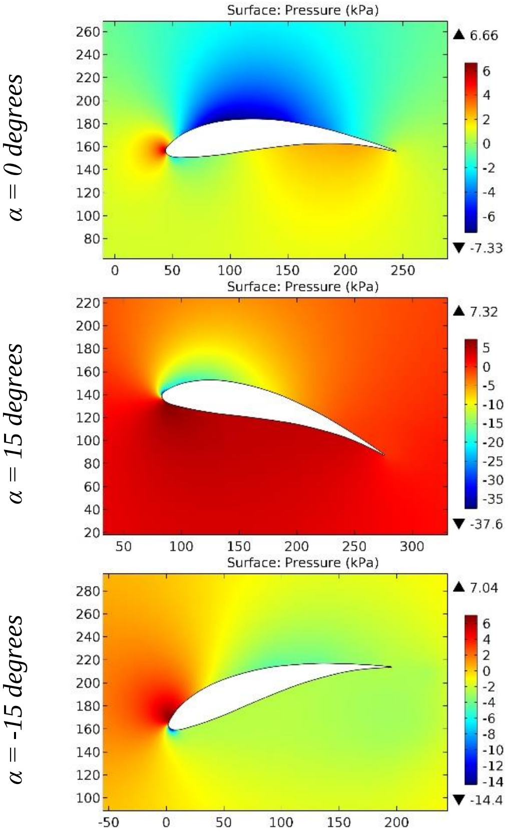

Figure 137. The pressure contours on the surfaces of the MVA-227 airfoil.

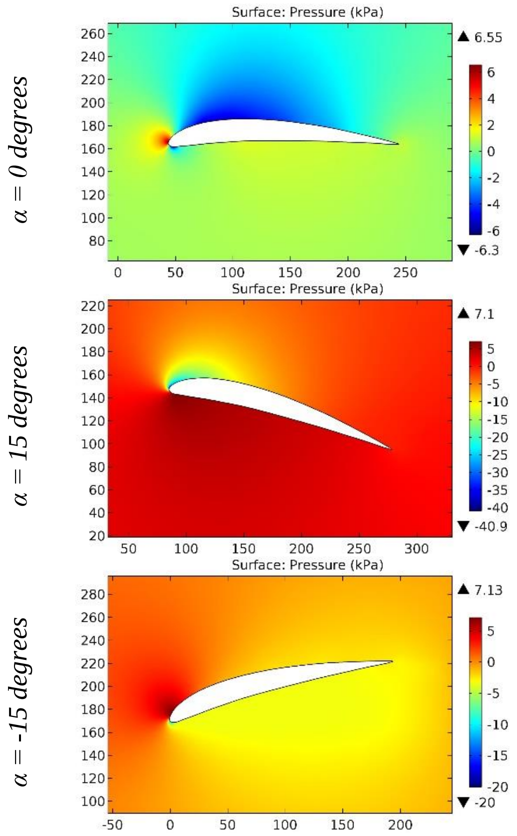

Figure 138. The pressure contours on the surfaces of the MVA-301 airfoil.

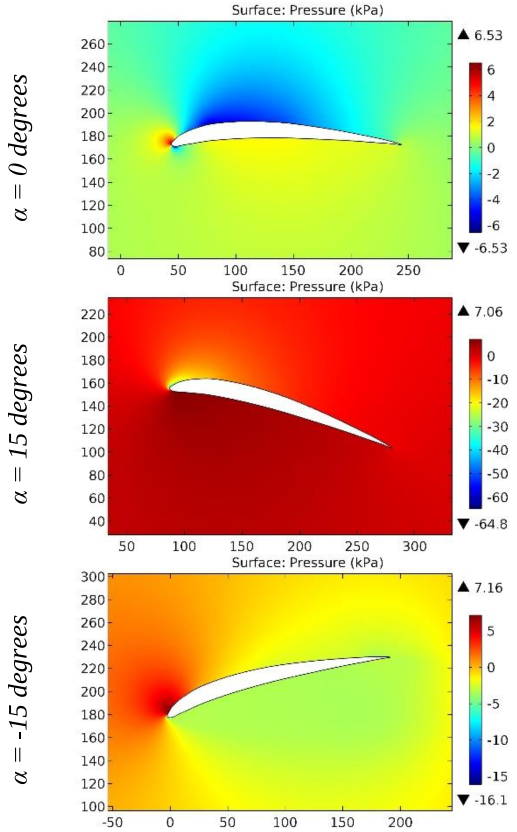

Figure 139. The pressure contours on the surfaces of the MVA30175 airfoil.

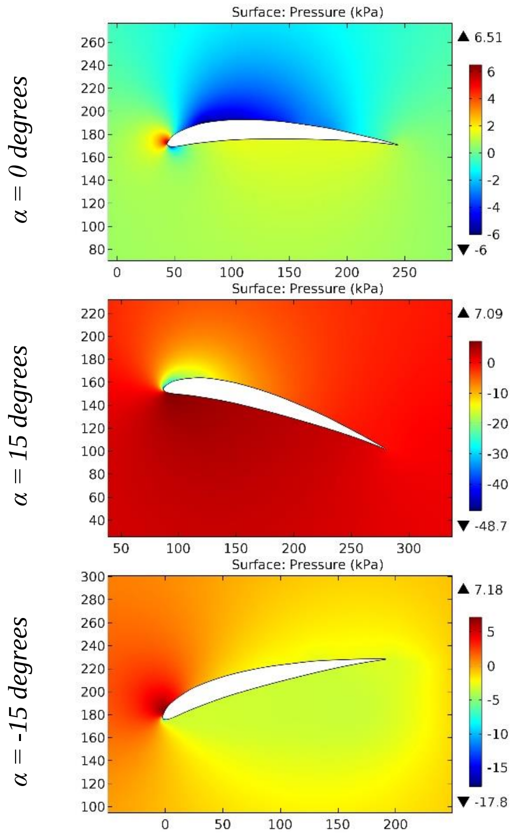

Figure 140. The pressure contours on the surfaces of the MVA-301M airfoil.

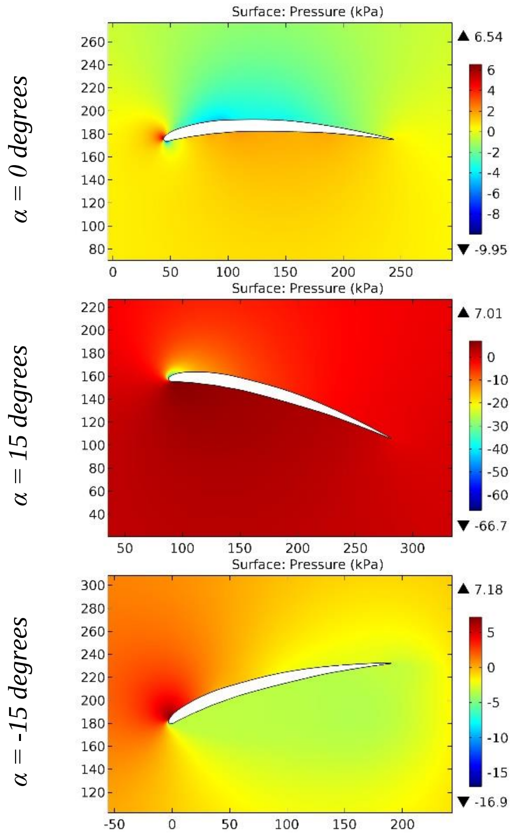

Figure 141. The pressure contours on the surfaces of the MVA-342 airfoil.

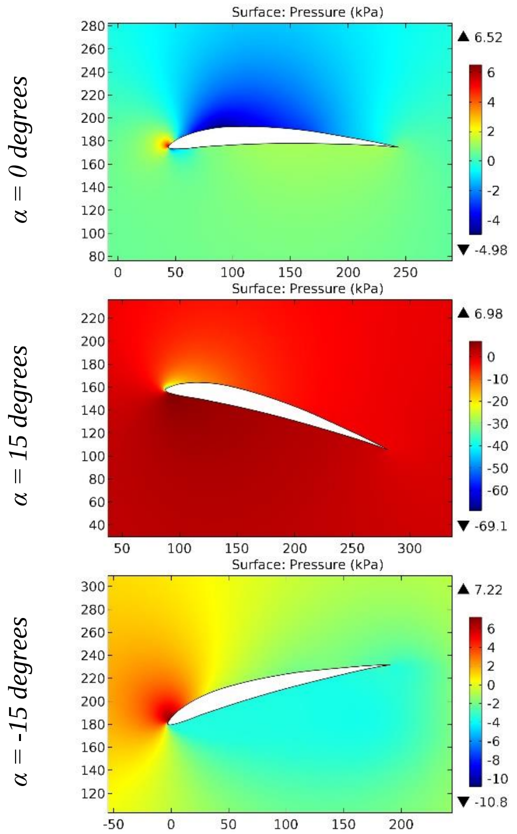

Figure 142. The pressure contours on the surfaces of the MVA-439 airfoil.

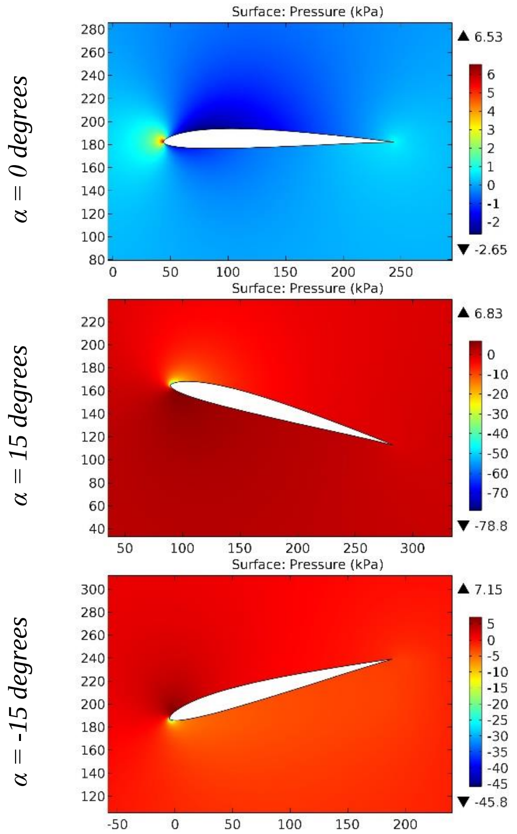

Figure 143. The pressure contours on the surfaces of the mve8.516 airfoil.

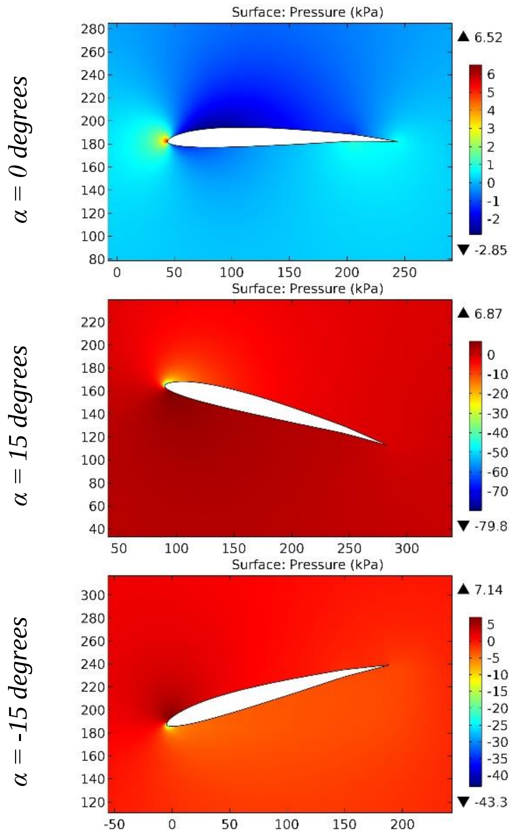

Figure 144. The pressure contours on the surfaces of the mve8516 f 3 airfoil.

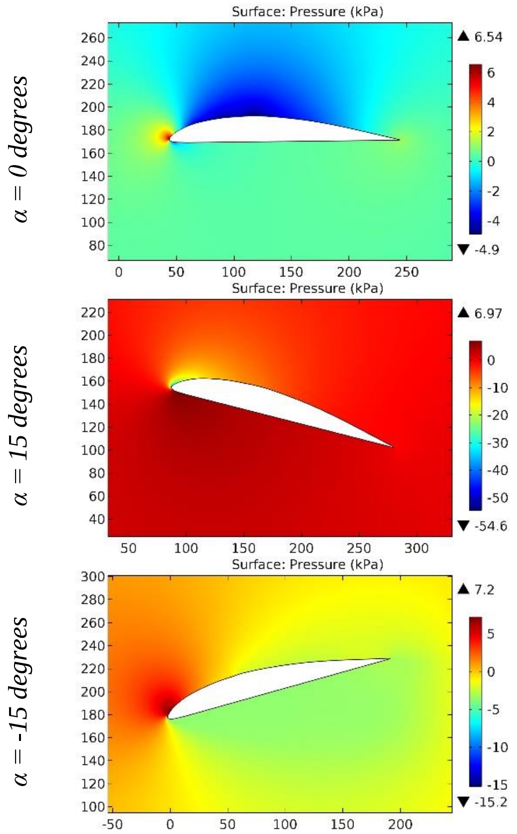

Figure 145. The pressure contours on the surfaces of the MZ 5411 airfoil.

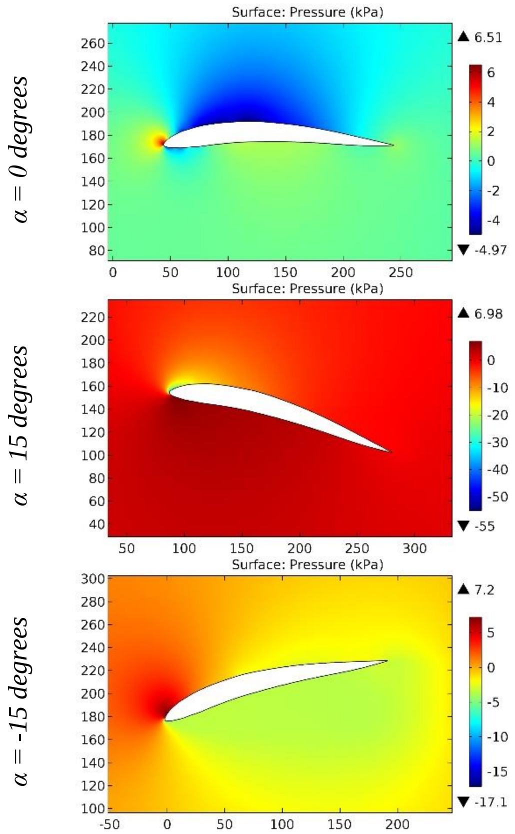

Figure 146. The pressure contours on the surfaces of the MZ 6409 airfoil.

Conclusion

Computer simulation makes it possible to determine the aerodynamic characteristics of the airplane wings under normal weather conditions. The presented calculated pressure contours, conjugated with the surfaces of the airfoils, create a complete picture of the influence of the geometry of the airfoil on the lift and drag value. Thus, the results of the calculation are relevant for choosing the advantageous configuration of the airfoil of the airplane wing under certain flight conditions, for example, the development of the maximum speed of horizontal flight. For all the considered airfoils, the greatest value of positive pressure occurs during the airplane descent, and the greatest value of negative pressure occurs both during the airplane climb and during the airplane descent.

References:

1. Anderson, J. D. (2010). *Fundamentals of Aerodynamics*. McGraw-Hill, Fifth edition.
2. Shevell, R. S. (1989). *Fundamentals of Flight*. Prentice Hall, Second edition.
3. Houghton, E. L., & Carpenter, P. W. (2003). *Aerodynamics for Engineering Students*. Fifth edition, Elsevier.
4. Lan, E. C. T., & Roskam, J. (2003). *Airplane Aerodynamics and Performance*. DAR Corp.
5. Sadraey, M. (2009). *Aircraft Performance Analysis*. VDM Verlag Dr. Müller.
6. Anderson, J. D. (1999). *Aircraft Performance and Design*. McGraw-Hill.
7. Roskam, J. (2007). *Airplane Flight Dynamics and Automatic Flight Control*, Part I. DAR Corp.
8. Etkin, B., & Reid, L. D. (1996). *Dynamics of Flight, Stability and Control*. Third Edition, Wiley.
9. Stevens, B. L., & Lewis, F. L. (2003). *Aircraft Control and Simulation*. Second Edition, Wiley.
10. Chemezov, D., et al. (2021). Pressure distribution on the surfaces of the NACA 0012 airfoil under conditions of changing the angle of attack. *ISJ Theoretical & Applied Science*, 09 (101), 601-606.

11. Chemezov, D., et al. (2021). Stressed state of surfaces of the NACA 0012 airfoil at high angles of attack. *ISJ Theoretical & Applied Science*, 10 (102), 601-604.
12. Chemezov, D., et al. (2021). Reference data of pressure distribution on the surfaces of airfoils having the names beginning with the letter A (the first part). *ISJ Theoretical & Applied Science*, 10 (102), 943-958.
13. Chemezov, D., et al. (2021). Reference data of pressure distribution on the surfaces of airfoils having the names beginning with the letter A (the second part). *ISJ Theoretical & Applied Science*, 11 (103), 656-675.
14. Chemezov, D., et al. (2021). Reference data of pressure distribution on the surfaces of airfoils having the names beginning with the letter B. *ISJ Theoretical & Applied Science*, 11 (103), 1001-1076.
15. Chemezov, D., et al. (2021). Reference data of pressure distribution on the surfaces of airfoils having the names beginning with the letter C. *ISJ Theoretical & Applied Science*, 12 (104), 814-844.
16. Chemezov, D., et al. (2021). Reference data of pressure distribution on the surfaces of airfoils having the names beginning with the letter D. *ISJ Theoretical & Applied Science*, 12 (104), 1244-1274.
17. Chemezov, D., et al. (2022). Reference data of pressure distribution on the surfaces of airfoils (hydrofoils) having the names beginning with the letter E (the first part). *ISJ Theoretical & Applied Science*, 01 (105), 501-569.
18. Chemezov, D., et al. (2022). Reference data of pressure distribution on the surfaces of airfoils (hydrofoils) having the names beginning with the letter E (the second part). *ISJ Theoretical & Applied Science*, 01 (105), 601-671.
19. Chemezov, D., et al. (2022). Reference data of pressure distribution on the surfaces of airfoils having the names beginning with the letter F. *ISJ Theoretical & Applied Science*, 02 (106), 101-135.
20. Chemezov, D., et al. (2022). Reference data of pressure distribution on the surfaces of airfoils having the names beginning with the letter G (the first part). *ISJ Theoretical & Applied Science*, 03 (107), 701-784.
21. Chemezov, D., et al. (2022). Reference data of pressure distribution on the surfaces of airfoils having the names beginning with the letter G (the second part). *ISJ Theoretical & Applied Science*, 03 (107), 901-984.
22. Chemezov, D., et al. (2022). Reference data of pressure distribution on the surfaces of airfoils having the names beginning with the letter G (the third part). *ISJ Theoretical & Applied Science*, 04 (108), 401-484.
23. Chemezov, D., et al. (2022). Reference data of pressure distribution on the surfaces of airfoils having the names beginning with the letter H (the first part). *ISJ Theoretical & Applied Science*, 05 (109), 201-258.
24. Chemezov, D., et al. (2022). Reference data of pressure distribution on the surfaces of airfoils having the names beginning with the letter H (the second part). *ISJ Theoretical & Applied Science*, 05 (109), 529-586.
25. Chemezov, D., et al. (2022). Reference data of pressure distribution on the surfaces of airfoils having the names beginning with the letter I. *ISJ Theoretical & Applied Science*, 06 (110), 1-7.
26. Chemezov, D., et al. (2022). Reference data of pressure distribution on the surfaces of airfoils having the names beginning with the letter J. *ISJ Theoretical & Applied Science*, 06 (110), 18-25.
27. Chemezov, D., et al. (2022). Reference data of pressure distribution on the surfaces of airfoils having the names beginning with the letter K. *ISJ Theoretical & Applied Science*, 07 (111), 1-10.
28. Chemezov, D., et al. (2022). Reference data of pressure distribution on the surfaces of airfoils having the names beginning with the letter L. *ISJ Theoretical & Applied Science*, 07 (111), 101-118.

Contents

Scientific publication

«ISJ Theoretical & Applied Science, USA» - Международный научный журнал зарегистрированный во Франции, и выходящий в электронном и печатном формате. **Препринт** журнала публикуется на сайте по мере поступления статей.

Все поданные авторами статьи в течении 1-го дня размещаются на сайте http://T-Science.org.

Печатный экземпляр рассылается авторам в течение 3 дней после 30 числа каждого месяца.

Импакт фактор журнала

Impact Factor	2013	2014	2015	2016	2017	2018	2019	2020	2021
Impact Factor JIF		1.500							
Impact Factor ISRA (India)		1.344				3.117	4.971		6.317
Impact Factor ISI (Dubai, UAE) based on International Citation Report (ICR)	0.307	0.829							1.582
Impact Factor GIF (Australia)	0.356	0.453	0.564						
Impact Factor SIS (USA)	0.438	0.912							
Impact Factor РИНЦ (Russia)		0.179	0.224	0.207	0.156	0.126		3.939	
Impact Factor ESJI (KZ) based on Eurasian Citation Report (ECR)		1.042	1.950	3.860	4.102	6.015	8.716	8.997	9.035
Impact Factor SJIF (Morocco)		2.031				5.667			7.184
Impact Factor ICV (Poland)		6.630							
Impact Factor PIF (India)		1.619	1.940						
Impact Factor IBI (India)			4.260						
Impact Factor OAJI (USA)						0.350			

Deadlines

	Steps of publication	Deadlines	
		min	max
1	Article delivered	-	
2	Plagiarism check	1 hour	2 hour
3	Review	1 day	30 days
4	Payment complete	-	
5	Publication of the article	1 day	5 days
	publication of the journal	30th of each month	
6	doi registration	before publication	
7	Publication of the journal	1 day	2 days
8	Shipping journals to authors	3 days	7 days
9	Database registration	5 days	6 months

INDEXING METADATA OF ARTICLES IN SCIENTOMETRIC BASES:

International Scientific Indexing ISI (Dubai, UAE)
http://isindexing.com/isi/journaldetails.php?id=327

Cl.An. // THOMSON REUTERS, EndNote (USA)
https://www.myendnoteweb.com/EndNoteWeb.html

Research Bible (Japan)
http://journalseeker.researchbib.com/?action=viewJournalDetails&issn=23084944&uid=rd1775

Scientific Object Identifier (SOI)
http://s-o-i.org/

РИНЦ (Russia)
http://elibrary.ru/contents.asp?issueid=1246197

Google Scholar (USA)
http://scholar.google.ru/scholar?q=Theoretical+t-science.org&btnG=&hl=ru&as_sdt=0%2C5

Turk Egitim Indeksi (Turkey)
http://www.turkegitimindeksi.com/Journals.aspx?ID=149

Directory of abstract indexing for Journals
http://www.daij.org/journal-detail.php?jid=94

DOI (USA) http://www.doi.org

CrossRef (USA) http://doi.crossref.org

Open Academic Journals Index (Russia)
http://oaji.net/journal-detail.html?number=679

Collective IP (USA)
https://www.collectiveip.com/

Japan Link Center (Japan) https://japanlinkcenter.org

PFTS Europe/Rebus:list (United Kingdom)
http://www.rebuslist.com

Kudos Innovations, Ltd. (USA)
https://www.growkudos.com

Korean Federation of Science and Technology Societies (Korea)
http://www.kofst.or.kr

AcademicKeys (Connecticut, USA)
http://sciences.academickeys.com/jour_main.php

Sherpa Romeo (United Kingdom)
http://www.sherpa.ac.uk/romeo/search.php?source=journal&sourceid=28772

Cl.An. // THOMSON REUTERS, ResearcherID (USA)
http://www.researcherid.com/rid/N-7988-2013

RedLink (Canada)
https://www.redlink.com/

Cl.An. // THOMSON REUTERS, ORCID (USA)
http://orcid.org/0000-0002-7689-4157

TDNet
Library & Information Center Solutions (USA)
http://www.tdnet.io/

Yewno (USA & UK)
http://yewno.com/

RefME (USA & UK)
https://www.refme.com

Stratified Medical Ltd. (London, United Kingdom)
http://www.stratifiedmedical.com/

THE SCIENTIFIC JOURNAL IS INDEXED IN SCIENTOMETRIC BASES:

Advanced Sciences Index (Germany)
http://journal-index.org/

SCIENTIFIC INDEXING SERVICE (USA)
http://sindexs.org/JournalList.aspx?ID=202

Global Impact Factor (Australia)
http://globalimpactfactor.com/?type=issn&s=2308-4944&submit=Submit

International Society for Research Activity (India)
http://www.israjif.org/single.php?did=2308-4944

CiteFactor (USA) Directory Indexing of International Research Journals
http://www.citefactor.org/journal/index/11362/theoretical-applied-science

International Institute of Organized Research (India)
http://www.i2or.com/indexed-journals.html

JIFACTOR
http://www.jifactor.org/journal_view.php?journal_id=2073

Journal Index
http://journalindex.net/?qi=Theoretical+%26+Applied+Science

Eurasian Scientific Journal Index (Kazakhstan)
http://esjindex.org/search.php?id=1

Open Access Journals
http://www.oajournals.info/

SJIF Impact Factor (Morocco)
http://sjifactor.inno-space.net/passport.php?id=18062

Indian citation index (India)
http://www.indiancitationindex.com/

InfoBase Index (India)
http://infobaseindex.com

Index Copernicus International (Warsaw, Poland)
http://journals.indexcopernicus.com/masterlist.php?q=2308-4944

Электронно-библиотечная система «Издательства «Лань» (Russia)
http://e.lanbook.com/journal/

Signed in print: 30.10.2022. Size 60x84 1/8

«Theoretical & Applied Science» (USA, Sweden, KZ)
Scientific publication, p.sh. 55.25. Edition of 90 copies.
http://T-Science.org E-mail: **T-Science@mail.ru**

Printed «Theoretical & Applied Science»